Using LiDAR Data to Estimate Effective Leaf Area Index, Determine Biometrics and Visualize Canopy Structure in a Central Oregon Forest with Complex Terrain

by

Evan Anthony Hayduk

A Thesis
Submitted in partial fulfillment
of the requirements for the degree
Master of Environmental Studies
The Evergreen State College
December 2012

This Thesis for the Master of Environmental Studies Degree

by

Evan Anthony Hayduk

has been approved for

The Evergreen State College

by

_____

Judith Bayard Cushing
Member of the Faculty (Ecology Informatics and Computer Science)

December 20, 2012

_____

Date

ABSTRACT

Using LiDAR Data to Estimate Effective Leaf Area Index, Determine Biometrics and Visualize Canopy Structure in a Central Oregon Forest with Complex Terrain

Evan Anthony Hayduk

Leaf Area Index (LAI), the total one-sided area of leaf tissue per unit ground surface area, is an important parameter in many ecological models. LAI is important for determining interception loss, and can be used potentially as a surrogate for other ecosystem parameters when studying ecosystem processes and services. Estimation of LAI at the watershed scale is difficult since traditional, direct destructive methods are cumbersome and possible only on small spatial scales. Furthermore, estimation of LAI in steep terrain has proven challenging for indirect methods using tools that utilize lasers to estimate light penetration through canopies. In this study, digital hemispherical photographs were used to ground-truth a Light Detecting and Ranging (LiDAR) method of estimating effective LAI at both the plot and watershed scales using canopy volume from LiDAR point cloud data. Effective LAI differs from true LAI in that it includes non-leaf material, such as branches, in the calculation. The LiDAR model seems to underestimate effective LAI when compared to ground based methods (R^2= 0.3346, $p<.001$) for 19 of the 133 vegetation plots in Watershed 1 of H.J. Andrews Experimental Forest.

LiDAR data were also used to calculate biometrics (height, crown diameter, and stem location) of individual trees and to visualize forest structure. When compared to vegetation surveys completed for all permanent vegetation plots, 82% of live trees were identified using LiDAR data. The results of this work can be used for modeling throughfall, canopy storage and interception loss for the watershed, either scaling from branch, to plot, to watershed leaf area or using allometric equations with the identified individual trees. The visualizations presented could assist researchers by allowing them to see gaps in the canopy and assess variability on a subplot scale. Future research includes assessing what factors affect the accuracy of tree identification and how software programs can be improved for more accurate tree identification and LAI estimation in complex terrain.

TABLE OF CONTENTS

Chapter 1- Introduction: Leaf Area Index, LiDAR and Motivation

Introduction……2
Leaf Area Index……...5
Direct Methods of LAI Measurement……..5
Indirect Methods of LAI Measurement…….....7
What is LiDAR? ……..……10
Study Site – The H. J. Andrews Experimental Forest……..….13
Geology……..13
Soils ...……...14
Vegetation and Management History…….……...15
Harvest History…..……15
Interdisciplinary Nature of this Research……..……16
Thesis Organization Overview……..……17

Chapter 2- Estimating LAI from Digital Hemispherical Photographs and LiDAR Data

Introduction and Background……20
Remotely Sensed LAI Measurements……20
LiDAR and LAI Estimation from the Literature……..……23
Selection of a LAI-LiDAR Model……..…25
Methods……..……26
Hemispherical Photograph Acquisition……26
Hemispherical Photograph Analysis……..…27
LiDAR Data Acquisition……...……31
LiDAR Data Analysis……32
FUSION Executables Used……33
Volume Calculation for LAI Model……..……36
Results……37
LAI Results from Digital Hemispherical Photographs using SLIM Software……37
Simple Linear Regression of LAI Values……..……39
LiDAR LAI Model Based on Surface Volume of CHM…...……41
Discussion……..……45
Underestimation of LAI from Hemispherical Photograph Analysis……..47
Slope Correction for Hemispherical Photograph Analysis……49
LiDAR LAI Estimates……...51
Alternative LiDAR Systems……..53
Conclusions……55

Chapter 3- LiDAR used to Describe Stand Characteristics and Identify Individual Tree Height and Location

Introduction and Background……59
Biomass and Carbon Stocks……...59
Using LiDAR Data to Describe Forest Structure and Cover…..…61

Stem Mapping……67
Methods……..……70
TreeVaW Individual Tree Identification and Stem Mapping……70
H.J. Andrews Vegetation Survey Data……..……71
DBH-Tree Height Relationship and Comparison……..……71
Results……72
Total Trees Identified in Plots……72
Vegetation Survey and TreeVaW Comparison by Plot……73
Discussion……..…84
New Methods in Tree Extraction from LiDAR Data……..…88
Conclusions……91

Chapter 4- LiDAR Data Visualization and Overview of Visualization in Natural Resource Management
Introduction and Background……94
Methods……101
Visualization of LiDAR Data for Plots and Transects……102
Visualization of TreeVaW Output Trees……103
Results……..103
Watershed 1 Visualizations……..103
Visualizations of LiDAR Point Cloud and TreeVaW Identified Trees……107
Discussion……114
Visualization in Ecosystem Monitoring and Processes……...116
Landscape Visualization……..118
Conclusions……..120

Chapter 5- Summary of Conclusions and Future Research
Objectives Revisited……123
Future Research Directions……..125

Literature Cited……..……128

Appendix A: LiDAR Calculated LAI, Surface Volume and Cover*Height Value for All Permanent Vegetation Plots……142

Appendix B: TreeVaW Tree Identification Results for all 133 Permanent Vegetation Plots……..……..…...146

LIST OF FIGURES

Figure 1. Study site map showing WS1 at H.J. Andrews Experimental Forest. Blue circles indicate all permanent vegetation plots in the watershed with red circles representing plots in which DHPs were taken. 12
Figure 2. Trigonometric calculation for scope setting in SLIM software for DHP photo analysis. 30
Figure 3. Q-Q plots for all LAI results: Plot LAI (right), Wide LAI (bottom left) and Cardinal LAI (top left). Axes represent theoretical and sample quantiles. Only Plot LAI is normally distributed. 38
Figure 4. Regression analysis for ln(Plot LAI) compared to ln(Wide_LAI). The relationship is not significant (alpha= .05). 39
Figure 5. Regression analysis for ln(Plot LAI) compared to ln(Cardinal LAI). The relationship is somewhat strong and statistically significant (R^2 = 0.3114, p = 0.013). 40
Figure 6. Simple linear regression model of Plot LAI from hemispherical photographs to LiDAR estimated LAI for each plot. 43
Figure 7. Simple linear regression between LiDAR calculated LAI and Cover*Height values for plots in which DHP were taken. 44
Figure 8. Results of simple linear regression for all plots between LiDAR calculated LAI and Cover*Height value. 45
Figure 9. Previous estimates of LAI in the FEEL network in Watershed 1 at H.J. Andrews. 47
Figure 10. Transect 1, plot 8. 74
Figure 11. Transect 1, plot 9. 74
Figure 12. Transect 1, plot 10. 75
Figure 13. Transect 2, plot 5. 76
Figure 14. Transect 2, plot 6. 76
Figure 15. Transect 2, plot 7. 77
Figure 16. Transect 2, plot 8. 77
Figure 17. Transect 2, plot 9. 78
Figure 18. Transect 2, plot 11. 78
Figure 19. Transect 2, plot 12. 79
Figure 20. Transect 2, plot 13. 79
Figure 21. Transect 6, plot 8. 80
Figure 22. Transect 6, plot 9. 80
Figure 23. Transect 6, plot 10. 81
Figure 24. Transect 6, plot 11. 81
Figure 25. Transect 6, plot 12. 82
Figure 26. Transect 6, plot 13. 82

Figure 27. Transect 6, plot 14. 83
Figure 28. Transect 6, plot 15. 83
Figure 29. Transect 6, plot 16. 84
Figure 30. Transect 6, plot 17. 84
Figure 31. A comparison of a) the newly developed HSCOI metric, and b) a CHM. The high point in the CHM is transformed to a low point in the HSCOI because it would be an area where penetration of LiDAR pulses would be very low (Lee and Lucas 2007) 89
Figure 32. A diagram representing new types of visual analysis of LiDAR data could occur because of research by Kao et al. (2005). 98
Figure 33. FUSION visualization of WS1 Digital Elevation Model (DEM) and LiDAR data of 19 vegetation plots where digital hemispherical photographs were taken. 104
Figure 34. Overhead view visualization of WS1 DEM and LiDAR data of vegetation plots. 105
Figure 35. Overhead view visualization of WS1 DEM and LiDAR data of vegetation plots with digital orthophotograph of vegetation in the Watershed overlaid. 106
Figure 36. Visualization of LiDAR data and DEM of vegetation plots in transect 2 (above) and transect 6 (below). 107
Figure 37. Transect 1, plot 9. 108
Figure 38. Transect 1, plot 10. 108
Figure 39. Transect 2, plot 5. 109
Figure 40. Transect 2, plot 6. 109
Figure 41. Transect 2, plot 7. 109
Figure 42. Transect 2, plot 8. 110
Figure 43. Transect 2, plot 9. 110
Figure 44. Transect 2, plot 12. 110
Figure 45. Transect 2, plot 13. 111
Figure 46. Transect 6, plot 8. 111
Figure 47. Transect 6, plot 9. 111
Figure 48. Transect 6, plot 10. 112
Figure 49. Transect 6, plot 11. 112
Figure 50. Transect 6, plot 12. 112
Figure 51. Transect 6, plot 13. 113
Figure 52. Transect 6, plot 14. 113
Figure 53. Transect 6, plot 15. 113
Figure 54. Transect 6, plot 16. 114
Figure 55. Transect 6, plot 17. 114

LIST OF TABLES

Table 1. Resulting resolution and accuracy of LiDAR data. 32
Table 2. LAI and gap fraction results from SLIM software. Plot LAI was calculated with a limited scope of view to capture LAI within each vegetation plot. Wide LAI used the default 60 degree scope for calculation and Cardinal LAI is the average of the four cardinal direction LAI values with a 60 degree scope. 37
Table 3. Plot LAI, Volume of Canopy Height Model, and LiDAR calucalted LAI for each plot studied. 42
Table 4. DBH-Height asymtotic equation and regression coefficients used for each species (Garman et al. 1995). 72
Table 5. Observed trees, trees predicted by TreeVaW and percentage of trees identified by TreeVaW in plots where digital hemispherical photographs were taken. 73

ACKNOWLEDGEMENTS

I would especially like to thank my reader, Judy Cushing, for all the guidance and expertise she provided throughout my time in the MES program. A special thanks to the last minute heroics of Fox Peterson, for helping in the final editing of this thesis. Also, thank you to Barbara Bond and Scott Allen for the framing of this research. Also, I would like to greatly thank everyone who assisted me in the completion of this thesis, including:

Jerilyn Walley, Nalini Nadkarni, Mark Schulze, Lee Zeman, Anne McIntosh, Adam Kennedy, Kirsten Winters, Jeff Richardson, Robert McGaughey, Soren Popescu, Jason Cornell, Lorrain Garr, Carri Leroy, Martha Henderson, Gerardo Chin-Leo, Ralph Murphy, my entire MES cohort and all the other MES'ers.

This thesis research is a part of the VISTAS project. The VISTAS project is supported by the U.S. National Science Foundation/ BIO/DBI 1062572. Any opinions, findings, and conclusions or recommendations expressed in this material are those of the author and do not necessarily reflect the views of the National Science Foundation. Data sets were provided by the H.J. Andrews Experimental Forest research program, funded by the National Science Foundation's Long-Term Ecological Research Program (DEB 08-23380), US Forest Service Pacific Northwest Research Station, and Oregon State University.

A final and thank you to my wonderfully patient and beautiful partner Jen Motley and my family.

Chapter 1- Introduction: Leaf Area Index, LiDAR and Motivation

The major motivation for this thesis, which focuses on estimating Leaf Area Index and related visualizations for Watershed 1 (WS1) in the H.J. Andrews Experimental Forest, is rooted in the Visualization of Terrestrial and Aquatic Systems (VISTAS) project. VISTAS is a collaboration among computer and social scientists, ecologists, and students at The Evergreen State College, Oregon State University, and the University of Minnesota. The project was born of necessity: to solve problems apparent in the current age of massive data stores and grand challenge environmental science. Adding to the challenge of addressing critical environmental science questions in the presence of massive amounts of data are difficulties inherent when dealing with multiple spatial and temporal scales, complex physical terrain, and highly distributed and heterogeneous data (VISTAS Summary). The VISTAS project posits that visualizing natural phenomena can help scientists develop intuition and hypotheses at multiple spatial scales, thus improving their ability to formulate new insights about ecosystem services, patterns and processes in complex systems and to communicate these insights to the wider community (VISTAS Summary). The objectives of the VISTAS project are:

1) Conduct EcoInformatics research to enable the required visual analytics and implement a proof of concept software tool
2) Co-develop VISTAS software with environmental scientists who will use it in studies spanning spatial and temporal scales
3) Apply social science methods to study the co-development and usability of VISTAS and its visual analytics.

Barbara Bond, co-principle investigator (coPI) of the VISTAS project and former PI of the Andrews Long Term Ecological Research (LTER) site, and her students have studied ecohydrological function in WS1 for decades. Her former Master's student, Scott Allen, now a PhD candidate at Louisiana State University, recently completed work in WS1. Allen and others' work examines the influence of spatial patterns of canopy storage, interception, and throughfall on isotopic composition of water in the watershed. A portion of his work is related to prior research including that by Keim et al. (2005) which used simulated rainfall on harvest branches to determine the storage capacity of branches with a known leaf area. This branch scale leaf area can then be scaled up to the tree level to estimate the capability of individual trees to intercept and store precipitation (Waring et al., 1977; Gholz et al., 1979; Laurenroth et al., 1993; Bond et al., 2002). Scaling Keim's work to the watershed level requires accurate measurement of Leaf Area Index for the watershed, the third objective of this thesis project (stated below).

The main objectives of this thesis are as follows:

1) Determine accurate LAI estimates for a subset of permanent vegetation plots in WS1 using digital hemispherical photography (DHP)
2) Use estimates of LAI obtained from DHP (1) to build a LiDAR based model of LAI for all 133 permanent vegetation plots
3) Calibrate the LiDAR based model (2) for LAI to create LAI maps for the entire watershed
4) Test the ability of software programs to extract and identify individual trees from LiDAR data in all 133 permanent vegetation plots in WS1

5) Create novel visualizations of individual trees in the vegetation plots using LiDAR data

LAI is not only important for measuring interception loss, but as a potentially easy way to measure ecosystem parameters that can be used as surrogates for calculating ecosystem processes and services. For example, relationships between LAI and biomass may facilitate the calculation of carbon (C) stores in forests, and relationships between LAI and stomatal aperture may facilitate the calculation of gas exchange and C fluxes from forests. Additionally, color-identification software may be used in conjunction with LAI to produce estimates of forest albedo, which can be used to study global heat flux, and the potential for forests to contribute to or protect us from, varying wavelengths of radiation. LAI may also be directly related to foliar biomass, which is often useful in biogeochemical analyses over time as a proxy for plant nutrient allocation, indicative of soil nitrogen (N) concentrations, and potentially related to rates of root development and turnover. Most importantly, LAI may be used in all of the above ways to aid in calculation of global net primary production (NPP) and net ecosystem exchange (NEE), which dictate the planet's ability to mitigate changes in atmospheric C concentrations. Accurate NPP and NEE calculations could be particularly useful from a management standpoint as they allow the assignment of a relative economic value to forests for their service as a carbon sink, may aid in the quantification of ecosystem services, help with management decisions, and be a useful measure for policy and decision makers to compare forest capacities worldwide.

Leaf Area Index (LAI)

Leaf area index (LAI) was first described by Watson (1947) as the "total one-sided area of leaf tissue per unit ground surface area." Watson labeled LAI as a dimensionless unit that characterizes the canopy of a forest stand. LAI determines canopy water interception and radiation extinction, thereby influencing water and carbon gas exchange, within- and below- canopy microclimates, and aiding in the understanding of biogeochemical cycling in ecosystems (Breda, 2003). Accurate measurements of LAI can contribute to a better understanding of water resource dynamics and photosynthetic productivity on an individual, stand, or watershed scale (Breda, 2003).

Since Watson (1947) first defined LAI, various techniques have been used to measure LAI in ecosystems from simple cropland to dense, complex temperate rain forests, and have also been summarized in review articles such as Breda (2003), Jonckheere et al. (2004) and Weiss et al. (2004). Breda (2003) breaks down *in situ* LAI measurement methods into two different categories: direct and indirect measurements.

Direct Methods of LAI Measurement

Direct methods of determining LAI include harvesting, allometric methods and litter collection. Harvesting is a destructive method of measurement that requires harvesting and measuring all vegetation within a given area. Leaf samples are collected from a site that has a known ground-surface area and then dried and weighed. LAI is then computed by multiplying leaf dry mass ($g\ m^{-2}$) by the specific leaf area ($m^2\ g^{-1}$ SLA). Since m^2 and g are present in both the numerator

(leaf area) and denominator (ground area) these measures cancel out, leaving LAI as a unitless value. This method is used extensively with crop species, but the destructive nature and tedious approach is not applicable to large areas, especially forest stands with large trees.

A less destructive method of sampling is the application of allometric relationships between directly (destructively) measured sapwood and leaf area of individual trees. The theory supporting this technique is based on the hypothesis that leaf area is directly proportionate to conducting tissue (Grier and Waring, 1974; Makela, 1986; Waring et al., 1977). Consequently, allometric relationships are sensitive to site and species, and in extreme cases, to the year of measurement. Breda (2003) also recommends replacing sapwood area as the base for measurement due to the difficulty in measuring conductive area. Using easily measurable variables, such as diameter at breast height (DBH), is a more efficient way to measure LAI using allometric relationships, and can be done without directly removing a core sample from trees to quantify sapwood.

The final direct method described by Breda (2003) consists of collecting leaves as litter in traps distributed below the canopy during leaf fall. This technique is used widely in deciduous stands that shed leaves during the fall season. Litter is collected in a set number of traps within a known collection area, and harvested often to avoid loss of litter and decomposition. The collected litter is dried and weighed, then scaled to trap size in m^2 to compute the dry mass of litter as g m^{-2}. Leaf dry mass is then converted to leaf area by multiplying the collected biomass by the Specific Leaf Area (SLA). SLA is found by measuring

the projected leaf area of leaves and dividing that value by the leaf area dry mass of the leaves. SLA relates biomass to cover and is indicative of photosynthetic processing and C allocation (Evans and Poorter, 2001). To obtain LAI, the total accumulated leaf area spanning collection times is calculated by adding together the leaf area calculations for each trap and from each collection and scaling to the plot or landscape scale.

Indirect Methods of LAI Measurement

Jonckheere et al. (2004) describe the benefits of indirectly measuring LAI whereby leaf area is inferred from one or more other variables. Indirect methods are faster and amendable to automation and thus allow for larger spatial samples. Additionally, these techniques do not require destructive sampling and can be applied in areas where destructive sampling is not possible. Indirect methods fall into one of two categories: indirect contact methods and indirect non-contact methods.

The first indirect contact method described by Jonckheere et al. (2004) is the inclined point quadrat technique used by Wilson (1960, 1963). According to Jonckheere (2004) this method "consists of piercing a vegetation canopy with a long thin needle (point quadrat) under known elevation (i.e., the angle between the needle and the horizontal plane when vertically projected) and azimuth angles (i.e., the bearing of the needle from North when horizontally projected) and counting the number of hits or contacts of the point quadrat with 'green' canopy elements." These data are then input into a simple equation based on a radiation penetration model:

$$LAI = 1.1 \times N(32.5)$$

where N (32.5) is the number of contacts with an elevation angle of 32.5 degrees. The more times the needle is dropped into a vegetative canopy, the more reliable are the estimates of LAI. When the needle is dropped repeatedly with different angles of insertion, the formula used becomes:

$$N_i = LK_i$$

where L is LAI, N_i is the number of contacts of the needle dropped with elevation i and K_i the extinction coefficient with elevation i. This method, according to Jonckheere et al. (2004) is attractive because it does not require an assumption of random leaf distribution, but its major drawback is the considerable field work involved, often requiring over 1000 insertions to obtain a reliable estimate of LAI. This method is also not applicable in canopies taller than 1.5 m, and thus it has been limited to determination of LAI on cropland.

Jonckheere et al. (2004) also consider allometric techniques for the measurement of LAI, as mentioned above, which they categorize as an indirect contact method, and which rely on destructive sampling to measure sapwood, or non-destructive measurement of basal area or diameter at breast height (DBH). The destructive sampling of sapwood would fall into the direct methods category, mentioned above. Measurement of other variables such as DBH and basal area are

considered indirect non-contact due to the non-destructive nature of the measurements. Other indirect non-contact measurements of LAI are based on measuring light transmission through canopies and are more commonly implemented.

Indirect non-contact methods apply the Beer-Lambert law, which accounts for the total radiation intercepted by canopy layers and depends on incident irradiance, canopy structure, and optical properties. Indirect non-contact methods require forest floor based measurement of total, direct, and/or diffuse radiation transmittance to the ground. In the last few decades, a wide range of instruments have been developed to measure LAI in real time within plant canopies. These instruments use either gap fraction analysis, or gap size distribution analysis, to determine LAI. Devices such as the Digital Plant Canopy Imager CI 100 MVI, measure gap fraction by incorporating canopy image analysis techniques. Other devices, such as Accupar, Demon, Licor LAI-2000 Plant Canopy Analyzer, use gap fraction and calculate LAI by comparing differential light measurements above and below the canopy (sensu Cutini, 1998). However, the maximum measurable LAI is lower for devices that measure gap fraction, because LAI reaches an asymptotic saturation level at a value of 5, which causes gap fraction saturation as LAI approaches and exceeds 5-6. Other devices use gap size distribution to measure LAI, including the Tracing Radiation and Architecture of Canopies (TRAC) instrument.

Hemispherical photography also uses gap size distribution to estimate LAI in forest canopies. Jonckheere et al. (2004) focus extensively on the use of

hemispherical photographs in their review of LAI measurement methods, and state that a hemispherical photograph provides a permanent record and is therefore a valuable information source for position, size, density and distribution of canopy gaps. Hemispherical photography requires the use of a fish-eye lens to photograph the canopy from the forest floor with the camera oriented towards zenith. This technique also captures the species-, site- and age-related differences in the architecture of canopies based on light attenuation and the difference in the photograph of light (sky) and dark (canopy).

TRAC and hemispherical photography, which use gap size distribution to measure LAI, do not distinguish photosynthetically active leaf tissue from other plant elements such as branches, stems and flowers. For this reason, alternative terms for LAI have been proposed, with Chen and Black (1992) settling on the most widely used term: "effective LAI".

What is LiDAR?

A description of Light Detecting and Ranging (LiDAR) systems and LiDAR data is found in the FUSION software manual (McGaughey, 2012): LiDAR systems use laser light to measure distances between the source of the LiDAR and the object(s) surveyed. Aerial laser scanning is an aircraft based LiDAR system which provides accurate, detailed 3D measurement of ground, vegetation, and buildings. In open areas, ground contours can be measured within 6 inches of actual elevation. In steep, forested areas accuracy is typically .3m to .6m, depending on density of canopy cover and the spacing of the laser pulses. The speed and accuracy of LiDAR systems allow for highly detailed mapping of large

areas previously possibly only with time-consuming and expensive ground surveys (McGaughey, 2012), and are increasingly being used to infer forest biometrics.

Aerial LiDAR systems are mounted on a single- or twin-engine plane or helicopter for data collection over a large area. An aerial LiDAR system consists of four pieces of equipment: 1) a laser emitter/receiver scanning unit on the aircraft, 2) global positioning system (GPS) units on the aircraft and on the ground, 3) an inertial measurement unit (IMU) attached to the scanner to measure roll, pitch, and yam of the aircraft, and 4) a computer system to control the entire system and store the data. Several types of LiDAR systems exist, with the most commonly used version for forestry being discrete-return, small-footprint systems. The term small-footprint refers to the size of the laser beam diameter at ground level, typically from .02m to 1m wide. Up to 200,000 pulses of light per second are emitted by the laser scanner, and the time it takes for the pulse to return to the receiver is measured. The times are used to compute the distance to the object on the ground, with the GPS and IMU units used determining the precise location and attitude of the laser scanner as the pulses are emitted. All this information is used to calculate exact coordinates for each point. Depending on the unit, an oscillating mirror or rotating prism on the laser scanner is used to sweep light pulses across a wide swath of the landscape. Large areas are surveyed using a series of parallel flight paths. The only weather conditions required are clear skies and flights can be performed day or night since the system emits its own light (Lefsky et al., 2002; Lefsky et al., 2005).

The laser altimetry calculated by the aerial system yields direct 3D measurements of the ground surface, vegetation, roads, and buildings. The millions of data points create a 3D point cloud. After the flight, additional calculations are performed to create the final data points, and results can be produced in weeks to months. The initial acre of the LiDAR flight is expensive, accounting for the costs of the aircraft, equipment and personnel. However, when large areas are measured, the costs can drop to as low as $1 to $2 per acre.

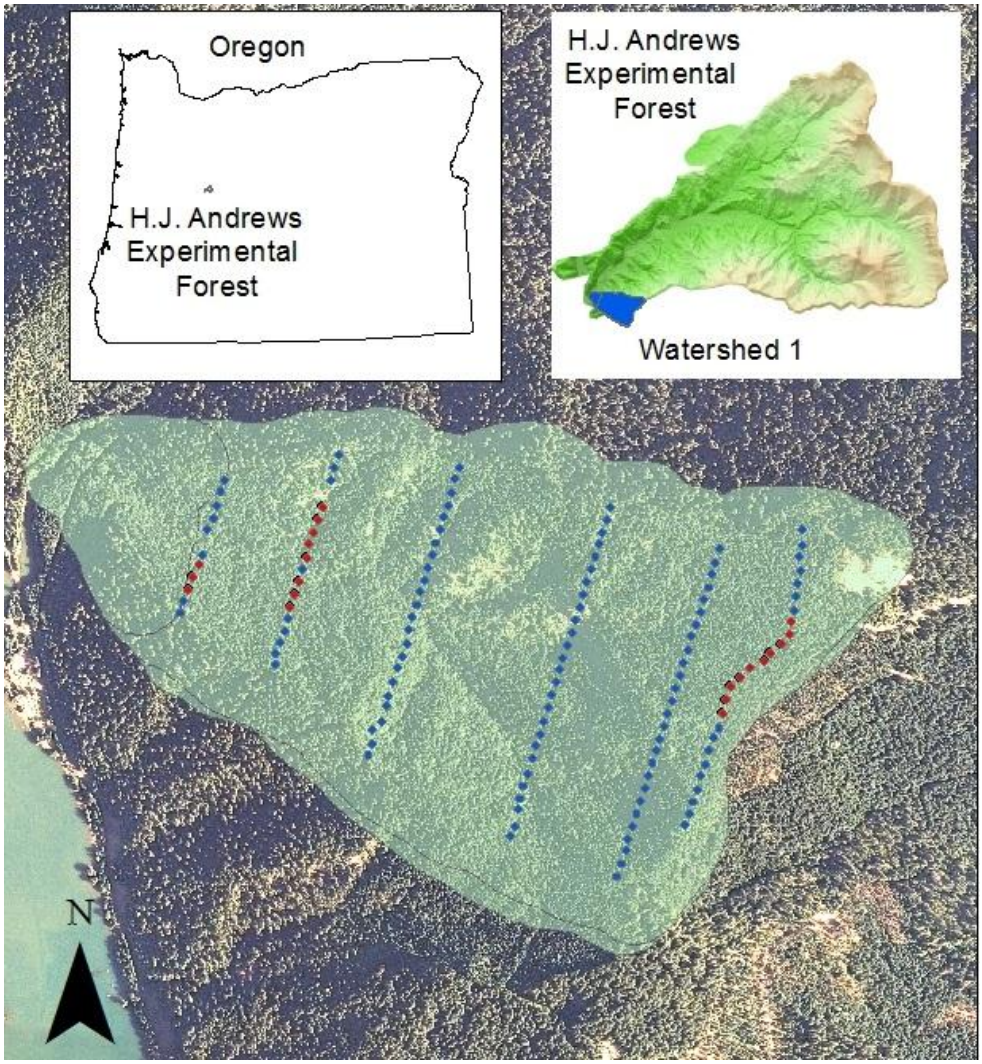

Figure 1. Study site map showing WS1 at H.J. Andrews Experimental Forest. Blue circles indicate all permanent vegetation plots in the watershed with red circles representing plots in which DHPs were taken.

Study Site – H.J. Andrews Experimental Forest

The site where this thesis research was conducted is Watershed 1 on the H. J. Andrews Long Term Ecological Research site near Blue River Oregon, USA, in the Cascade Mountains (Figure 1). Study site information for Watershed 1 (WS1) was obtained from the H.J. Andrews website (andrewsforest.oregonstate.edu/). WS1 is a small watershed of 96 ha located on a first order stream draining to Lookout Creek along the McKenzie River in the Western Cascades range of Oregon. The bounding coordinates (in decimal degrees) for WS1 are North: 44.20851700, South: 44.19901700, East: -122.23581300, and West -122.25683100. WS1 is a well-known low-elevation watershed nestled within the greater H.J. Andrews Experimental forest and exhibits "complex terrain" characteristic of the region. The minimum elevation on WS1 is 450 meters, maximum elevation is 1027 meters, the mean slope measured using ground based clinometry is 59.35% and the watershed outlet faces an aspect of 286 degrees. Mean January temperature is 35 F (1.6 C), mean July temperature is 69 degrees F (20.6 C), although heating and cooling patterns are asymmetric, with cold air pooling occurring on approximately 80% of summer nights (Rothacher, 1965; Pypker et al., 2007).

Geology: Swanson and James (1975) describe the geology of WS1 and the H.J. Andrews (HJA). The HJA is underlain by bedrock of volcanic origin of mixed mineralogy. Three geologic formations have been mapped for the HJA and correspond roughly with elevation. Little Butte Formation bedrock (approximately 760 m elevation), dated as Oligocene to lower Miocene, consists

of massive tuffs and breccias derived from mudflows and pyroclastic flows. Sardine Formation bedrock (760 m to 1200 m), dated as middle to late Miocene, consists of two units: a lower unit containing welded and non-welded ash flows, and an upper unit containing basalt and andesite lava flows. Andesitic and basaltic lava flows (>1200 m), or the "Pliocascade" Formation, were deposited during the Pliocene and overlie Sardine Formation material. Watershed 1 spans the Little Butte-Sardine contact area. A large caprock, visible in aerial photography, particularly after harvest, and in LiDAR bare earth images, demarcates a distinct separation in mineralogy observed by Peterson (2012). Watershed 1 has both basaltic and andesitic mineralogy: in the extreme northeast corner of WS1, the upper elevations are underlain by deposits of Sardine andesitic flow rock. Most of the bedrock of this type in WS1 is slow to weather, displaying rugged escarpments and outcroppings (Swanson and James, 1975). However, recent research by Pett-Ridge (Peterson, personal communication) suggests that weathering rates on parts of WS1 may be relatively rapid; these analyses are based on silicate material losses in dissolved water and stream outflow.

Soils: Soils have not been formally mapped for WS1, although Rothacher (1965) characterized several potential soil groups. Additionally, several soil pits have been dug on the watershed (1957, mid-1960's, 1982, 2002, 2010) which indicate high heterogeneity in soil physical and chemical characteristics (Peterson and Lajtha, 2012). Land movements of varying duration and intensity are common on the HJA; glacial, fluvial and mass wasting processes are the main factors affecting soil development and spatial distribution, especially in geologic contact zones and

steeper areas. In WS1, soils vary from shallow and stony to moderately deep with well-developed profile features. These soils may affect the establishment and survival of vegetative communities.

Vegetation and Management History: Rothacher et al. (1967) describe the pre-logging condition of WS1. Douglas-fir (*Psuedotsuga menziesii*) was the dominant species, ranging in age from 100 to 500 years. Western Hemlock (*Tsuga heterophylla*) was intermixed and generally younger; some western red-cedar (*Thuja plicata*) was also present, mostly in drainage areas. Pacific yew (*Taxus brevifolia*) was present in the understory. Hardwood species were common in stem density, but had relatively low biomass compared to conifers. However, hardwoods were first to establish on many plots, and created environments on which conifers would later thrive. Current hardwoods, in terms of relative abundance (number) and in decreasing order are big-leaf maple (*Acer macrophyllum*), Pacific dogwood (*Cornus nuttallii*), golden chinkapin (*Chrysolepis chrysophylla*), and red alder (*Alnus rubra*). Some of these, such as *Alnus rubra*, are found mixed within the coniferous plots, while others, such as *Chrysolepis chrysophylla*, clearly dominate dry plots. Six understory plant communities were present: 1) hazel-salal (10% of watershed area), 2) rhododendron-salal (10%), 3) vine maple-salal (10%), 4) vine maple-Oregon grape (25%), 5) gold-thread (25%) and 6) sword-fern (20%).

Harvest History: Watershed 1 was originally part of a paired watershed study with a control watershed (WS2) and a patch clear cut watershed (WS3) of similar size and topographic characteristic. WS1 was 100% clear-cut over four year period

from fall 1962 to summer 1966. Initially, it was suspected that high lead logging could be used, but the method was switched to skyline following the harvest of one unit. Even the skyline logging techniques of the day, however, proved to be difficult for the initially hired group, Ballinger Logging, and Swiss contractors (Wyssen Logging) were called in to construct a method for harvesting larger trees. During this time between logging events, regrowth of understory species, specifically *Ceanothus spp* occurred, which may have impacted soil conditions. After the entire watershed was harvested, it was burned in 1967 in a burn that was "hot and satisfactory," and all debris littering the stream was removed. Since 1952, the watershed stream outflow has been monitored and regrowth inventoried approximately on a six year basis. These inventories and stream measurements are the fundamental components of the current biomass and nutrient studies conducted on WS1 to assess the impacts of harvest on watershed productivity and nutrient budgets (Peterson 2012).

Interdisciplinary Nature of this Research

This thesis follows the VISTAS project with an interdisciplinary approach to completing stated objectives. The work's major goals are those related to ecology and pose fundamental questions about how forest ecosystems function. However, the methods used to answer these questions are based in the computer sciences, including computer programming and data visualization, and the researcher wears both hats to carry out the work. It would be difficult for a computer scientist to complete field work to acquire hemispherical photographs that are later analyzed for LAI calculations. Similarly, it would be difficult for most ecologists to write

code to create an executable program, or even to use the complex software needed for such work. Furthermore, the results of this study can be used to accomplish goals in several disciplines. The estimates of LAI for the watershed can be used by ecologists to determine how precipitation interacts with the canopy, either being stored or falling as throughfall, and as the first check to the water balance of the system. The estimates of total trees in the plots and watershed can be used for biogeochemical cycling models to determine nutrient transport and carbon sequestration within the watershed. The methods of visualization and tree counts could be used by natural resource managers for decision making. And, finally, the suggestions offered for improvement of the LiDAR analysis and visualization software can be used by computer scientists to improve these tools, and to build even better tools in the future.

Thesis Organization Overview

This thesis is organized into four chapters as follows. In Chapter 2, the use of remote sensing to estimate LAI is explored. Then, we describe how we used digital hemispherical photography (DHP) of 19 plots to estimate LAI for all 133 plots in WS1, and how we subsequently used LAI estimates from those plots to 'ground-truth' a LiDAR based model to determine LAI for the remaining plots and the watershed as whole. In Chapter 3, we present an overview of how LIDAR has been used to estimate canopy and stand characteristics. We then describe how we used the TreeVaW software to extract and identify individual trees in all 133 permanent vegetation plots in WS1. TreeVaW results for the 19 plots we surveyed are compared to comprehensive vegetation surveys completed at about

the same time as the LiDAR data were collected; and TreeVaW and survey data of individual tree height are compared. Chapter 4 provides background information about forest data visualization and then presents visualizations of LiDAR data from WS1 created with the FUSION software, as well as visualization of trees identified in 19 plots by TreeVaW. Chapter 5 concludes this thesis, and proposes future directions for related research.

Chapter 2- Estimating LAI from Digital Hemispherical Photographs and LiDAR Data

INTRODUCTION AND BACKGROUND

Remotely Sensed LAI Measurements

Breda (2003) chose to consider only ground based measurements of LAI, but noted that remotely sensed vegetation indices, either from satellite or aerial high-resolution imagery, have novel potential for estimating LAI at larger scales. His review mentions that remotely sensed indices at the time (2003) required a site- and stand-specific calibration with ground-based measurements of LAI since remote sensing in itself does not yield accurate LAI measurement for complex canopies, especially those with high LAI values. Jonckheere et al. (2004) also describe air- and space-borne methods for LAI determination at the forest and landscape level, but note that the description of those techniques were beyond the scope of their review.

Zheng and Moskal (2009) offer a complete review of estimating LAI using remote sensing techniques including theoretical background, methods used and sensors utilized. This paper covers the ground based methods discussed above, but focuses on the use of remote sensing technologies and includes a discussion of sources of error and scaling issues. Aerial passive sensors are superior to images obtained from satellites because of their much finer spatial resolution. Unfortunately greater resolution produces in shadows from tree canopies that obscure each other and adds bias to estimation of LAI and makes simulating a radiation regime difficult without using a geometric optical model.

In a forest canopy, different angular distributions of foliage elements result in solar radiation interaction with foliage at four different scales: a) within

groups of trees, b) within individual tree crowns, c) within branches, and d) within shoots (Zheng and Moskal, 2009). To correctly estimate LAI, a geometric-optical model must use the calculated shape of canopy crowns and spatial distribution of canopy elements. The proportion of shadows cast as a function of view direction, relative to the hot spot direction, are then calculated, and spectral characteristics are obtained based on geometrical shape and arrangement. Finally, the spectral reflectance of individual trees or whole canopies can be calculated with the geometric optical model (Zheng and Moskal, 2009).

Satellite retrieval of LAI measurements is based on the unique spectral response characteristic of green leaves as opposed to other materials such as bark. The absorption of solar radiation of green leaves, with high absorption of visible light and red light make vegetation indices such as Simple Ratio (SR), Normalized Difference Vegetation Index (NDVI), Enhanced Vegetation Index (EVI) and the Reduced Simple Ratio (RSR) possible (Zheng and Moskal 2009). Each of these indices has certain advantages over the others, depending on the forest or ecosystem type being evaluated.

Other passive sensors discussed by Zheng and Moskal (2009) are Landsat series sensors and hyperspectral remote sensing data sets. The Landsat series sensors, including thematic mapper and enhanced thematic mapper are used most often because of the balance of spectral, spatial and temporal resolution possible with the sensors. These sensors have been developed to estimate and map LAI at landscape and global levels, based on linear regression relationships between

vegetation indices and LAI, as well as on the linear and non-linear estimation model.

The final type of remotely sensed LAI methods reviewed by Zheng and Moskal (2009) are those that use active sensors that emit a certain wavelength signal and capture the echoes reflected by target objects without receiving the reflected solar radiation by land surfaces. Radio Detection and Range (RADAR) and Light Detection and Ranging (LiDAR) are the two most commonly used active remote sensing systems. LiDAR and other active remote sensing have a distinct advantage over optical passive remote sensing in their ability to capture detail of three-dimensional structure of the forest. The passive systems can only provide two-dimensional information. LiDAR systems can be terrestrial, airborne, or satellite-based, and either discrete or full waveform. Discrete LiDAR systems provide single or multiple returns for each laser pulse, while the full waveform LiDAR provides the waveform for one pulse. Terrestrial LiDAR is a discrete system, yet only one return is recorded for each laser pulse, while most other discrete systems have three or more echoes bounce back for each laser pulse. Discrete systems measure the distance between the emitting sensor and objects by recording the time of flight of the laser. Each laser pulse returns two different types of information: spatial information in x,y,z coordinates and a corresponding intensity value. Aerial, discrete LiDAR systems have been used extensively to characterize and explore forest canopies.

LiDAR and LAI Estimation from the Literature

One of the more recent methods to determine LAI of forest stands uses LiDAR data. Morsdorf et al. (2006) evaluated the potential of aerial discrete return LiDAR systems to derive fractional cover and LAI for a stand in Switzerland. The objective of their work was to establish a predictor variable of LAI that resembles the way LAI is estimated using indirect methods in the field. Morsdorf et al. (2006) started with an equation from previous literature (Weiss et al. 2004) in which LAI at a certain heights is a function of leaf density. The authors added contact frequency as a predictor and set the projection function to 0.5, assuming a spherical foliage distribution in a study area dominated by conifer species. The LAI proxy from LiDAR data used by Morsdorf et al. follows:

$$NLAI = \frac{\sum EFE}{\sum ELE + \sum ESE}$$

where E_{FE}, E_{LE}, and E_{SE} stand for first echo, last echo, and single echo, which were recorded by the LiDAR system used by the authors. The authors used the results of the LAI model to produce maps of LAI for the study area.

In similar research, Riano et al. (2004) also estimated LAI and canopy properties, as well as covered ground using hemispherical photography in three oak (*Quercus myrenaica*) and eight pine (*Pinus sylvestris*) forest plots in the Sierra de Guadarrama mountains of central Spain. The purpose of their research was to assess the capacity of LiDAR data to estimate LAI and covered ground at different spatial scales. To accomplish this, LiDAR data were processed for

different radii, from 0.5 to 2.5 meters (0.5 meter increments) and from 2.5 to 20 meters (2.5 meter increments). The LiDAR predictive variables were: 50, 75 and 90 percentile of heights, average height, maximum height and percentage of canopy hits (returns above 3 meters). The best LAI prediction radius for the oak-dominated forests was from 7.5-10 meters, while the prediction radius for pine forests was 10-12.5 meters. Overall, estimations of LAI for the oak forests were more accurate than those for the pine forests. The results of the regressions of hemispherical LAI and the LiDAR parameters were then used by the authors to map LAI and covered ground for both the oak and pine forest stands.

Solberg et al (2006) examined the use of LiDAR derived gap fraction measurements taken before and after an insect outbreak in a Scots pine stand in Norway. The authors compared LAI obtained from a LICOR 2000 device and digital hemispherical photographs with gap fraction values obtained with discrete return LiDAR data. By ground-truthing the discrete return LiDAR data, Solberg et al. (2006) validated the hypothesis that airborne laser scanning could be used to map defoliation at high spatial resolution over large areas. The authors concluded that this application of LiDAR data could be used for: 1) ad-hoc mapping of acute forest damage, 2) routine monitoring of crown density in stands, and 3) producing large-scale ground-truth data sets for satellite surveys.

Lim et al. (2003) focused LiDAR and LAI research on sugar maple (*Acer saccharum* Marsh.) and yellow birch (*Betula alleghaniensis* Britton) stands in the Turkey Lakes watershed of Sault Ste. Marie, Ontario, Canada. LiDAR derived metrics for the research included maximum laser height, mean laser height, and

mean laser height calculated from LiDAR returns based on a threshold applied to the intensity of return values. Maximum laser height was found to be the best estimator of LAI for the study area. The authors concluded that 'laser height metrics' are a viable option for estimation of plot heights, stem density, aboveground biomass and volume, and other canopy related measures, including LAI.

Selection of a LAI-LiDAR Model

Research by Richardson et al. (2009), reviewed four models from the literature for estimating LAI using aerial LiDAR in the Washington Park Arboretum in Seattle, WA. The four LAI models reviewed used LiDAR metrics based on the mean elevation of returns (Lim et al. 2009), fraction of canopy returns to total returns (Riano et al. 2004), the ratio of returns above 2m to returns below 2m (Solberg et al. 2006), and a canopy volume metric (Lefsky et al. 1999). Similar to work done by Coops et al. (2009), Richardson et al. (2009) adapted the methods of Lefsky et al. (1999) to use discrete return LiDAR rather than the full waveform LiDAR used by Lefsky et al. (1999). These four models were considered for the determination of LAI from LiDAR data for this project. The model created by Lefsky et al. (1999) was chosen for two reasons: 1) the research took place in a similar forest type similar (namely, watershed 1(WS1) at H.J. Andrews), and 2) the range of viable LAI produced by the model fell within the expected range of LAI for WS1 (Nadkarni, personal communication). The other models were calibrated for different forest types and produced lower LAI values: 0.5-4.0 for Lim et al. (2003), 0-3 for Riano et al. (2004) and 0-1.6 for Solberg et al. (2006).

Richardson et al. (2009) noted that these models performed poorly in "saturated" conditions where LAI is high.

METHODS

Hemispherical Photograph Acquisition

For the research reported in this thesis, Digital Hemispherical Photographs (DHPs) were taken over two days in May 2012 in Watershed 1 at the H.J. Andrews Experimental Forest. The camera used was a Canon PowerShot S3IS with an Opteka for Canon 58 mm super wide fisheye lens (0.20X). DHPs were taken early in the morning and late in the evening when the sun was below the horizon or otherwise blocked by the surrounding terrain, since uniform overcast skies were not present. Uniform overcast skies are needed for accurate analysis to limit sunflecks and direct sunlight affecting the photograph. The camera setting mode button was adjusted to F1 function, the setting used for hemispherical photographs with a resulting circular image. The settings were also set to P, or programmed automatic, so that the camera automatically adjusted the shutter speed to the amount of light available. The camera was also set to 'auto-bracket' mode, which takes three photographs at three slightly different exposures: underexposed, normal and overexposed. The DHP showing the greatest contrast between foliage and sky was then used for analysis.

The camera was mounted to a tripod and leveled with a bubble level roughly one meter above the ground level. The top of the camera was oriented to the north with a compass, so that the top of the resulting DHP was due north. The 10-second self-timer function was utilized to limit shaking of the camera while

depressing the picture button. Five sets (3 auto-bracketed photos for each) DHPs were taken for each 9m radius plot: one in the center of the plot, and four in each cardinal direction (N, S, E, and W) roughly 4.5 meters from the center of the plot.

Immediately after taking a set of DHPs, the photos were transferred to a computer and coded according to how other data in the watershed were collected. Information included in the code was plot [P], unit [1], watershed [1], transect [1,2,6], plot number [01-26], direction [C-center, N-North, E- east, S- south, W-west], and camera exposure [N-normal, U-underexposed, O-overexposed]. For example, a normal exposure DHP taken in the center of Plot 8 of transect 1 would be coded as P1108CN.

DHPs were taken in 21 of 133 permanent vegetation plots. Before analysis, two plots (P11108 and P11211) were removed from the data due to low light conditions (P11108) and high light conditions (P11211) at the time the plots were photographed. These plots were included in the stem mapping and comparison of stem counts derived from LiDAR data with TreeVaW and actual tree surveys in the plots (See chapter 3).

Hemispherical Photograph Analysis

DHP analysis was completed with the SLIM (Spot Light Interception Model) software package (www.ualberta.ca/~pcomeau/Light_Modeling/Lite_and_slim_intro.html) developed by Phil Comeau. The program is part of the SLIM/LITE software package. SLIM is designed to estimate LAI, gap fraction, and fractional transmittance from DHPs.

Analysis of the DHPs is subjective (Comeau, SLIM). SLIM analyzes DHPs by classifying each pixel as either a sky or canopy pixel. This converts the true color digital photograph into a black and white, 'thresholded' image. Since uniform sky and light conditions were not present when the DHPs were taken, each DHP was analyzed individually for the light and sky conditions at the time each photo was taken by hand-selecting areas of the DHP that were sky or canopy. Five left clicks on the mouse were used to denote sky and five right clicks denoted canopy. The resulting image was visually analyzed to make sure that fine details, such as a single branch, were visible in the thresholded image. If fine detail was not visible, the brightness of the image was adjusted using a slide bar to ensure all canopy features were recognized. SLIM converted the thresholded image to a Below Canopy Readings (BCR) image. This grayscale image divided the thresholded image into 480 segments. The BCR was then used by the program to estimate Leaf Area Index and Canopy Gap Fraction.

SLIM estimates LAI in three different ways: Poisson, Binomial and Linear Average. The Poisson model assumes a random canopy distribution and random location of leaves and needles in the plane of projection (Jonckheere et al. 2004). The canopy layers are considered thin enough to decrease the probability of having more than one contact between incoming rays of light and vegetation within one layer (Jonckheere et al. 2004). In most natural systems, this is not the case. Binomial models for estimating LAI are described by Nilson (1971) and reviewed by Jonckheere et al (2004). The negative binomial model is more appropriate for canopies with clumped or more regularly distributed leaves. The

final SLIM method for estimating LAI, Linear Average, was first proposed by Lang and Xiang (1986), and combines local linear averaging with larger-scale logarithmic-linear averaging of transmittance data. The Linear Average method in SLIM requires an estimation of leaf angle, data which was not available for this research. The Binomial method requires an estimation of clumping, which was available from previous work done in WS1 (Kennedy, personal communication). Due to its availability of clumping and presence of non-random leaf distribution, the Binomial method was used to calculate LAI values in this research.

For this thesis research, three methods were used to estimate and compare LAI for the vegetation plots and surrounding area. The SLIM program uses scope as an input parameter, which determines the angle of view for analysis of canopy attributes. The default setting for the program is a scope of 60 degrees, resulting in a 120 degree view for analysis. The 60 degrees refers to the angle from zenith (directly above) that is analyzed. The three methods for determining LAI were: 1) LAI for only the plot (LAI_plot), 2) LAI for the plot and immediate area (scope 60 degrees), and 3) a wider view of LAI around the plot.

The first method, LAI_plot required trigonometric calculations and ArcMap (ESRI, 2012) analysis to determine the correct scope that would only calculate the LAI for the 9 meter radius plot. First, a raster layer provided by the HJA for vegetation height was used. This layer was created by researchers at HJA and is similar to a Digital Elevation Model (DEM). In ArcMAP (ESRI, 2012), this layer was loaded, as well as the shape file for all 133 vegetation plots. The plots where the DHPs were taken were selected and a new layer of only these 19 plots

was created. From this layer, the *create buffer* tool was used to create polygons of the 9 m radius DHP plots. The polygons represented the borders of the plots. The *zone by mask* tool was then used to clip the vegetation raster to the vegetation plots, creating a new layer that only held raster data for the vegetation plots. The *zonal statistics* tool was used to determine the mean value of the vegetation raster for each plot. The clipped plots then represented the average canopy height inside each plot. Average canopy height was used to calculate the correct scope of view for analysis in SLIM. Because average canopy height and plot radius transposed to canopy were known, the angle of scope could be calculated with basic trigonometry (see Figure 2).

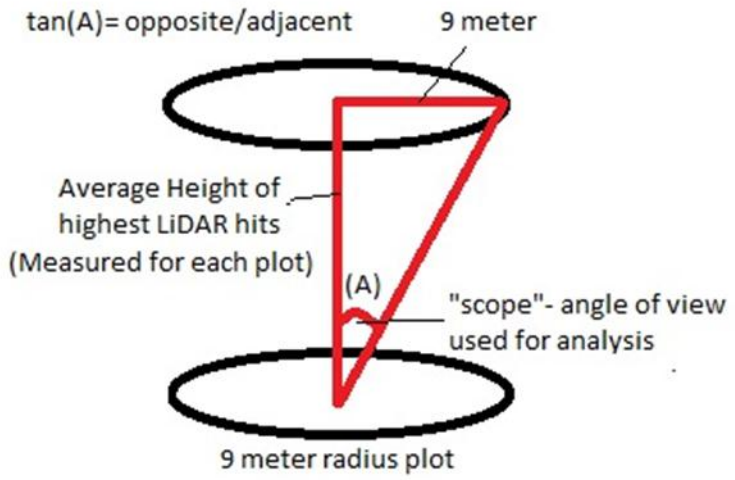

Figure 2. Trigonometric calculation for scope setting in SLIM software for DHP photo analysis.

The second and third methods required less computation. The second method used the same center DHP as the previous method, but used a default 60 degree setting for LAI analysis. The third method used DHP and computed average values of all four cardinal directions ~4 meters from the center of each plot. For these DHPs, a default scope of 60 degrees was also used. The average

LAI values determined by SLIM were calculated as the 'wider view' of LAI around each plot. The plot LAI was compared to both the wider LAI and the average cardinal direction LAI values using a simple linear regression.

LiDAR Data Acquisition

LiDAR data were collected by Watershed Sciences, Inc., (WS) at the HJA and the Willamette National Forest on August 10th and 11th, 2008. The total collection area, including a 100 meter buffer, was 19,493 acres. The LiDAR survey used a Leica ALS50 Phase II laser system with a sensor scan angle of ±14 degrees from nadir (the perpendicular vector to the ground directly below the aircraft) and a pulse rate of ≥ eight points per square meter of terrestrial surfaces. All areas were surveyed with an opposing flight line side-lap of ≥50% (≥100% overlap) to reduce laser shadowing and increase surface laser painting. The system allows for up to four range measurements (returns) per pulse, and all discernible laser returns were processed for the output data set. An onboard differential GPS unit measured the aircraft position twice per second (2 Hz) to accurately solve for laser point position (geographic coordinates, x, y, z). Aircraft attitude was measure 200 times per second (200 Hz) as pitch, roll, and yaw (heading) with an onboard inertial measurement unit. Aircraft/sensor position and attitude were indexed by GPS time to allow for post-processing correction and calibration.

Table 1shows the resulting resolution and accuracy with specification and achieved values (Watershed Sciences Report, 2008).

	Targeted	Achieved
Resolution:	≥ 8 points/m^2	9.14 points/m2
Vertical Accuracy (1 sd)	< 13 cm	2.1 cm

Table 1. Resulting resolution and accuracy of LiDAR data.

LiDAR Data Analysis

LiDAR data form a point cloud that represents areas in which the light pulse from the plane is reflected back to the receiver after it intercepts canopy or ground. The visualization software tool FUSION (McGaughey, 2012 http://forsys.cfr.washington.edu/JFSP06/lidar_&_ifsar_tools.htm), was developed as specialized remote sensing software to process, analyze and display extremely large LiDAR data sets. FUSION creates 3-dimentional terrain and canopy surface models and fuses LiDAR data with 2-dimentional imagery such as orthophotographs, topographic maps, and satellite images. FUSION also includes algorithms that allow users to manually measure individual tree attributes or automatic capabilities to characterize individual trees.

The analysis and visualization software consists of two programs, FUSION and LiDAR data viewer (LDV), and several other task-specific command line programs (FUSION manual, McGaughey 2012). The primary user interface for FUSION is a graphical display window and a control window. The display window shows all project data in a 2D display, similar to geographic information systems. Input for FUSION consists of several data types, including shapefiles, images, digital terrain models, canopy surface models, and LiDAR return data. The LDV program creates and displays 3D visualizations for examination and measurement of spatially explicit data subsets. The command

line programs provide specific analysis and data processing capabilities to make FUSION suitable for processing large LiDAR acquisitions. Command line programs utilities (or executables) used for this thesis project include *CanopyModel, ClipData, CloudMetrics*, and *PolyClipData*.

FUSION Executables Used

In addition to the two main programs of FUSION and LDV, the FUSION package includes numerous task-specific executables, or command line utility and processing programs. As a part of the FUSION program download, a comprehensive manual provided guidance and instructions on proper use of the executables.

The first executable used was *ClipData*, which creates a sub-sample of the LiDAR data for use in other analysis. The options for these selections are rectangular or round, and can be created around any point, such as a plot center or GPS point. For this project, selections of the LiDAR data were clipped for each plot. The syntax for the command line program for *ClipData* follows:

ClipData [switches] InputSpecifier SampleFile [MinX MinY MaxX MaxY]

where ClipData refers to the program to be used, and

- [switches] identifies options that can be utilized
- InputSpecifier identifies the raw LiDAR data files to be clipped
- SampleFile is the output file created

- [MinX MinY MaxX MaxY] are the spatial coordinates for the sample area to be clipped.

Switches used were “Shape: 1” to denote a circle selection, and “dtm:file” and “height” to identify the bare earth model and to normalize the elevation data from the raw LiDAR data.

The second executable used was *CloudMetrics*, which computes various statistical parameters describing a sub-set of LiDAR data. *CloudMetrics* was executed on each of the plots using the output of the *ClipData* executable mentioned above. The output of *CloudMetrics* is a .csv file. The syntax for *CloudMetrics* follows:

CloudMetrics [switches] InputDataSpecifier OutputFileName

where CloudMetrics refers to the program to be used, and

- [switches] to specific options that can be utilized
- InputDataSpecifier to the raw LiDAR data files
- OutputFileName to the newly created output .csv file

Switches used included “minht:#” and “above:#” which compute additional metrics above a given height break, in this case 3 meters (Fusion Manual, McGaughey 2012).

The next executable utilized was *CanopyModel* to create a canopy surface model from the LiDAR point cloud for the entirety of WS1, as well as for each individual plot where DHPs were taken. *CanopyModel* assigns the elevation of

the highest return in each grid cell to the grid cell center, and smooths the surface using a median or a mean value for the grid cells. When a bare earth model is used with a switch, a canopy height model (CHM) is created. The output of *CanopyModel* is in a PLANS format DTM file that uses floating point elevation values and contains coordinate projection information for easy input into GIS systems. The syntax for *CanopyModel* follows:

CanopyModel [switches] surfacefile cellsize xyunits zunits coordsys zone horizdatum vertdatum datafile1 datafile2

where CanopyModel refers to the program used, and

- [switches] to specific options that can be utilized
- surface file to the name of the output file
- cellsize to the desired grid cell size (0.5 meters)
- xy units and y zunits to units for LiDAR data (M for meters)
- coordsys to the coordinate system for the canopy model (1 for UTM)
- zone to the coordinate system zone for the canopy model (10)
- horizdatum to the horizontal datum used (2 for NAD83)
- vertdatum to the vertical datum used (2 for NAVD88) and datafile1
- datafile2 to the raw LiDAR data files used to create the canopy model.

The switch "ground:file" was used to specify the corresponding bare earth model used to normalize the LiDAR data and create a canopy height model. The canopy height model created a canopy volume metric that was used in the LAI LiDAR

model; the canopy volume metric was also input into TreeVaW for identification and stem mapping of individual trees.

The final executable used was *PolyClipData*. This program is similar to the *Clipdata* executable, but uses a shapefile to clip data rather than a set square or circle. For this executable, a shapefile of WS1 was used to clip the LiDAR data to the extents of the watershed. The syntax for *PolyClipData* follows:

PolyClipData [switches] PolyFile OutputFile Datafile

where PolyClipData refers to the program used, and

- [switches] to specific options that can be utilized
- PolyFile to the name of the ESRI shapefile containing polygons
- OutputFile to the name of the output file
- Datafile to the name of the LiDAR data file or a list of data files with a .txt extension

Volume Calculation for LAI model

A CHM model created with FUSION was used to estimate canopy volume for the LAI_LiDAR model. The CHM was loaded in FUSION, and the *export terrain model* tool was used to export the CHM as an ASCII grid file. In ArcMap, the *ASCII to raster* conversion tool was used to create a raster from the CHM. The new CHM raster output was loaded into ArcMap, along with the bare earth model mentioned above. The *volume surface calculate* tool in ArcMap was used to measure the volume of canopy present above the bare earth model for each plot. These values were stored in a .csv file for regression analysis using the statistical package R (The R project).

After the surface volume was calculated for each plot in which DHPs were taken, a simple linear regression was performed between those values and the LAI plot values from DHP analysis. The regression coefficients, slope and intercept, were then used for the LAI from LiDAR model.

RESULTS

LAI Results from Digital Hemispherical Photographs using SLIM Software

PLOT	Plot LAI	Plot Gap Fraction	Wide LAI	Wide Gap Fraction	Cardinal LAI	Cardinal Gap Fraction
P11109	8.24	13	6.42	20.3	6.5	18.525
P11110	2.91	58.7	6.68	21.1	6.63	19.675
P11205	6.18	30.9	8.41	8.8	7.875	10.525
P11206	9.08	9.6	7.06	13.7	7.5625	11.125
P11207	7.42	20.2	7.78	11.8	7.555	12.5
P11208	9.32	9.3	7.58	9.7	7.7275	10.8
P11209	10.39	7.7	7.48	11	7.7425	13.65
P11212	5.95	32.7	6.29	22.8	6.41	20.85
P11213	6.97	14.5	6.03	17.7	6.92	14.275
P11608	8.67	7.5	7.17	10.1	7.4475	9.775
P11609	7.15	22.8	7.57	9.7	7.725	8.925
P11610	7.66	19	7.31	11.6	7.35	11.025
P11611	7.5	13.8	7.19	10.4	7.2425	10.325
P11612	9.85	7.3	7.21	11.9	7.595	9.775
P11613	8.34	10.8	7.51	9.7	7.6925	9
P11614	9.22	7.2	7.85	8.1	7.9	8.7
P11615	8.01	20.9	7.96	11.3	7.8825	9.8
P11616	9.54	6.1	7.33	10.5	7.555	8.975
P11617	8.55	11.5	7.44	11.8	7.5225	9.55

Table 2. LAI and gap fraction results from SLIM software. Plot LAI was calculated with a limited scope of view to capture LAI within each vegetation plot. Wide LAI used the default 60 degree scope for calculation and Cardinal LAI is the average of the four cardinal direction LAI values with a 60 degree scope.

Table 2 displays the results of analysis by SLIM software. Plot LAI is computed for a scope of view that captured only canopy directly above individual plots. LAI for the plots ranged from 2.91 to 10.39. Wide LAI was computed using a scope of 60 degrees (from zenith, 120 degrees of view). Wide LAI showed both less variation among values and overall lower values in comparison to Plot LAI (means). The lowest value for the Wide LAI was 6.03, while the highest was 7.96.

Cardinal LAI is the average of the four DHPs taken in the four cardinal directions from center for each plot (also with a 60 degree scope, 120 degrees of view for analysis). The Cardinal LAI values are relatively consistent among plots, ranging from a 6.41 to 7.8825.

Before analysis of LAI values, a Q-Q plot of each set of LAI values was performed to test for normal distribution. Figure 3 displays the Q-Q plots for each set of LAI values. According to these plots, only the Plot LAI measurements are normally distributed. Consequently, a natural log transformation was performed on the data for regression and correlation analysis in order to reduce variability in the tail ends of the distribution.

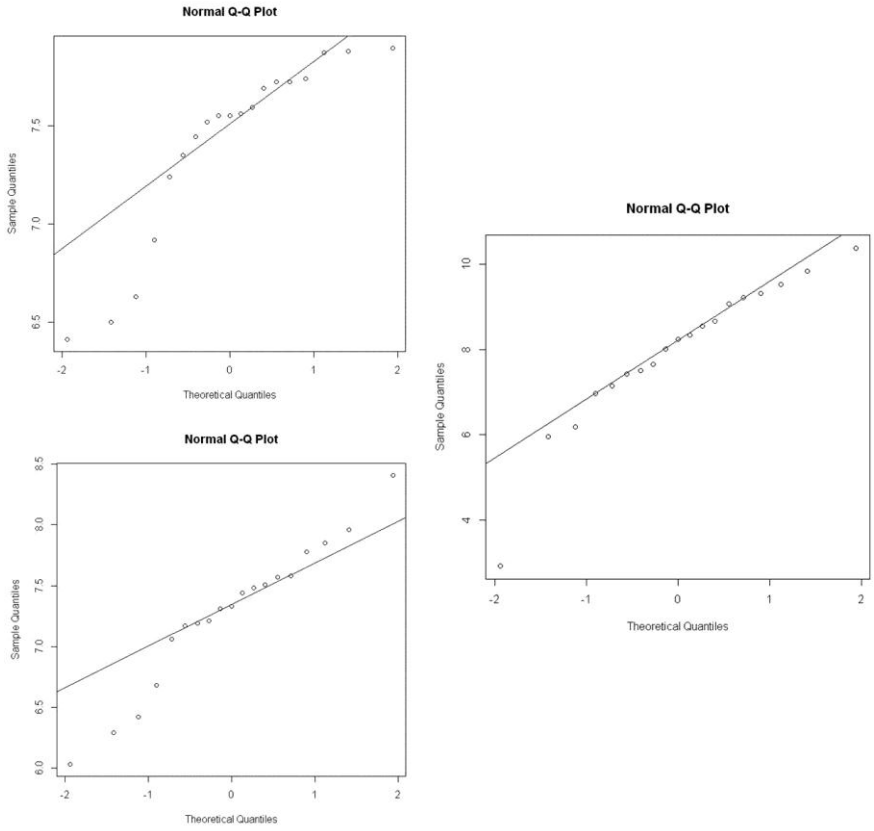

Figure 3. Q-Q plots for all LAI results: Plot LAI (right), Wide LAI (bottom left) and Cardinal LAI (top left). Axes represent theoretical and sample quantiles. Only Plot LAI is normally distributed.

Simple Linear Regression of LAI Values

After natural log transformations were performed on all three sets of LAI values, a regression analysis was performed to assess how the Wide LAI and Cardinal LAI values compare to the Plot LAI values (Figures 4 and 5).

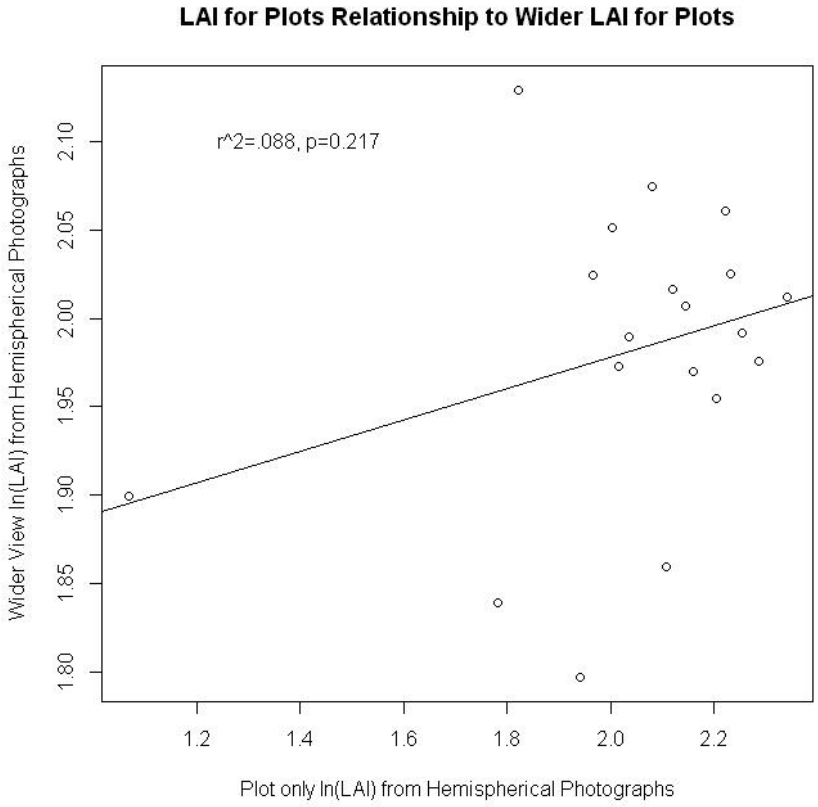

Figure 4. Regression analysis for ln(Plot LAI) compared to ln(Wide_LAI). The relationship is not significant (alpha= .05).

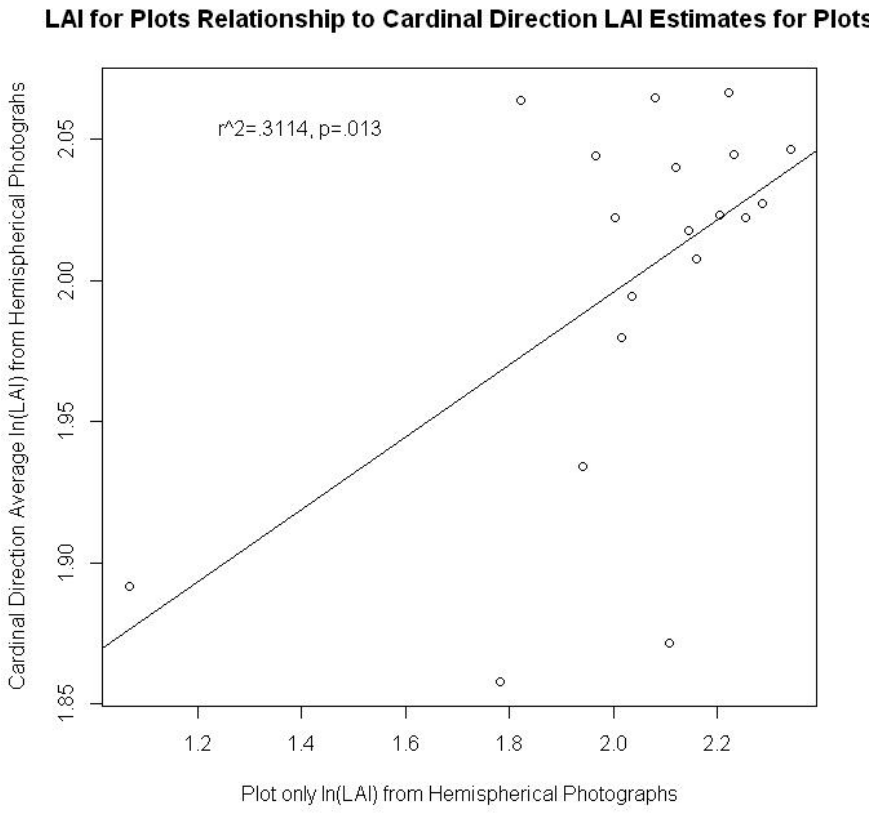

Figure 5. Regression analysis for ln(Plot LAI) compared to ln(Cardinal LAI) (R^2 = 0.3114, p = 0.013).

The relationship between Plot LAI and Wide LAI is neither strong (R^2= 0.08) nor significant (p= 0.217). The analysis reveals a statistically significant relationship between Plot LAI and Cardinal LAI (R^2 = 0.31, p = 0.013). Outlier plots heavily influence the relationships between both plot LAI and wider LAI and plot LAI and cardinal LAI. We suspect that although a strong correlation may exist, it may be driven primarily by the presence of extremely high and low values of cardinal LAI. If the correlations do have physical meaning, however, correlations between cardinal LAI and plot LAI as opposed to plot LAI and wider LAI is indicative of anisotropy in LAI patterns on the watershed, and suggestive that some form of

topographic directionality, potentially driven by mechanisms such as downslope water movement or solar angle, may exist in LAI.

The Plot LAI values were the only normally distributed values. They also represent the highest values for the LAI measurements. These values were closest to what was expected for LAI range for an even aged, mostly Douglas fir stand (Nadkarni, personal communication). For these reasons, only the LAI plot values were used for subsequent analysis.

LiDAR LAI Model Based on Surface Volume of CHM

In order to assess the relationship between DHP Plot LAI and LiDAR, the Plot LAI values were used in a simple linear regression model against the surface volume metric from the LiDAR data. Table 3 shows the volume of the Canopy Height Model (CHM) for each plot, as well as the corresponding Plot LAI value for each plot.

The coefficients (slope and intercept) of the best fit line from the simple linear regression performed between Plot LAI and the volume of each plot was used to estimate the value of LAI from LiDAR. The equation, from Richardson et al. (2009) was derived by work originally completed by Lefsky et al. (1999), but adapted for use with discrete return aerial LiDAR data.

PLOT	Plot LAI	Volume	LiDAR LAI
P11109	8.24	4313.057	8.323283
P11110	2.91	3457.183	6.120263
P11205	6.18	3481.565	6.183021
P11206	9.08	3984.748	7.478215
P11207	7.42	3992.862	7.4991
P11208	9.32	3793.143	6.985023
P11209	10.39	4104.921	7.787541
P11212	5.95	3682.819	6.70105
P11213	6.97	4412.353	8.578869
P11608	8.67	4208.022	8.052922
P11609	7.15	4046.029	7.635951
P11610	7.66	4153.8	7.913353
P11611	7.5	4704.49	9.330831
P11612	9.85	4419.239	8.596594
P11613	8.34	4625.235	9.126827
P11614	9.22	4697.408	9.312602
P11615	8.01	4299.383	8.288085
P11616	9.54	4674.676	9.254088
P11617	8.55	4109.038	7.798137

Table 3. Plot LAI, Volume of Canopy Height Model, and LiDAR calucalted LAI for each plot studied.

The slope of the best fit line (0.0026) is the value for α and the intercept (-2.7785) is the value for β. The following equation from Richardon et al. (2009) was used:

$$\text{LiDAR LAI} = \alpha + \beta(\text{Volume})$$

This equation was applied to each plot and the results are presented in Table 3. The LiDAR calculated LAI was then compared to the Plot LAI values obtained from the DHP by running a simple linear regression (Figure 6). The regression revealed a somewhat strong (R^2= 0.3314) and statistically significant (p=0.0099) relationship.

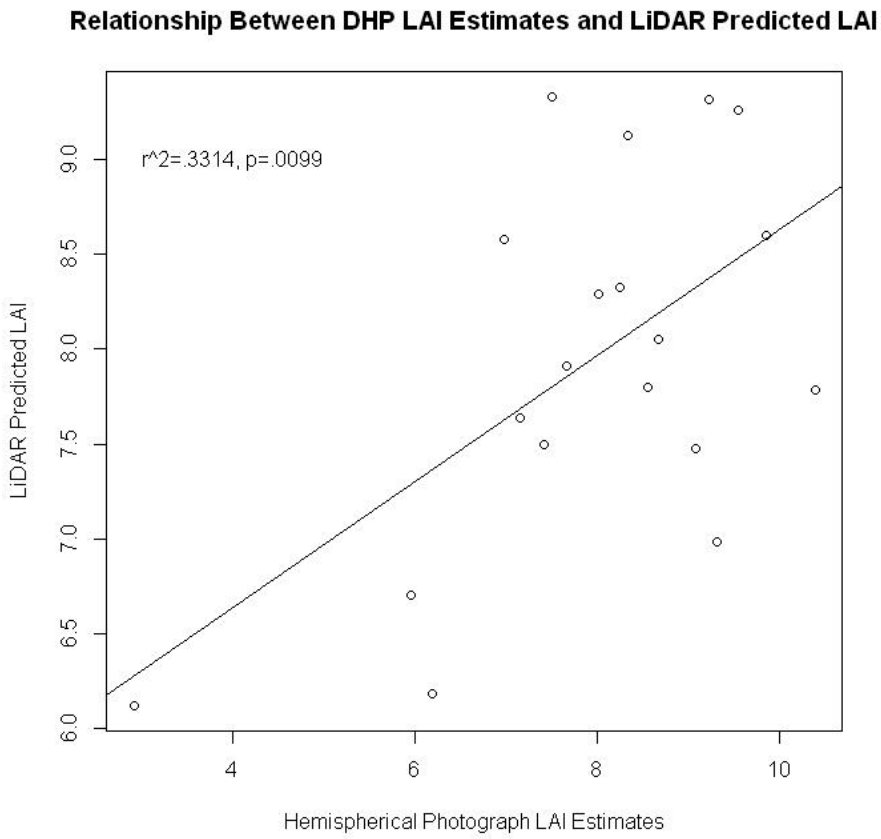

Figure 6. Simple linear regression model of Plot LAI from hemispherical photographs to LiDAR estimated LAI for each plot.

The LiDAR LAI model was applied to the rest of the permanent vegetation plots in WS1. Plots P11108, P11202, P11417, P11418, P11427 and P11519 were excluded due to missing values. The surface volume values, LiDAR calculated LAI and Cover*Height value for all plots are displayed in Appendix A. Cover*Height was originally created as a proxy for biomass in prior research in the watershed. Peterson and Lajtha (2012) exponentially regressed a Cover*Height metric derived from the 1m LiDAR onto allometrically calculated values of biomass using the equations in the Pacific Northwest Biomass Component Equation Library (Halpern and Means, 2011). These equations were

validated against similar sets presented by Lutz (2005). Two simple linear regressions were completed between the LiDAR LAI calculations and Cover*Height values. First, for plots in which DHP were taken (Figure 7) and second for all plots in the watershed (Figure 8). The relationship for the DHP plots was very strong (R^2= 0.75) and statistically significant (p< 1.578e-8). This relationship for all plots was strong (R^2= 0.5467) and statistically significant (p< 2.2e-16).

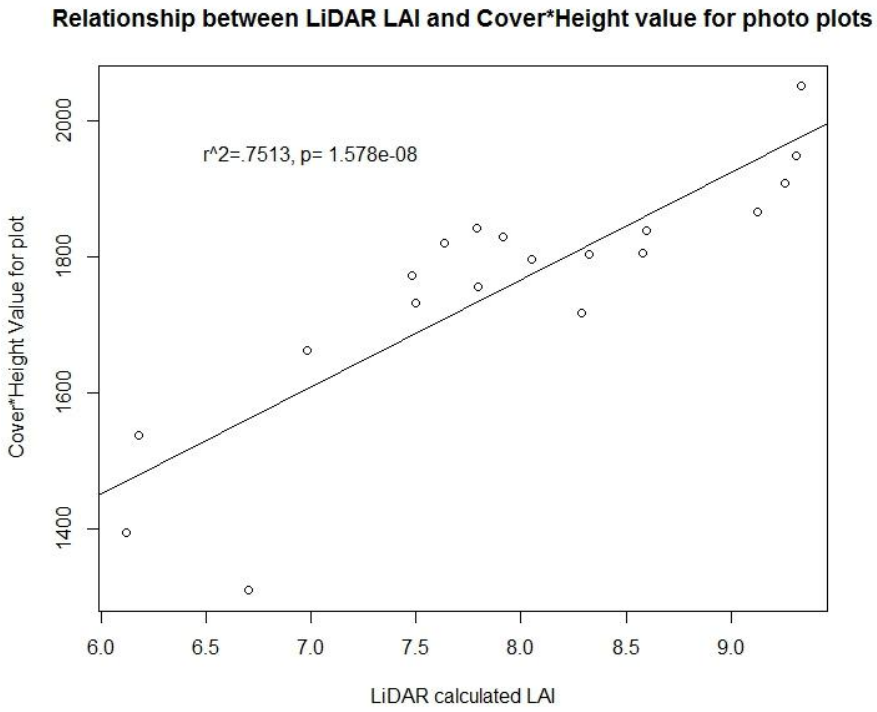

Figure 7. Simple linear regression between LiDAR calculated LAI and Cover*Height values for plots in which DHP were taken.

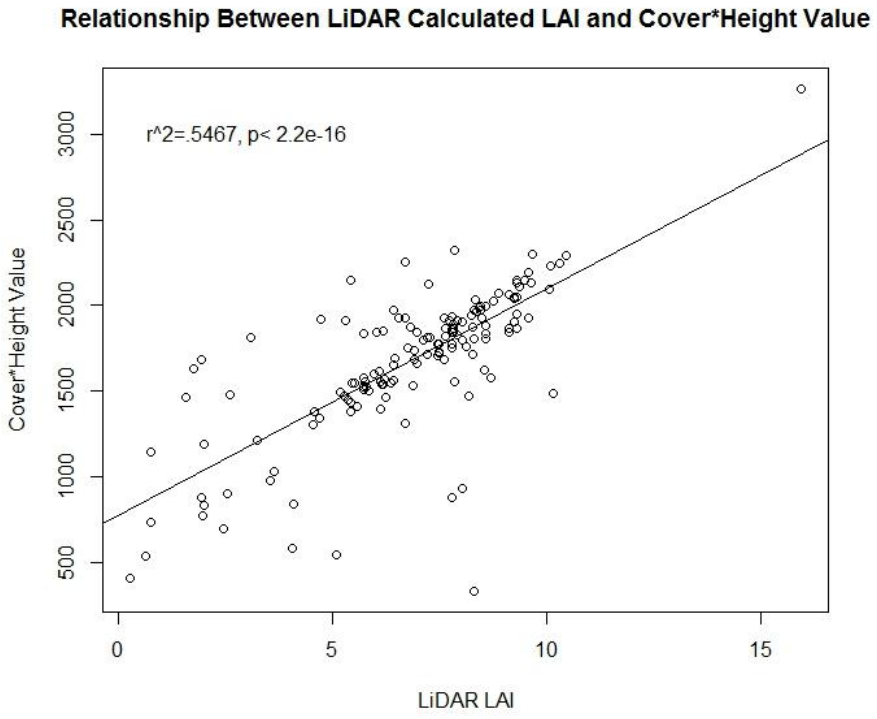

Figure 8. Results of simple linear regression for all plots between LiDAR calculated LAI and Cover*Height value.

DISCUSSION

In this research, a model of LAI from LiDAR data was successfully run to estimate LAI for 133 plots in a small watershed at the H.J. Andrews Experimental Forest in Central Oregon. The LiDAR based estimates, and the hemispherical photograph LAI estimates, with which the model was calibrated, are both slightly less than what would be expected for LAI in the area. The LAI for an even aged, dense, roughly 40 year old mostly Douglas fir stand would be expected to be in the range of 9-12 (Vose et al. 1994; Waring, 1998). Both estimates, from DHP and LiDAR produced estimates ranging from 7-10. The slightly lower estimates in DHP and LiDAR may be due to sub-optimality of field and sky conditions on the days of measurement.

Previously, a LICOR-2000 device was used to estimate LAI in the watershed and, among other errors, also resulted in underestimation of expected values. An informal document produced by previous researchers working in the watershed detailed issues retrieving LAI for the 133 permanent vegetation plots and the whole watershed (Peterson, 2010). The document states that protocol for the use of LI-COR in mountainous terrain (i.e., WS1) is complicated because the hill slope may shade the hemispherical instrument lens. As mentioned in the site description, slopes on WS1 average nearly 60% when measured in the field, such that they intercept the view of the hemispheric lens. Special covers exist to direct the view to open space away from the hillslope, but experimental error in this case is high. Because of this, previous attempts at estimating LAI in the Forest Ecohydrology and tELemetry Transect (FEEL), which corresponds with transect 1 of WS1 have been highly variable (Figure 9). Peterson (2010) also attributes this error to both variation in tree foliage over time and the experimental error mentioned above. On the FEEL transect, tree species present include *Psuedotsuga menziesii*, *Tsuga heterophylla*, *Arbetus menziesii*, *Alnus rubra, Acer circinatum*, and *Acer macrophyllum*. During the early summer season of the most recent measurement, the abundance of *Acer spp.* understory contributed severely to the perceived canopy cover, whereas in measurements made prior and in other season, hardwood species did not have such prolific coverage. Allometric equations have also been used in the watershed with similar results showing variability in foliar contribution depending on the selection of species, stand age, and stand vigor used. Kennedy (personal communication) suggested that a scalar

correction factor of 1.89 be used to express the density of coniferous leaf area that would not be accounted for in measurements of hardwoods in the watershed. However, recent calculations of LAI using sapwood values did not use this correction factor (Peterson, 2010). As a result of these prior results, I chose for this thesis project digital hemispherical photography as the best non-LiDAR method of estimation of LAI for the watershed. However, the results of my research suggest that this method is prone to errors similar to previous methods.

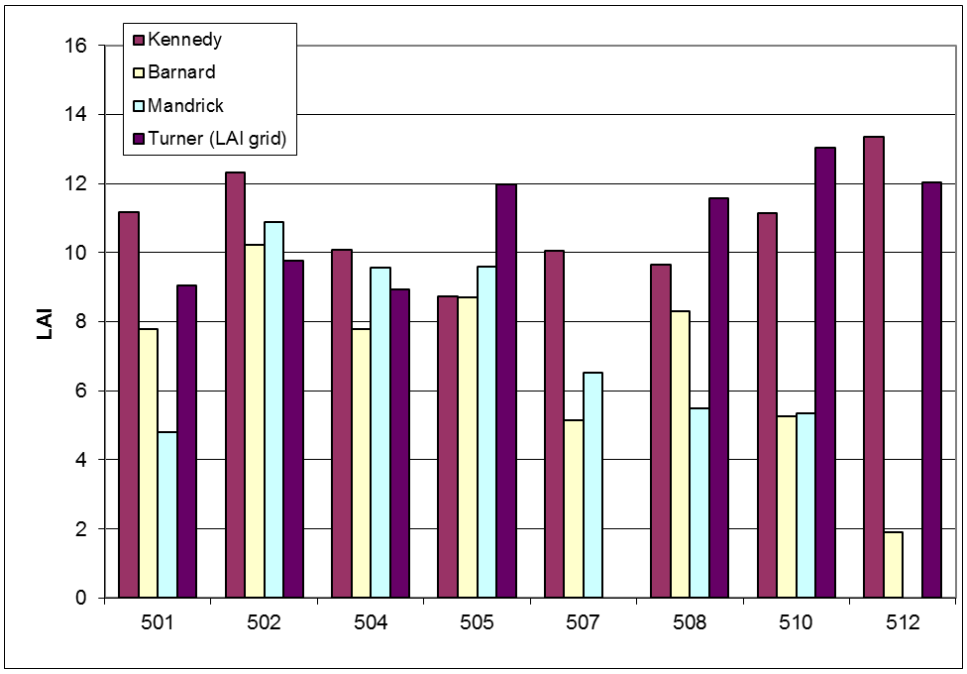

Figure 9. Previous estimates of LAI in the FEEL network in Watershed 1 at H.J. Andrews.

Underestimation of LAI from Hemispherical Photograph Analysis

A review of the literature reveals that underestimation and other issues surrounding estimation of LAI from hemispherical photographs is common. Martens (1993) used four different instruments to estimate LAI in conifer and

hardwood forest stands. These instruments fell into two categories: line and hemispheric sensors, with the latter including hemispherical photography. Different methods in obtaining LAI from hemispherical photographs either underestimated (Campbell's method) or overestimated LAI (Beer-Lambert method) when compared to direct measurements taken in the same area. These methods are similar to how SLIM estimates LAI in three different ways. Most estimation methods for LAI require the assumption that canopy elements are randomly dispersed, which is highly unlikely in any natural forest stand. This conclusion is similar to that drawn by Dufrene and Breda (1995) in their research using one semi-direct and three indirect measurements of LAI in a deciduous forest. All three indirect methods underestimated LAI due in part to local clumping of architectural canopy components, and in particular, the spatial dispositions of branchlets and leaves not being independent. This results in a non-random distribution of these two canopy elements.

Clark and Murphy (2011) thoroughly outline the issues surrounding hemispherical photography in the estimation of gap fraction and LAI. The limitations start with equipment used, including camera spatial, radiometric and spectral resolution and software. Accurate estimates are also dependent on weather conditions, time of day, crown closure, ground slope, and many other factors. Sunny conditions (present at the time of capture of DHPs for this thesis), time of day (early morning and late evening) and low crown closure can all lead to increased direct sunlight, which can saturate photographs and negatively impact the accuracy of gap fraction and effective LAI estimates. The camera and

lens used to acquire photographs can also affect LAI estimates. Color blurring in digital pictures can result in measurement errors in canopy gaps, edge detection, and lead to "blooming", especially near zenith (straight up) in sunny conditions. Clark and Murphy point out that leaf clumping can affect gap fraction and LAI measurements; with the threshold level of light between "gap" and "plant" being a subjective measure that varies with individual users and which is subject to bias.

Slope Correction for Hemispherical Photograph Analysis

Hemispherical photographs are taken to capture the canopy directly above the plot or area that is being studied. When this area is flat, capturing the area directly above the camera is straightforward. However, when the area is sloped, as is much of WS1, capturing the area directly above is more difficult. Some researchers have taken this into account, and slope correction for hemispherical photograph analysis is an option to correct errors due to slope. Walter and Torquebiau (2000) addressed this matter, noting that although much of the world's forests grow on sloped terrain, the issue of ground slope has not been addressed in indirect measurements of LAI.

Schleppi et al. (2007) considered how LAI estimates are obtained from hemispherical photographs. LAI is indirectly estimated by measuring the light transmission through canopies, and the angle at which the transmission is measured enters the calculation at two distinct points: 1) as the angle of incidence determining the travel distance of a light ray through the whole canopy, and 2) relative to the zenith for the statistical distribution of the angle at which the single foliage elements are seen. Schleppi et al. (2007) note that any angle on flat ground

is sufficient to describe the zenith angle. However, on sloped ground the angle of incidence is not identical to the zenith angle, and each direction in the canopy must be classified according to both angles.

Schleppit et al (2007), referencing Nilson (1971) note that the transmission of light through and ideal canopy is described as a function of the zenith angle θ:

$$G(\theta)L = K(\theta) = -\ln T(\theta)\cos(\theta), \quad \theta < \pi/2$$

where L is Leaf Area Index, G(θ) is the mean projection ratio of leaves in the zenith angle, which is a function of the statistical distribution of the leaf inclination angles, T(θ) is the light transmission at angle zenith θ, and K(θ) is the 'contact number', which represents the average number of contacts that a light probe would make by passing through the canopy at the zenith angle, relative to the thickness of the canopy. This equation is only valid on flat ground. On sloped ground, with an angle of (v), and the sensor held horizontally, light travels a shorter way through the canopy in the downhill compared to the uphill direction. If an observer looked downhill the canopy would appear lighter, and darker when looking uphill. Therefore, the zenith angle (θ) can be replaced in the equation on the right side by the angle of incidence (τ):

$$G(\theta)L = K(\theta) = -\ln T(\theta, \tau)\cos(\tau), \quad \theta < \pi/2, \tau < \pi/2$$

This correction would necessarily have to occur within the computer software algorithms used to estimate LAI from hemispherical photographs.

LiDAR LAI Estimates

Since the LiDAR estimates of LAI were calibrated based on the DHP estimates of LAI, they are slightly less than expected as well. However, the high r-squared value (R^2= 0.57) when the estimates for all plots were compared to the Cover*Height measurements for each plot is promising in that they compare to a widely used metric within the watershed. One way to reassess LAI for the plots would be to use a so-called LiDAR only metric, or a model that only uses metrics derived from the LiDAR data itself, and does not rely on possibly unreliable hemispherical photograph estimates of LAI.

Many of these LiDAR only models exist in the literature. Jensen et al. (2008) noted that most previous attempts to estimate LAI from remote sensing have relied on empirical relationships between field-measured observations and various spectral vegetation indices (SVIs) derived from optical imagery or the inversion of canopy radiative transfer models. Jensen et al. (2008) used LiDAR data along with SPOT5- derived SVIs to estimate LAI, but found that LiDAR data alone was adequate to do so. The researchers calculated many LiDAR-derived model covariates, including canopy height metrics, canopy cover metrics, and height distribution metrics. These covariates were compared to known LAI values for plots within a multiple regression framework. In estimated LAI for two stands in Idaho, nine different models were created and tested, with r-squared values ranging from 0.6971 to as high as 0.8612 (Jensen et al. 2008).

Overall, the LiDAR derived covariates explained the largest proportion of variation in LAI, with most models incorporating LiDAR covariates associated with upper story metrics, and all models containing the covariate MAX_HEIGHT. The authors point out the logic for including LiDAR: increases in canopy height should correlate to increases in LAI. However, the covariate MAX_HEIGHT alone did not significantly correlate with the known LAI quantities. When considering the vertical foliage distribution covariates, the calculated differences in percentile heights played an important role. Similarly to the MAX_HEIGHT covariate, the covariate L95_C25, or the 95^{th} percentile value minus the 25^{th} percentile value, is present in each LAI model.

Morrison et al. (2011) also set out to compute LAI using LiDAR with minimum field data for use in remote areas like the Canadian boreal forest. Their research reviewed many LiDAR metrics from articles mentioned above (Lim et al. 2003, Riano et al. 2004, Solberg et al. 2006, and Lefsky et al. 1999), but concluded that each model was developed for a specific forest type and required calibration. Instead, the authors modified an intensity based gap fraction model developed by Hopkinson and Chasmer (2007). This model classified LiDAR returns into four echo classes (first, single, intermediate, last) and generated grids of intensity by summing returns within a raster cell, and takes into account two-way power transmission loss by intermediate and last return hits using a square root function. The subset of first and single hits at or below 1.3 meters represents ground returns and an equation combining all these values is used to estimate gap

fraction. The gap fraction (P) estimates are then used to estimate effective LAI (LAI_e) based on the Beer-Lambert Law:

$$LAI_e = -\ln(P)/k$$

where k is the extinction coefficient, which is a function of leaf angle distribution, radiation type and direction, and canopy structure and clumping. A standardized, mid-value of 0.5 was used by the researchers to represent a spherical (random) projection coefficient for leaves of any shape. Using the standard 0.5 extinction coefficient, LAI_e for conifer species was underestimated, and LAI_e was overestimated for broad-leaved aspen species. The authors then optimized the extinction coefficient for each species studied using DHP LAI estimates. This resulted in better LAI_e estimates from the LiDAR data.

Alternative LiDAR Systems

The LiDAR system used for collection of data for this thesis was a discrete return, small footprint system, with similar systems used extensively in the research field to estimate LAI and other forest attributes. However, two other systems hold promise for estimation of LAI: full waveform aerial LiDAR and ground-based terrestrial LiDAR systems. Full waveform systems have already been described in this thesis, and were used by Lefsky et al. (1999) for their estimation of LAI. Adams et al (2012) utilized full waveform LiDAR in their research, noticing that with all uses of LiDAR, performance was hindered by an inability to distinguish the source of the LiDAR returns as foliage, stems, understory and the ground,

other than the relative position of the return. The goal of their research was to determine whether drawing distinctions between the type of material that a return was hitting would improve analysis with LiDAR data, and if full waveform metrics could provide information on foliage density and improve forest health and growth measurements.

Adams et al. (2012) also cover the major differences between waveform systems and discrete return systems and why using full waveform systems might better suit the needs of researchers. The major drawback of discrete return systems is a 'blind-spot' that occurs following each detected return, during which no other returns can be detected. Adams et al. (2012) quantified waveform shape with various curve-fitting methods, including peak height, half-height width and an exponential decay function attributed to each return. However, due to the complexity of the surfaces encountered and the multitude of angles, textures and paths each new waveform metric showed more potential variation within a surface type that it did between surface types. However, ground peaks on average showed waveforms with higher peaks, shorter widths and faster decays. Foliage returns in turn averaged lower peaks, wider pulses and slower decays. This classification could lead to more accurate DEM production from full waveform LiDAR, but the clear distinction between surface types still seems impractical for the time being.

Terrestrial LiDAR systems represent an alternative approach for collecting LiDAR data, where collection occurs from below the canopy rather than from an aircraft or satellite. Seidl et al. (2012) examined the use of ground-based laser

scanning in the analysis of mature forest structure and compared their findings to hemispherical photography methods. In all, 35 groups of trees were analyzed by the researchers to generate 3D point clouds of the tree axes and leaves. The images were used to generate hemispheric views of the canopy. These images were compared to actual hemispherical photographs taken in the same area. The authors found that their method was problematic for identifying small canopy gaps, and wind-induced movements at the time of collection further complicated the issue. However, improvements in the systems should speed up the operation of the system and/or produce a smaller beam, both of which would help alleviate the issue. The authors see a future application of this work being the creation of canopy models of growth and photosynthetic carbon gain in mature trees based on the 3D canopy structure data collected, which their study showed was well represented by terrestrial laser scanning.

CONCLUSIONS

Estimation of Leaf Area Index in Watershed 1 at H.J. Andrews Experimental Forest using prior methods had proven difficult. The use of hemispherical photographs to estimate LAI in this thesis seems prone to the same difficulties. The steepness of the terrain and the high density of the vegetation make the estimation of LAI very uncertain. However, using LiDAR data to estimate LAI seems promising for the watershed. The strong correlation between the LAI LiDAR estimates from this work to the Cover*Height metric used in the watershed provide evidence that the results are validated against a metric known and often used by researchers in the area.

The lack of correlation of the plot level LAI to the wider scope LAI and cardinal direction LAI is curious. This may be caused by either the hill slope affecting the two wider measures of LAI, or the different ways in which light is being measured in the photographs within the software itself. Exploring how light is reacting differently on the sloped terrain compared to a flat surface may provide insight and better results for the wider LAI measurements. Developing new algorithms within software programs for specialized use on sloped terrain could perhaps solve to this issue.

A possible next step in the estimation of LAI for the watershed is to develop and test a LiDAR model that does not rely on ground-truthed LAI estimates. In theory, a model of LAI from LiDAR data that used hemispherical photographs, or other methods, as a ground-truth will only be as good as those original LAI estimates. A LiDAR only model may be the answer to estimating LAI in a steep, densely vegetated watershed, since it has been proven that LiDAR can adequately measure these areas.

Finally, exploration into alternative LiDAR systems may be helpful in the estimation of LAI in the watershed. An examination of how full waveform or terrestrial systems could improve estimates is certainly possible. The discrete return, aerial system used for this thesis seems capable of providing information on the upper canopy, but seems to lack the capability to accurately measure and assess lower canopy and understory features. An interesting approach to solve this issue could be linking the aerial LiDAR data with terrestrial LiDAR data. This

would provide a perspective from above and below the canopy, and may provide a more complete picture and insight into the complete structure of the forest.

Chapter 3- LiDAR used to Describe Stand Characteristics and Identify Individual Tree Height and Location

INTRODUCTION AND BACKGROUND

LiDAR data have been used extensively in recent years and have the potential to generate high resolution digital terrain surfaces accurately. The resulting surface, precise within 15 cm, represents complex natural and semi-natural environments at a range of scales (Large and Heritage 2009). One of the first commercial uses of LiDAR data in the United States was the identification of encroaching vegetation on power line corridors (FUSION manual). Federal agencies in the United States, such as the Federal Emergency Management Administration (FEMA) and the U.S. Geological Survey (USGS), have used LiDAR with county and state agencies to map flood plains and earthquake hazard zones (FUSION manual). The following represents a fraction of LiDAR applications in the forestry sector: a) the estimation of biomass and carbon stocks, b) description and quantification of forest structure and cover, and c) identification of individual trees and stem mapping.

Biomass and Carbon Stocks

Omasa et al. (2007) assessed the capability of LiDAR to measure carbon (C) stocks in forests. Using LiDAR to quantify forest C stocks leads to a more complete understanding of terrestrial C cycling, which is important to quantify in light of recent climate change research. The ability of a forest to store and sequester C is often valued as ecosystem services, so an apt understanding of their capacity to do so is essential for both ecological and economical decision making. LiDAR is a novel tool for quantifying forest biomass because it allows for remote sensing of highly specific biomass components. For example, Garcia et al. (2010)

also evaluated LiDAR use to estimate total aboveground, branch and foliar biomass in an unmanaged forest in Spain using models based on LiDAR extracted height, LiDAR point cloud intensity, or height and intensity data combined. The researchers determined that normalizing LiDAR intensity data to a standard range removed the range dependence of the intensity signal. The intensity-based models proved the most effective and provided more accurate predictions of the breakdown of biomass into branch and foliar fractions. They also found that using species-specific models of the dominant species in the area improved estimates for biomass. Overall, the research demonstrated that LiDAR intensity data could be used to segment above ground to branch and foliar biomass from total biomass determination. Other variables, derived from LiDAR data and similar to those created using *CloudMetrics* and FUSION software (see Chapter 2), were included as explanatory variables in these biomass models.

Zhao et al (2009) conducted further work with LiDAR data and forest biomass, but aimed to move beyond scale-dependent the models that first need to be fitted and applied at the same scale or pixel size. The research goal was to create methods for scale invariant estimation of forest biomass using LiDAR data, and resulted in two models: a linear functional model that used LiDAR-derived canopy height distributions and a functionally equivalent nonlinear model that used canopy height quantile functions as parameters. These models used a LiDAR tree delineation approach to create a fine-resolution biomass map that captured individual tree component biomass in Eastern Texas, and the authors' work validated the use of canopy height distributions and canopy height quantiles as

LiDAR metrics for estimating biomass, as well as for mapping biomass at a range of spatial scales. Furthermore, the results of this work are viable for estimating other forest characteristics including belowground biomass, timber volume, crown fuel weight and Leaf Area Index.

Using LiDAR Data to Describe Forest Structure and Cover

Aerial LiDAR data have been used extensively for describing, measuring and quantifying canopy cover and structure of forests all over the world. Magnussen and Boudewyn (1998) used canopy-based quantile estimators to derive stand height from LiDAR data. Knowing that the proportion of laser pulses returned from or above a given reference height is directly proportional to the fraction of leaf area above it, the authors hypothesized that an unbiased estimate of this relationship could be obtained using the quantile of LiDAR derived canopy heights matching the fraction of leaf area above a desired height. Their work found a strong relationship between field and LiDAR estimates of stand height, and statistical tests supported their hypothesis. Their work demonstrated that estimating stand height from LiDAR data based on maximum canopy height value in each cell of a fixed grid has been and is likely to continue to be successful.

Smith et al. (2009) used discrete return LiDAR data to compare estimates of forest canopy cover from LiDAR and spectral methods and ground based measurements. This research used imagery from the Advanced Spaceborne Thermal Emission and Reflection Radiometer (ASTER), and explored sources of error if this technology were used on a large scale. The researchers found that

78% of the variability in field-based canopy cover metrics could be described by the derived LiDAR metric for canopy cover. They surmised that the other 22% is likely due to challenges of using LiDAR to sense understory vegetation and shrub dominated plots.

Hopkinson and Chasmer (2009) compared four models of fractional cover to hemispherical photograph fractional cover measurements across five distinct ecozones, eight forest species and multiple LiDAR survey configurations. Their models used four different LiDAR metrics: 1) a canopy-to-total first returns ratio, 2) a canopy-to-total returns ratio, 3) an intensity return ratio, and 4) a Beer's Law modified intensity return ratio. Although they found that the intensity based forest cover model had the highest R^2 value, the forest cover method using Beer's law was more useful since its best fit line passes though the origin and has a slope near unity. The models used showed promise across all the ecozones, but short canopies (less than 2m) and open canopy forest plots posed the greatest challenge to the models when predicting forest cover.

In research by Coops et al. (2007), the authors noted that the variation in vertical and horizontal forest structure is difficult to quantify with labor-intensive field methods or with passive optical remote sensing techniques that are limited in their ability to distinguish structural changes below the top of the canopy. Working in primarily Douglas-fir (*Pseudotsuga menziesii*) and western hemlock (*Tsuga heterophylla*) stands on Vancouver Island, Canada, the researchers chose stands that represented a wide range of stand development ages. This research built on previous work that used full waveform data to examine open and filled

volumes within the canopy itself (Lefsky et al. 1999). The resulting model produced a three dimensional canopy structure that was termed "canopy volume profiles" or 1 meter tall cells or voxels that were classified either as empty or filled depending on whether a LiDAR return was present within the 1m voxel. The voxels in the upper most 65% of the canopy were considered "euphotic", and those below that threshold deemed "oligophotic". The euphotic zone refers to the area that intercepts the majority of light within the canopy. Oligophotic refers to the area beneath the euphotic zone, which receives less light compared to the euphotic zone.

Coops et al. (2007) adapted the full waveform SLICER LiDAR methods used by Lefsky et al. (1999) for their discrete return LiDAR data. The returns present into 5x5 meter plot subsets were 'binned', and the number of returns within each subplot was counted at 1m height intervals. Bin areas were then classified as oligophotic or euphotic depending on their placement within the canopy, thus creating canopy volume profiles for the plots, that were found to correlate with ground measured stand attributes including crown volume, stem density and basal area. The overall canopy surface structure was shown to suitably characterize the total amount of open gap area using the methods of binning LiDAR into 1m voxels. The limited number of observations precluded developing regression models to estimate forest parameters, but the authors concluded that the relationship between the canopy volume variables and structural attributes suggest that models could be developed for this forest type regardless of stand age.

Concurrent with the work of Lefsky et al. (1999) was a research paper by Means et al. (1999). Using the same SLICER system, the authors compared ground measurements for height, basal area, total biomass, and leaf biomass to those obtained from the full waveform LiDAR system. The SLICER derived measurements correlated well with ground-measured attributes, with R^2 values of 0.95 for height, 0.96 for basal area, 0.96 for total biomass and 0.84 for leaf biomass. The relationships found were strong up to a height of 52m, a basal area of 132 m2/ha, and a total biomass of 1200 Mg/ha.

Much research has compared LiDAR estimates of forest attributes to field measured data, but Smith et al (2009) also considered spectral estimates when comparing field and LiDAR estimates of forest canopy cover. This work, situated in northern Idaho over an area of 25,000 hectares of mixed conifer forest, compared cover measurements from reflective spectral satellite data, and LiDAR and field collected measurements with variables measured using spherical densiometers. . The research had two goals: 1) to evaluate the overall accuracy of spectral and LiDAR derived cover metrics, and 2) to determine whether LiDAR data could quantify and reveal the sources of error observed in the spectral-based canopy cover metrics. The LiDAR metrics outperformed the spectral metrics when compared to field gathered data. However, all metrics were sensitive to the presence of herbaceous vegetation, shrubs, seedlings, saplings, and other subcanopy vegetation. This work is particularly relevant to this analysis because the stand type and site analyzed is similar to the one addressed at H.J. Andrews.

Lovell et al (2003) highlighted the importance of obtaining canopy structure from LiDAR data since that information is not available from other remote sensing methods but is essential for ecological assessments in forest inventory. Canopy architecture is particularly relevant to predictions of moisture and gas exchange that describe the overall functionality and productivity of the forest ecosystem. Their work used both aerial laser scanning, as well as ground based ranging systems in measuring important forestry parameters compared to standard field inventory, hemispherical photographs, and optical point-quadrat sampling. Simple models were developed, including determining predominant height of stand by aerial LiDAR, and Leaf Area Index from the ground based scanning system. The results of this work justify the further development of instrumentation and analysis to combine results from multiple systems to describe forest attributes such as height, cover, LAI, and foliage profile.

Many models using LiDAR data to describe forest structure are based on where the LiDAR points are distributed, namely by height. However, Hopkinson and Chasmer (2007) used LiDAR intensity values in modeling canopy gap fraction by using a modified Beer-Lambert approach. This may be more physiologically appropriate since a Beer-Lambert calculation reflects the capacity of the canopy to absorb radiation and deflect moisture, whereas a height distribution is a descriptive metric with less direct physiological significance. The authors related the ratio of ground return power/total return power to the canopy gap fraction derived from digital hemispherical photographs. They found that the LiDAR intensity based power distribution ratio provided a higher correlation to

the DHP gap fraction than the more often used ground to total return ratio. Furthermore, they modified the intensity power distribution ratio to account for secondary two-way pulse transmission losses within the canopy. This step created a model that requires no calibration and provides an accurate estimate of overhead canopy cover.

Hyde et al (2005) pointed out that LiDAR has been used extensively for measuring forest attributes in many ecosystems, including tropical, boreal, and mid-latitude forests. However, the authors noted that few studies have taken place in montane forests, and examined the ability of large footprint LiDAR systems to retrieve forest structural attributes in highly variable terrain and different canopy conditions in the Sierra Nevada mountains in California. The authors examined the effects of slope, elevation, aspect, canopy cover, crown shape, and spatial arrangement of canopy forming trees on the accuracy of the LiDAR estimates of height, cover and biomass and found good agreement between field and LiDAR measurements of height, cover, and biomass at the footprint level, and canopy height and biomass at the stand level. The differences encountered between field and LiDAR measurements was attributed to the spatial configuration of canopy elements, and were less affected by topography, crown shape, or canopy cover.

LiDAR data have also been utilized to measure, quantify and map the structure of understory characteristics. Korpela (2008) used LiDAR data to identify and map understory lichens in a barren pine grove in Southern Finland, using two different LiDAR data sets and examining the backscatter properties and intensity of LiDAR returns to differentiate bare ground from ground covered by

reindeer lichen. The remote sensing capabilities of the LiDAR made large scale mapping of lichen possible, whereas conventional field methods would have proved time-consuming and thus impractical.

Stem Mapping

LiDAR data have been used extensively to describe forest structure and cover, and to estimate biomass and C stocks, and more recently to identify individual trees and take 'inventory' of forest stands at various spatial scales. These techniques replace older, time consuming field measurements that identify individual trees one at a time during forest surveys (Hawk, 1970). Identifying individual trees in a stand with LiDAR data is important for this thesis as it suggests an alternative to mapping LAI at the watershed scale. If all trees can be identified in a stand, then allometric equations of DBH to height (Curtis 1967; Waring et al., 1977; Garman et al. 1995) and stem/crown dimension and biomass/needle area ratios (Bartelink, 1996) might be used to correctly estimate the amount of leaf area for individual trees. The estimates could then be used to scale up tree-based estimates to LAI at the stand, watershed or even landscape scale.

Strunk et al (2008) used aerial LiDAR data to estimate basal area for a complex forest on the Fort Lewis Military Installation in southeast Puget Sound (now Joint Base Lewis-McChord). The authors used the program FUSION (McGaughey, 2012) and similar software cited in Chapter 2 of this thesis (*ClipData, CloudMetrics, GridMetrics*) to produce LiDAR metrics that describe canopy size and vertical distribution. These metrics calculated basal area using

regression analysis. While the research did not explicitly identify individual trees from the stands studied, the estimation of basal area of a stand as well as stand density, predominant height, crown cover, foliage projected cover, and foliage branch projected cover are structural variables that are used to characterize forests in inventory, mapping programs and conservation (Specht and Specht, 1999).

Popescu and Wynne (2004) first set out to develop processing and analysis techniques to facilitate the use of discrete return LiDAR data to estimate plot-level tree height and measure individual trees from three-dimensional LiDAR surfaces. Popescu has been a leader in this field, developing TreeVaW, the tree extraction software used in this research. His work was conducted in both deciduous and coniferous stands, and the methods of using LiDAR derived tree metrics with regression models and cross validation of tree heights were more successful in the conifer stands than in the deciduous. The process included filtering the point cloud data with a circular window for the conifer stands, and a square window for the deciduous stands, and calibrating the search window based on forest type led to better results overall.

Similar to methods used by Popescu and Wynne (2004), Tiede et al. (2005) used local maximum filtering within a GIS environment to extract and delineate single trees from the LiDAR data point cloud. After using local maxima to identify individual trees from the point cloud, the authors developed a region-specific growing algorithm to delineate tree crowns from their data. This method used the original laser points rather than a derived raster data set. The authors achieved their stated goal for this research, developing and demonstrating a

complete GIS-based method from LiDAR data pre-processing, algorithm development, analysis and visualization, but noted that a complete count and validation of findings required field-verification, especially in complex multi-tiered deciduous and young stands.

Chen et al (2006) also derived local maxima in a canopy height model to identify individual tree tops using variable sized windows. However, in this research the window size was determined by the lower-limit of the prediction intervals of the regression curve between crown size and tree height. This was done because of 'commission errors', or non-treetop local maxima that were incorrectly classified as treetops. The authors manually measured tree crown size and tree height from the CHM used for analysis. This method was preferable to measuring in the field since: 1) it was easy to identify individual trees from the LiDAR data set due to the high pulse density present, and 2) sampling within the CHM greatly reduced workload and was not limited by factors such as accessibility in the field. The authors then used a watershed segmentation method by inverting the CHM so local maximums became local minimums, and a canopy minimum model (CMM) was produced. The 'flooding' of the CMM took place and the algorithm developed built 'dams' along the divide line between neighboring catchment basins (trees). The 'dams' were called watershed lines and were used to partition individual trees from the flooded CMM.

Korpela et al (2007) used large-scale aerial imagery, a Digital Terrain Model (DTM), and LiDAR data to develop a single-tree remote sensing (STRS) system to identify 3D treetop positioning, height estimation, species recognition,

crown width estimation, and model-based estimation of individual stem diameter. Each step was a part of a semiautomatic system using the tree data sources listed above. LiDAR-based crown width estimates were completed using crown modeling, where parametric crowns were iteratively fitted with LiDAR data. Image-based 3D treetop position and crown width estimation was down with multi-scale template matching, and species recognition was done manually by visual photo-interpretation. Overall, this method underestimated stem diameters, and calibration of the system again would require time-consuming field observations and measurements.

METHODS

TreeVaW Individual Tree Identification and Stem Mapping

For this thesis, a canopy height model (CHM) was created using FUSION and LiDAR data for WS1 (see Chapter 2). This CHM was clipped to the extents of each plot in the watershed using the *extract by mask* tool in ArcMap (ESRI). Because TreeVaW reads an older ENVI file format, with a .dat extension, the ArcMap *copy raster* function was utilized so that these files could be imported into TreeVaW, . The *copy raster* tool also creates an .hdr, or header file, that TreeVaW requires. Files were converted for each plot, after which the .dat extension was removed, which is the final step before TreeVaW would read the data. TreeVaW also requires unique parameters to calibrate its algorithms to the forest type present. Keith Olsen, a researcher at Oregon State University completing similar work at H.J. Andrews using TreeVaW provided these values (Keith Olsen, personal communication). Each plot file was input into TreeVaW

one at a time, and the software output a .csv file with XY location, crown diameter, and tree height for each tree identified. The following equation relating crown diameter (y) to height (x) was used for TreeVaW input:

$$y = 0.0000310796916048496 * x^3 - 0.00267405906767456 * x^2 + 0.195530509685481 * x + 1.61296048520958$$

H.J. Andrews Vegetation Survey Data

To compare the output of individual trees produced by TreeVaW, I used a data set from the H.J. Andrews website detailing comprehensive vegetation surveys completed in WS1 (http://andrewsforest.oregonstate.edu/). The most recent data were used (2007) since it would closest temporally to the date when the LiDAR data were collected (2008). The HJA data set required pre-processing to allow for comparison to the TreeVaW output: 1) Because the data set contained plots for both WS1 and WS3, all WS3 data were removed, 2) Next, all trees that were noted as "mortalities" were removed, so to analyze only live trees, 3) Finally, trees that were too small to measure diameter at breast height (DBH) were removed, since those trees would also be too small for the TreeVaW program to recognize.

DBH-Tree Height Relationship and Comparison

After the HJA data were prepared it was then compared to the TreeVaW output for each plot. However, there was no direct way to 'match up' the trees present in each data set because TreeVaW identified individual trees by XY location, crown

diameter and tree height, while the HJA data set identified trees only by DBH and quadrant location (NW, NE, SW, SE). In order to identify which trees TreeVaW was finding, asymptotic equations to convert DBH to height were used for each individual species (Research Contribution 10, Garman et al. 1995). The equations from that report provide predictive regional estimates of height-diameter trends for 24 tree species over a wide range of diameters, and used the same equation for each species, with regression coefficients for each derived from trees measured in 8,727 fixed and variable radius plots representing managed and natural stands. The equation used along with coefficients for each species converted in this thesis is found in Table 4.

Height = 1.37 + (b0[1-exp(b1*DBH)]^b2

Species	CODON	B0	B1	B2
Douglas Fir (*Pseudotsuga menziesii*)	PSME	61.6358	-0.01469	0.92706
Big Leaf Maple (*Acer macrophyllum*)	ACMA	30.4131	-0.03425	0.6821
Western Hemlock (*Tsuga heterophylla*)	TSHE	57.4756	-0.01677	1.02854
Red Alder (*Alnus rubra*)	ALRU	35.55	-0.02832	0.79602
Chinkapin (*Castanopsis chrysophylla*)	CACH	40.6648	-0.01778	0.87363

Table 4. DBH-Height asymptotic equation and regression coefficients used for each species (Garman et al. 1995).

RESULTS

Total Trees Identified in Plots

Overall, in all the plots of WS1 TreeVaW identified 2,810 trees of the 3,407 trees observed (82.48%) in the vegetation surveys (see Appendix B for complete list of trees by plot). Trees identified and trees observed for all the plots in which DHPs were taken are presented in Table 5. When TreeVaW was used to identify all trees

in the watershed, 74,299 trees were identified. However, since all trees in the watershed have not been counted, there is no way to assess the accuracy of this measure.

Plot	Observed Trees	Predicted Trees	% of Trees Id'ed
P11108	28	12	42.86%
P11109	23	17	73.91%
P11110	23	18	78.26%
P11205	17	17	100.00%
P11206	17	15	88.24%
P11207	15	18	120.00%
P11208	12	14	116.67%
P11209	25	11	44.00%
P11211	38	15	39.47%
P11212	46	22	47.83%
P11213	28	17	60.71%
P11608	24	17	70.83%
P11609	15	12	80.00%
P11610	18	14	77.78%
P11611	19	14	73.68%
P11612	21	17	80.95%
P11613	30	15	50.00%
P11614	19	15	78.95%
P11615	25	20	80.00%
P11616	21	14	66.67%
P11617	13	14	107.69%

Table 5. Observed trees, trees predicted by TreeVaW and percentage of trees identified by TreeVaW in plots where digital hemispherical photographs were taken.

Vegetation Survey and TreeVaW Comparison by Plot

In plot P11108, TreeVaW identified 12 of 28 live trees (42.86%). The trees identified were the tallest 12 trees present in the plot, according to the vegetation survey. Also, the height of the trees calculated by TreeVaw was consistently higher than the actual trees in the plot.

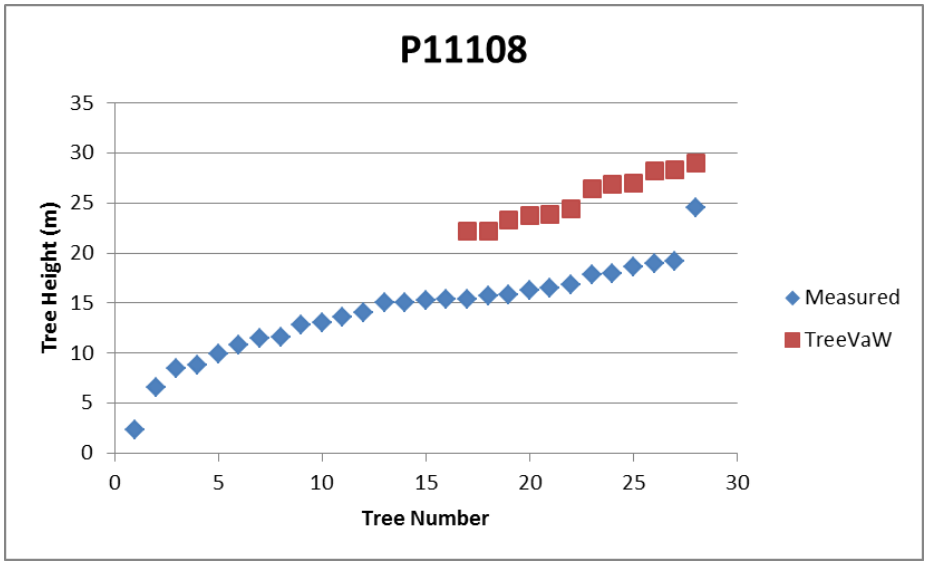

Figure 10. Transect 1, plot 8.

In plot P11109 TreeVaW identified 17 of 23 live trees present (73.91%). Similarly to P11108, the 17 trees identified by TreeVaW were the tallest 17 trees present in the plot. Also, the heights of the trees identified by TreeVaW were (again) consistently taller than those in the actual vegetation survey.

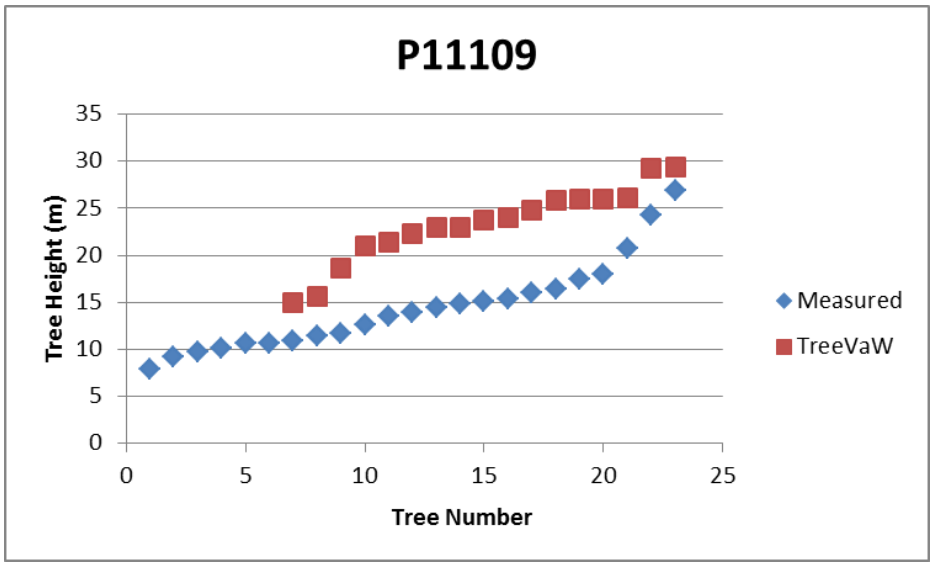

Figure 11. Transect 1, plot 9.

In plot P11110, TreeVaW identified 18 of 23 live trees present (78.26%). Unlike P11108 and P11109, however, TreeVaW identified both tall and short trees, but not trees in the middle of the height range. The heights of the taller trees identified

by TreeVaw were overestimated and the heights for the shorter trees underestimated.

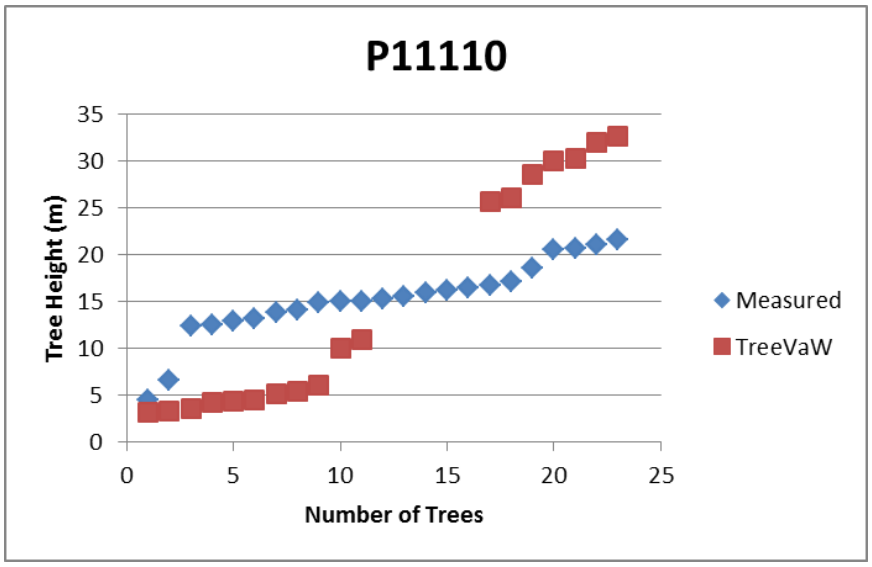

Figure 12. Transect 1, plot 10.

In plot P11205, TreeVaW identified 17 of 17 live trees (100%). The heights of all the trees identified by TreeVaW were very similar to the actual tree heights from the vegetation survey, although heights of the three smallest trees were underestimated. This may be due to the fact that these trees were ACMA (*Acer macrophyllum*, or bigleaf maple), while the rest of the trees \ were PSME (*Psuedotsuga menziesii*, or Douglas Fir). Additionally, the DBH data for the ACMA (and *Castanopsis chrysophylla* or CACH) trees on WS1 is difficult to incorporate into single bole models such as TreeVaw because it represents the average DBH of a clump of stems, so that the stem representing the main structural bole (likely the tallest bole) will be de-emphasized by the presence of thinner copice stems of secondary boles.

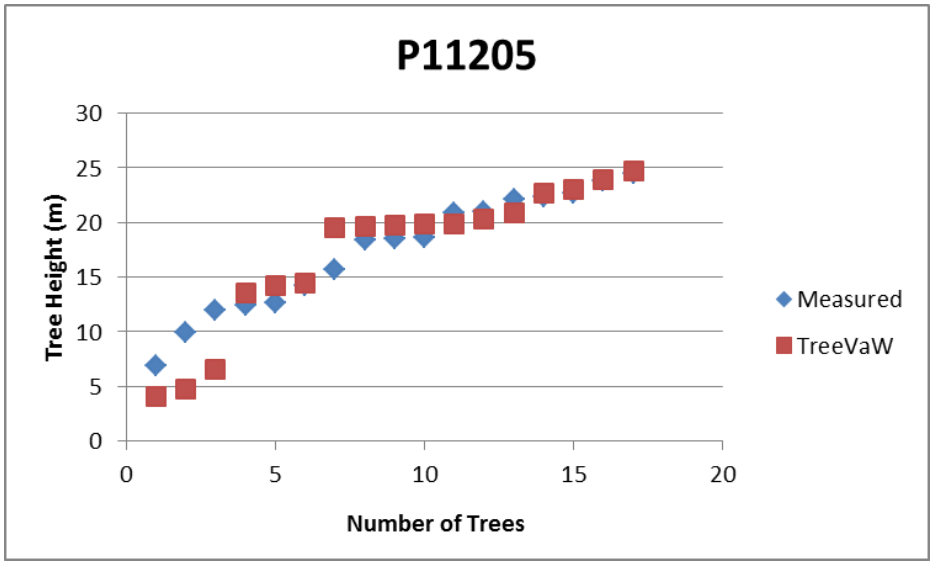

Figure 13. Transect 2, plot 5.

In plot P11206, TreeVaW identified 15 of 17 live trees present (88.24%). The heights of the trees identified by TreeVaW were slightly overestimated for the 11 taller trees and slightly underestimated for the 4 shortest trees.

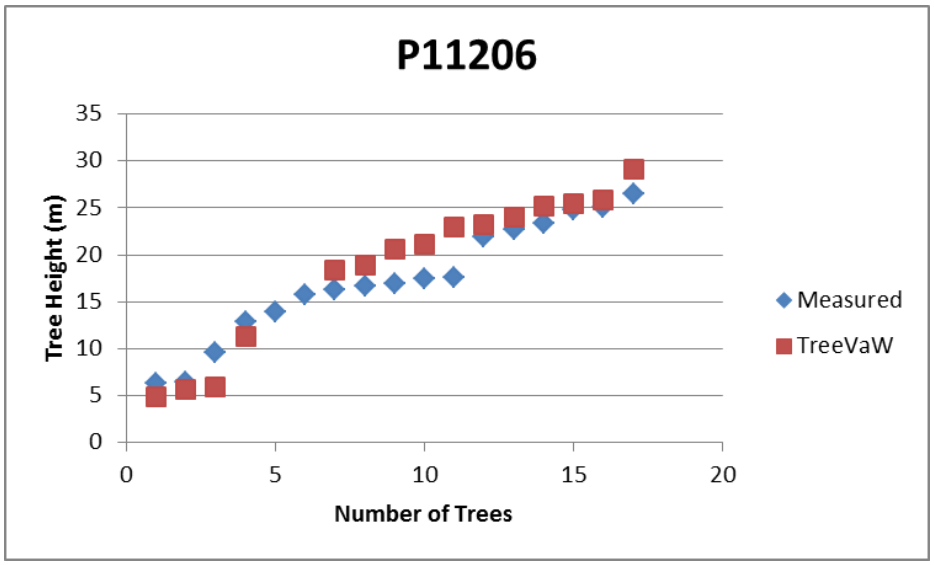

Figure 14. Transect 2, plot 6.

In plot P11207, TreeVaW identified 18 trees although only 15 live trees were present (120%). Heights for the taller trees identified by TreeVaW were overestimated while the heights of the shorter trees were quite close to the measured trees heights. The identification of three extra live trees not present may be due to identification of snags (dead trees) by TreeVaW that were removed from the vegetation survey.

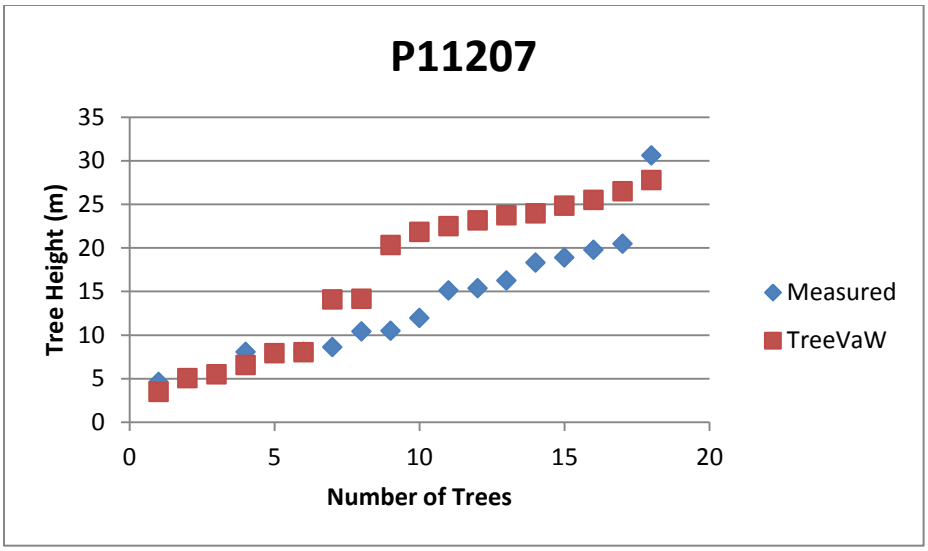

Figure 15. Transect 2, plot 7.

In plot P11208, TreeVaW identified 14 trees while only 12 live trees were present (116.67%). The two extra trees identified by TreeVaW were smaller than any live tree present in the vegetation survey. These extra trees may have been small snags that were removed from the vegetation survey. The heights of all trees identified by TreeVaw in this plot were overestimated, consistently about 3m taller than the trees present according to the vegetation survey.

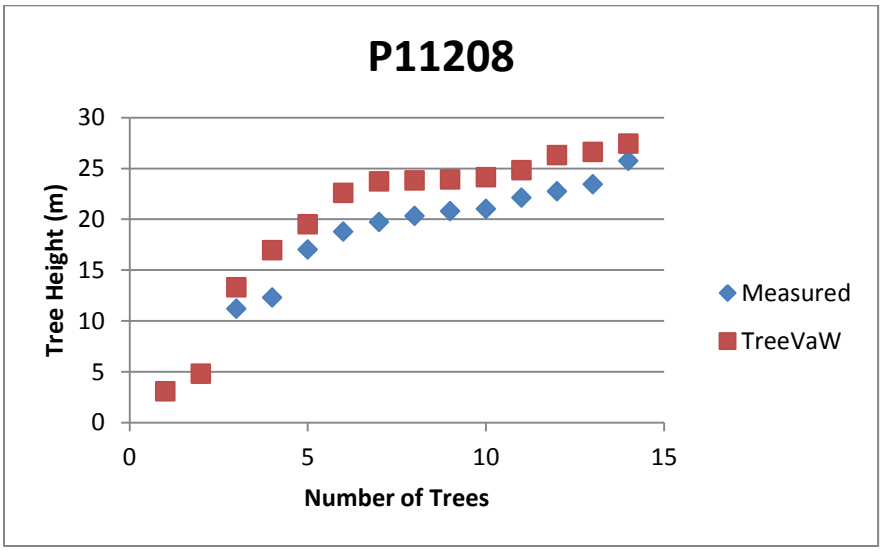

Figure 16. Transect 2, plot 8.

In plot P11209, TreeVaW identified 11 of 25 live trees present (44%). The trees identified by TreeVaW for this plot were the tallest trees present according to the vegetation survey. Also, the heights of the trees identified by TreeVaW were consistently overestimated by about 1-2 meters.

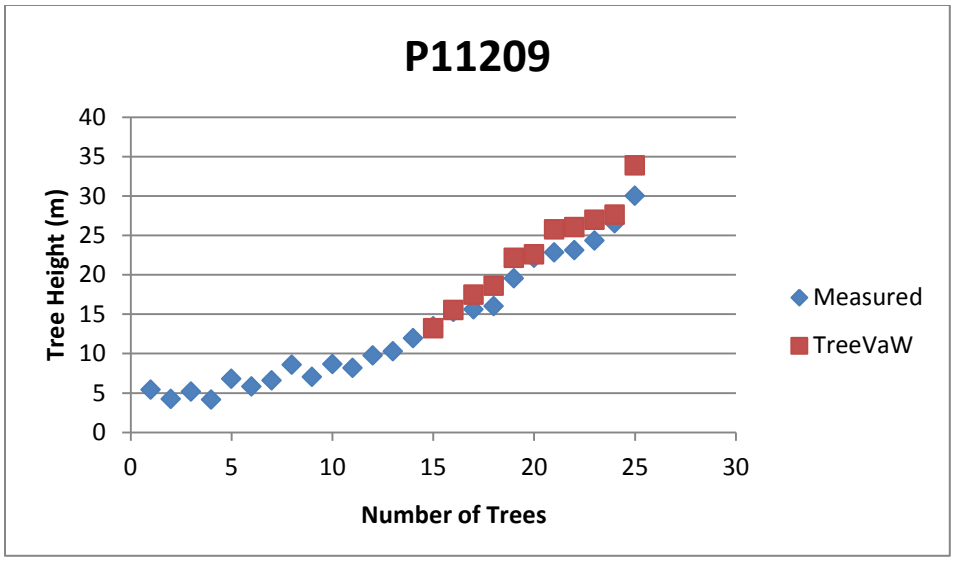

Figure 17. Transect 2, plot 9.

In plot P11211, TreeVaW identified 15 of 38 live trees present (39.47%). The trees identified by TreeVaW were the tallest trees present according to the vegetation survey, and the heights of the trees identified were consistently 7-8 meters taller than the trees present. Plot 211 is a particularly unique plot on WS1 because a mortality event occurring on the plot above it, Plot 212, has led to the bending and breakage of many trees on Plot 211. We would expect to see this over-estimation of height on the model versus the field because the model does not take into account the poor tree morphology on this plot due to local disturbance.

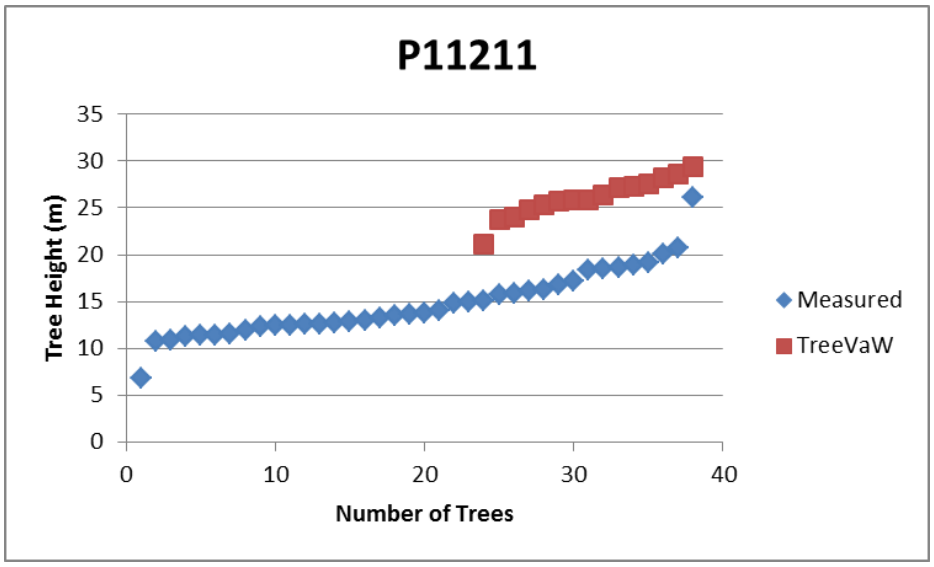

Figure 18. Transect 2, plot 11.

In plot P11212, TreeVaW identified 22 of 46 live trees present (47.83%). TreeVaW identified both the tallest and the shortest trees present in this plot. For

the shorter trees, TreeVaW consistently underestimated the height of the trees and consistently overestimated the height of the tallest trees. Again, the local mortality event on this plot may play a role. While large and small trees may have survived the event due to structural resilience or flexibility, respectively, mid-sized trees may have been damaged to the extent that they are unrecognizable in LiDAR imagery.

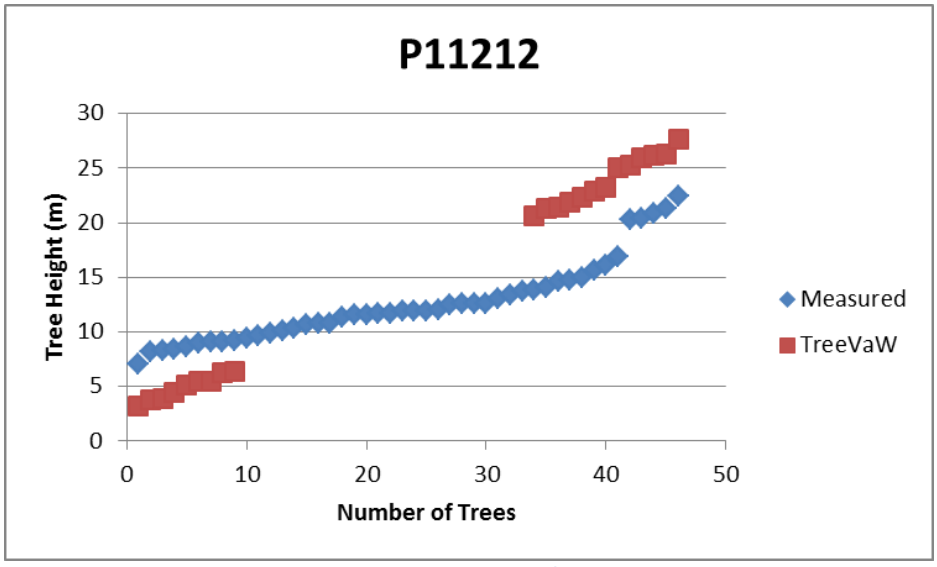

Figure 19. Transcect 2, plot 12.

In plot P11213, TreeVaW identified 17 of 28 live trees present (60.71%). All of the trees identified by TreeVaW except one were the tallest trees in the plot. TreeVaw overestimated the height of all trees identified.

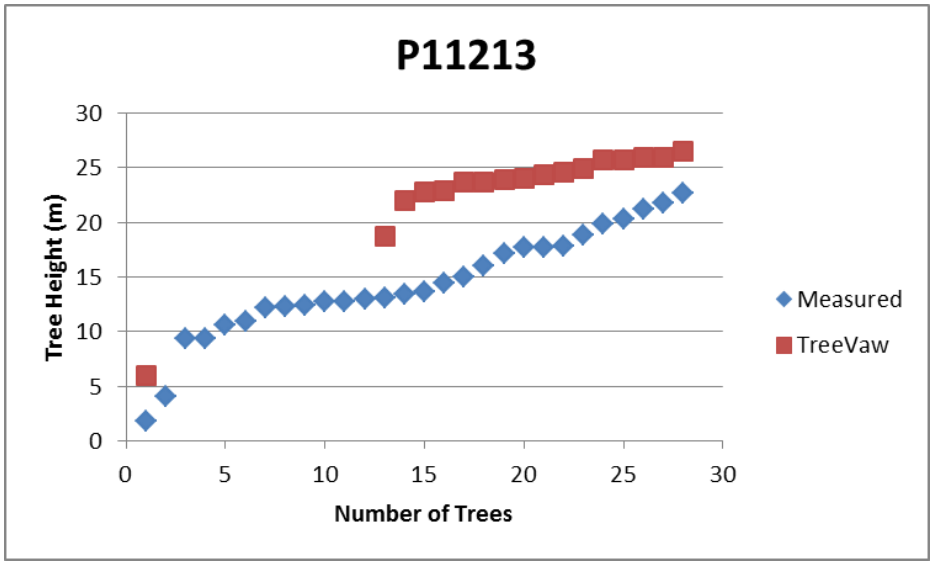

Figure 20. Transect 2, plot 13.

In plot P11608, TreeVaW identified 17 of 24 live trees present (70.83%). TreeVaW identified the 17 tallest trees in this plot with exceptional precision, only overestimating one tree by roughly three meters.

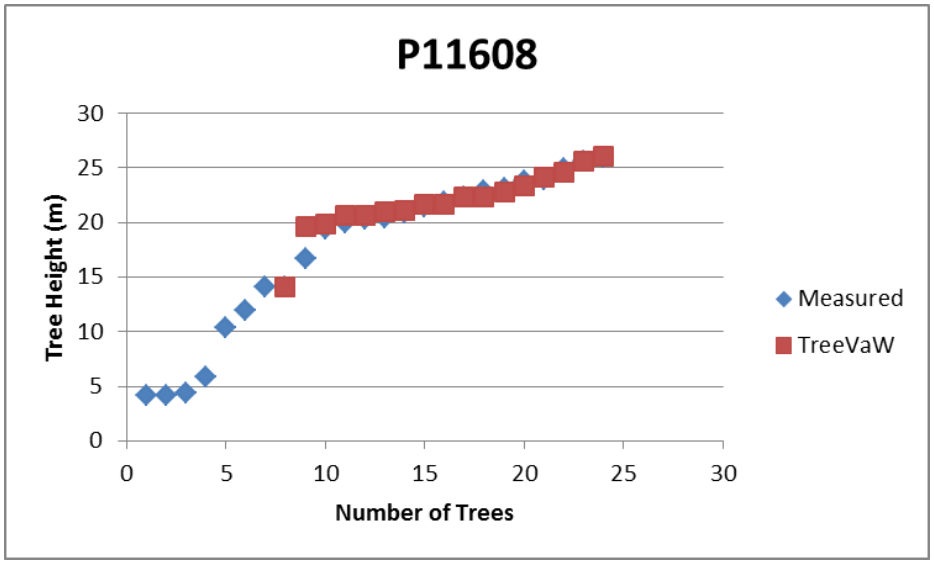

Figure 21. Transect 6, plot 8.

In plot P11609, TreeVaW identified 12 of 15 live trees present (80%). TreeVaW identified the 11 tallest trees as well as the shortest tree in this plot. It overestimated the height for three trees by 2-8 meters and underestimated the height of the tallest tree present in the plot.

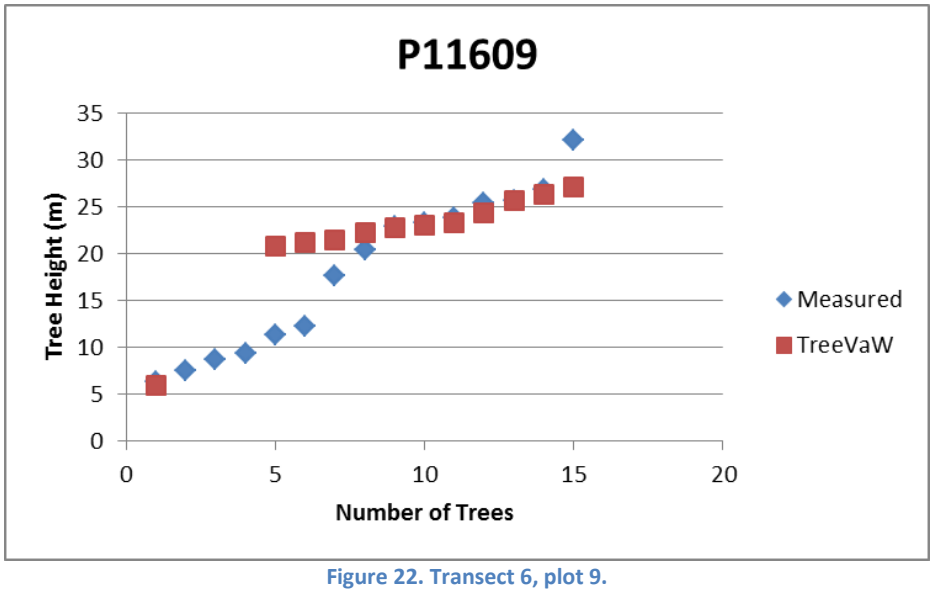

Figure 22. Transect 6, plot 9.

In plot P11610, TreeVaW identified 14 of 18 live trees present (77.78%). TreeVaW identified the 12 tallest trees as well as the two shortest trees in this

plot. The five tallest trees and two shortest trees were identified accurately for height, but TreeVaW slightly overestimated the height for the remaining 7 trees.

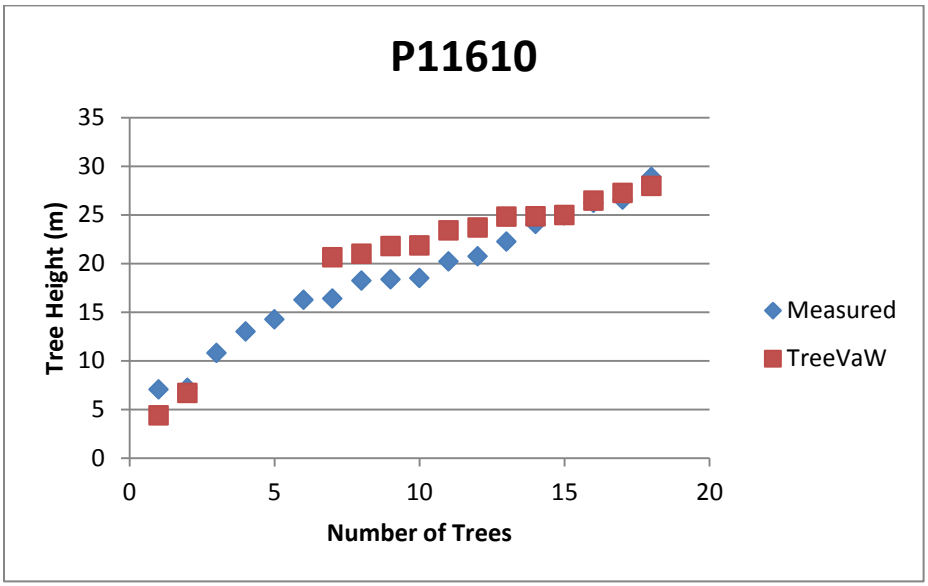

Figure 23. Transcect 6, plot 10.

In plot P11611, TreeVaW identified 14 of 19 live trees present (73.68%). TreeVaW again estimated the 14 tallest trees in this plot, fairly accurately with all estimated heights falling within two meters of the actual measurements.

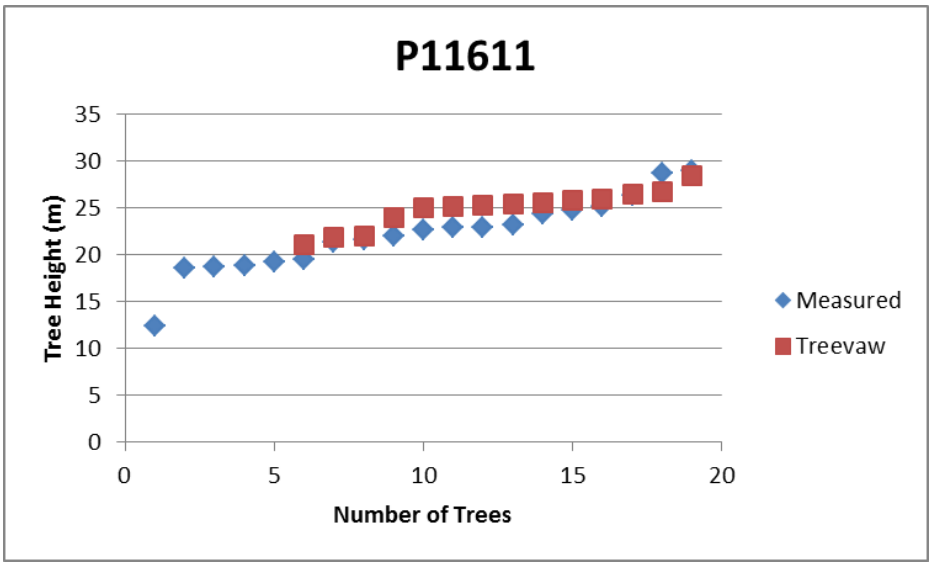

Figure 24. Transcect 6, plot 11.

In plot P11612, TreeVaW identified 17 of 21 live trees present (80.95%). The four trees that TreeVaW failed to identify were in the lower third of tree heights. The heights for the three smallest trees identified were accurate, and TreeVaW slightly overestimated the majority of the other trees identified.

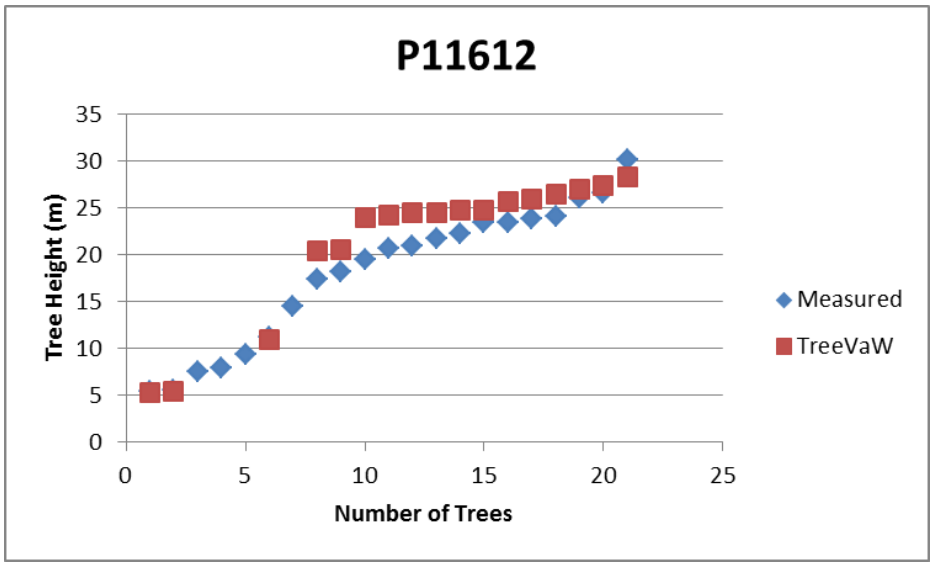

Figure 25. Transect 6, plot 12.

In plot P11613, TreeVaW identified 15 of 30 live trees present (50%). The shortest tree and the 14 tallest trees were identified by TreeVaW within this plot. TreeVaW slightly underestimated the height of the shortest tree and slightly overestimated (1-2 meters) the remaining tallest trees identified.

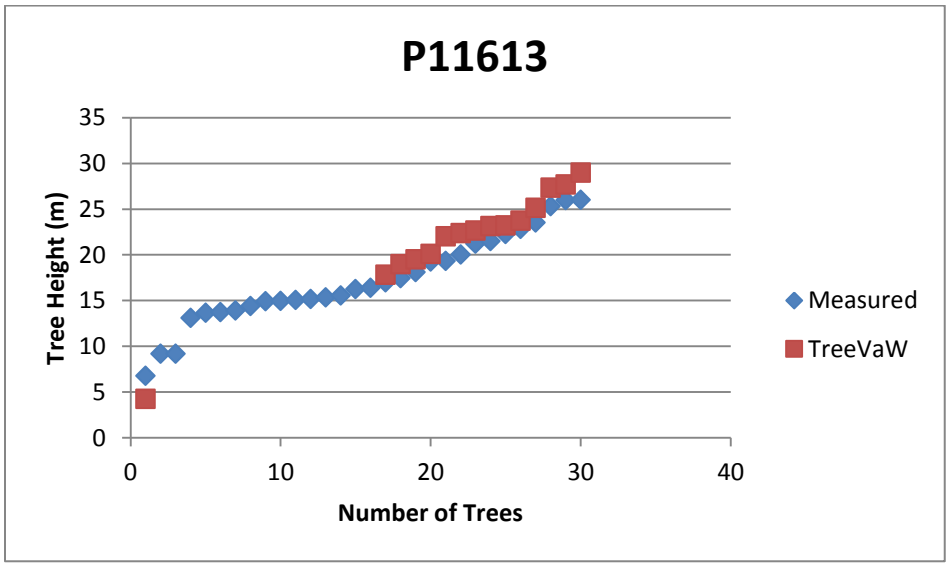

Figure 26. Transect 6, plot 13.

In plot P11614, TreeVaW identified 15 of 19 live trees present (78.95%). The four trees not identified were the four smallest trees within the plot. Overall, TreeVaW slightly overestimated height for all trees identified, with higher overestimations for the tallest trees (2-3 meters each).

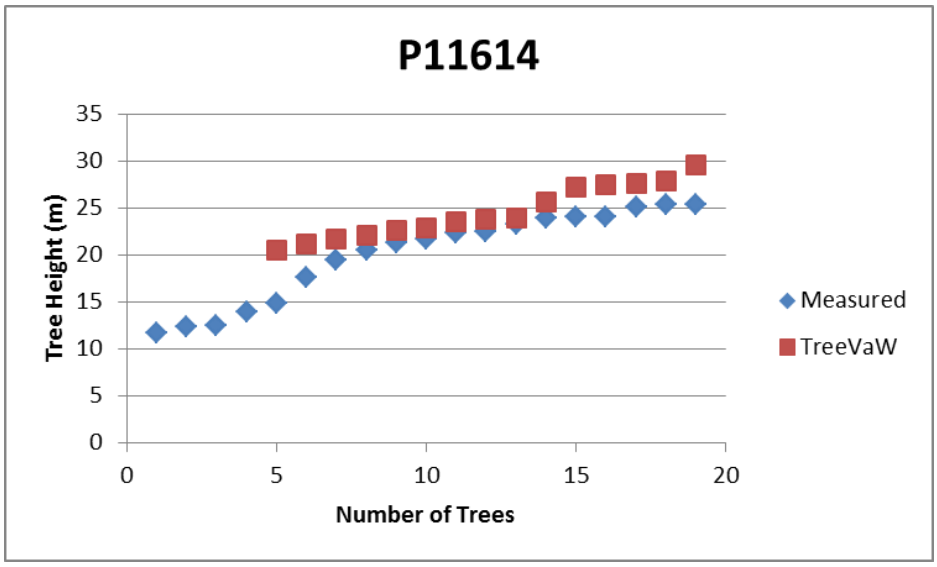

Figure 27. Transcect 6, plot 14.

In plot P11615, TreeVaW identified 20 of 25 live trees present (80%). Trees identified were among the tallest and shortest trees. For shorter trees identified, over- and under-estimation of height occurred while all of the heights for taller trees identified were overestimated by TreeVaW.

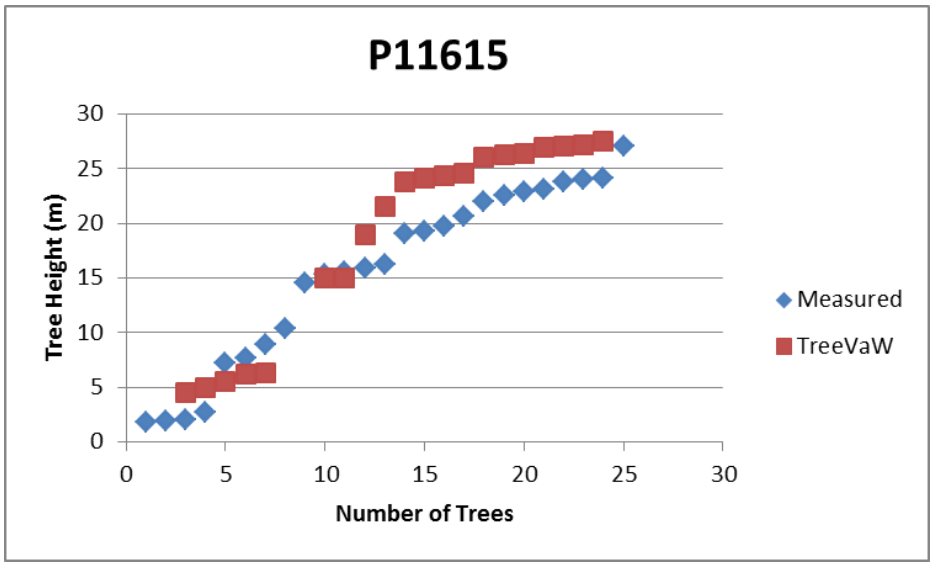

Figure 28. Transect 6, plot 15.

In plot P11616, TreeVaW identified 14 of 21 live trees (66.67%). The tallest trees in this plot were the trees that TreeVaW identified, and the heights of each were overestimated by 1-5 meters.

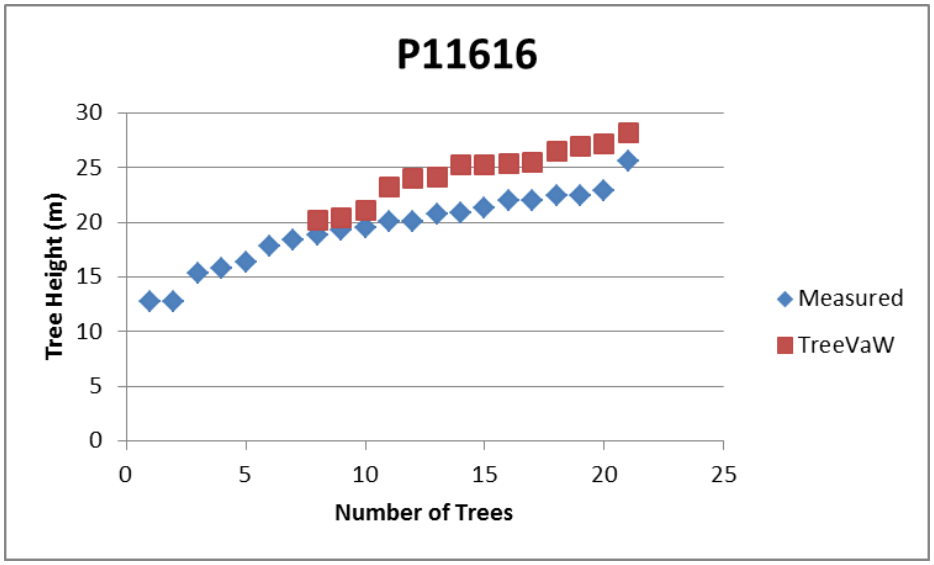

Figure 29. Transcect 6, plot 16.

In plot P11617, TreeVaW identified 14 live trees with only 13 live trees present (107.69%). The heights of all but the shortest and tallest trees were overestimated.

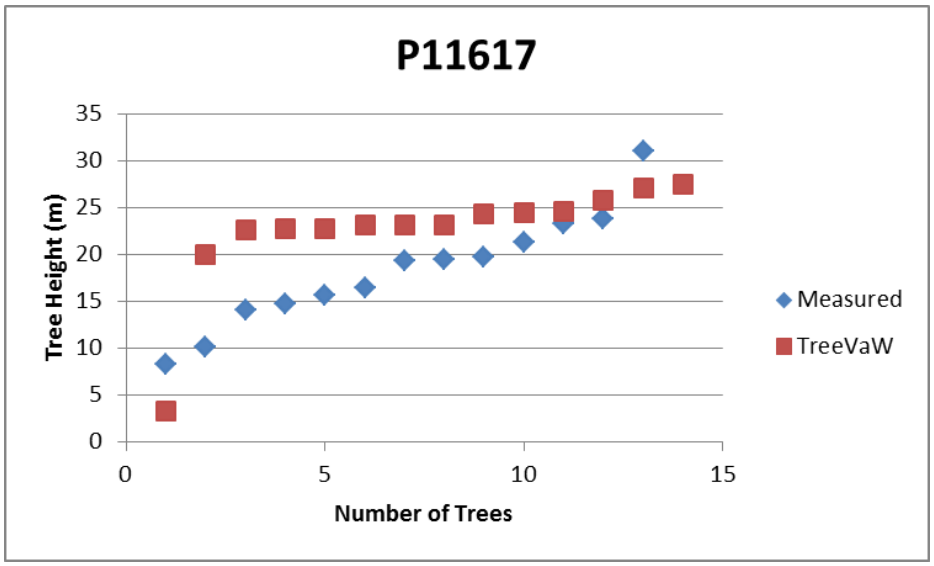

Figure 30. Transcect 6, plot 17.

DISCUSSION

The TreeVaW software identified most of the tallest trees in most of the plots surveyed. This was evident in the graphs for each plot in which DHPs were taken

for LAI analysis. These results are expected, given that the method used to identify trees uses a CHM. The tallest trees in stands form the peaks and valleys of the CHM, and thus are easier to segment and identify (Richardson and Moskal 2011). In a dense stand such as WS1, the tallest trees would mask or cover the smaller trees in the understory, and any existing software or method to identify trees would likely miss them. Richardson and Moskal (2011) found that the precision of their method was higher for the two taller height classes than the two shorter height classes. These findings, also supported by previous studies, strongly indicate that LiDAR data are consistently accurate in identifying the tallest, or dominant, trees in a stand. Additionally, on WS1, due to complex terrain, dominance is in part a function of slope. On steeper slopes, which are found deeper "within" the watershed (for example, P11108 and P11211), dominant trees are codominant with respect to the plots "above" them on the slope. Along the ridgeline (for example, all plots on transect 6, dominance is more representative of actual tree heights.

Andersen et al. (2001) encountered similar results when using LiDAR data to create a canopy surface model that measured individual trees. The morphologically based tree measurement algorithm performed better where tree crowns were larger and more widely dispersed. In denser areas, the canopy surface algorithm output errors of omission and commission. Morphologically, there are also distinct differences in tree DBH to tree height relationships on WS1, especially with respect to aspect. For PSME of the same age, individual trees on the north-facing slope are of smaller DBH and closer spacing than those on the

south-facing slope. We suggest that the ecological mechanism driving these morphological differences is soil moisture availability; although trees on the south facing slope will likely have greater radiation, soil moisture on these exposed slopes is generally low and weathering is more extensive than on north-facing slopes. The initial establishment of the plantation on these slopes was poor, and young PSME benefited from growing further apart and slowly under the protection of drought-tolerant hardwoods. On the north-facing slope, initial establishment of the plantation was highly successful, and PSME with adequate soil water and nutrients allocated much biomass to stem height to compete for limited radiation. This more rapid height growth of PSME on the north-facing slope lead to trees of the same age being at different stages of stand development, with north facing PSME undergoing canopy closure sometime between 1995 and 2001. This led to local mortality events and overall productivity decline. Although model algorithms are able to identify general patterns in PSME height and foliar component based on DBH, the specifics of stand physiology on WS1 due to complex terrain may not be fully represented, and this may account for a number of discrepancies we see in modeled versus measured height.

Hirata et al (2009) tested individual tree identification in stands of variable thinning by using a digital canopy model (DCM) and assessed the pulse penetration of the LiDAR itself. The researchers inverted the DCM and performed watershed segmentation in the basins and drainage divides to identify individual trees. The total number of trees identified (607 of 748 or 81.1%) is remarkably similar to the tree identification results in this thesis. More trees were accurately

identified in the areas where heavy or moderate thinning occurred compared to an area that was not thinned. A potential explanation for this is that plots with a comparatively sparse distribution of trees allowed for LiDAR penetration of the understory. Furthermore, the ratio of unidentified trees to all standing trees was higher for trees in the smallest height classes compared to the taller height classes of trees. Also similar to some plots in this thesis (P11108, P11110 and P11212), Hirata et al. (2009) found that LiDAR underestimated the heights of trees shorter than 15 meters, and overestimated heights of trees taller than 15 meters.

In their research, Edson and Wing (2011) used three different tree extraction methods to identify individual trees in mixed conifer stands. They used a watershed segmentation method of inverting a canopy height model, manual extraction using the FUSION software, and automatic extraction using TreeVaW (as in this thesis). These three methods had varying results, but the FUSION method was quickly abandoned because how long it took to find individual trees and issues in identifying understory trees in dense stands. The authors also noted that where and how many LiDAR pulses strike and reflect off trees impacts the identification and measurement of individual trees. Especially with conifer species, the odds of a pulse striking the highest, single apex point of a tree are low. The odds decrease further when the apex of the tree is below the upper canopy. Similar to the research previously discussed, Edson and Wing found it relatively easy to identify upper trees in dense plots, but smaller trees were shrouded by larger ones, and identification of smaller trees was difficult at best. They found identifying young conifers in a clear cut also difficult: even with a

pulse rate of 8-10 pulses per square meter, the sparseness of young conifer foliage caused only one or two LiDAR pulses to strike individual trees, making identification difficult to impossible.

New Methods in Tree Extraction from LiDAR Data

Seeking to improve upon known methods of individual tree identification, Lee and Lucas (2007) noted that most previous work focused primarily on the use of Canopy Height Models, and this approach has proven only mildly successful for mapping and attributing stems in complex, multilayered forests. They therefore developed a novel complementary approach using a Height-Scaled Crown Openness Index (HSCOI), which provides a quantitative measure of the penetration of LiDAR pulses into the canopy. To quantify the penetration of LiDAR pulses into the canopy, the data were transformed into a 3D voxel matrix of 1 cubic meter squares. Within the 3D matrix, canopy voxels containing returns were attributed with the tallest recorded LiDAR height value within the voxel space. The HSCOI was then constructed using the weighted summation of a proxy variable of the inverse canopy density, or 1/the number of voxels containing returns per 1 square meter vertical column. The HSCOI metric thus translates the LiDAR point observations into a measure of relative penetration of the LiDAR pulses by scaling them from the top of the canopy so that 0% indicated no penetration and 100% full penetration of the pulse to the ground. Figure 31 shows the difference between the created HSCOI and a traditional CHM.

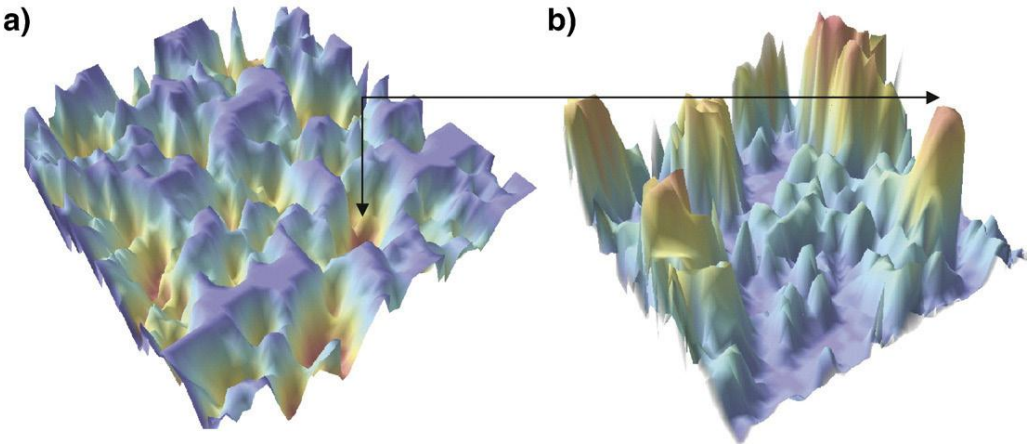

Figure 31. A comparison of a) the newly developed HSCOI metric, and b) a CHM. The high point in the CHM is transformed to a low point in the HSCOI because it would be an area where penetration of LiDAR pulses would be very low (Lee and Lucas 2007) .

Lee and Lucas (2007) applied the new metric (HSCOI) to mixed species forests in Queensland, Australia, which facilitated the mapping of the forest areas, delineation of tree crowns and clusters, and estimation of canopy cover. Computed tree densities compared well with field measurements at the stand level, and the most consistent results were from stem densities of less than 700 stems/hectare. This metric was combined with the CHM shown above to estimate dominant stem height, crown cover, and foliage and branch projective cover to sufficient levels of inventory for the stands. However, this method resulted in less accurate measurements when applied to a different forest type with increased average height and canopy closure.

Li et al (2012) also set out to develop a new approach that built on the use of CHMs in order to segment individual trees, using a similar LiDAR system as this thesis, and begun by separating ground returns from aboveground returns. The data were ‘normalized’ by subtracting the vegetation point cloud from the ground point DEM. As a result, the elevation value at any point represented its

height from the ground. The new method relies on the relative spacing between trees, which tends to increase from the base of trees to the top of trees. The authors note that, although there is overlapping of trees in dense forests, spacing between trees exists at higher parts of the canopy. Coniferous trees have, in simplicity, a conical shape, such that the crown radius at the base of the crown (where it would be measured from a ground based measurement) will be greater than that at the top of the crown. Thus, the point density of LiDAR returns, or any metric modeling canopy architecture, will be sparser at heights further from the canopy base. This method works from the top of a tree, and 'grows' the tree by including nearby points and excluding points from other trees based on their relative spacing, and becomes more of a challenge farther down the tree as spacing decreases and trees overlap. However, classifying points sequentially, from highest to lowest, overcomes this challenge. By developing and defining appropriate spacing thresholds, most points can be assigned to their corresponding trees. Trees are segmented using three variables: 1) either these fixed or adaptive thresholds, 2) a minimum spacing rule, and 3) a horizontal profile of tree shape. Reducing undersegmentation is accomplished by using a small threshold, and oversegmentation is reduced using the shape and distribution of the points. This top to bottom approach is iterated until all points have been classified into their corresponding sets, with each set corresponding to an individual tree.

The authors tested their algorithm in a conifer stand in the Sierra Nevada range of California and found that it increased the accuracy of individual tree detection compared to other methods. 86% of trees were identified, and 94 % of

the segmented trees were correct. The authors state that this method holds promise for use in similar, mixed and complex coniferous forests, but its effectiveness in other forest types, namely deciduous forests, requires further evaluation. This method is similar to other methods that use a CHM in that it identifies local maxima as the top of a tree, differing in that the new algorithm identifies the global maximum (highest point), segments that tree, and then removes the data points associated with that tree from the point cloud. Then, the process starts again, finding the 'next' global maximum and segmenting that tree, iterating until all points have been classified. Using untransformed LiDAR data avoids interpolation errors that emerge when a point cloud is transformed into a CHM.

CONCLUSIONS

LiDAR data have been used extensively to measure canopy characteristics and attributes, and this thesis has continued that work by using LiDAR data to identify individual tree location, height, and crown width within the H. J. Andrews Experimental Forest. The software used, TreeVaW, was originally developed for a much different forest type, and species and site specific parameters are available, problems still persist. These problems are most evident for crown width estimates, which were not used for analysis since they seemed unreasonably small. The stand type for which TreeVaW was developed consists of much less dense, more spread out trees, and the program seems to have issues delineating points for individual trees for the crown width estimates in denser stands. Also, the denseness of the canopy seems to limit the ability of TreeVaW to identify shorter trees in the understory. This is not entirely surprising since the software

relies on a canopy height model (CHM) for extraction of individual trees, and the taller trees are the most visible in the CHM.

TreeVaW performed very well in some plots, but in many plots it underperformed by failing to identify all or most trees). The program seemed to perform better in plots lower density, and well as in plots with mostly taller trees. TreeVaW tended to slightly overestimate heights of taller trees, and when it did identify shorter trees it often underestimated the heights of those trees. Reliance on the CHM for tree extraction may be why these errors occur and the use of a Height-Scaled Crown Openness Index (HSCOI) presented by Lee and Lucas (2007) might solve these issues. This said, the overall percentage of trees identified by TreeVaW in all 133 vegetation plots (~82%) compares well to other published results.

Chapter 4- LiDAR Data Visualization and Overview of Visualization in Natural Resource Management

INTRODUCTION AND BACKGROUND

The use of data-driven visualizations in forestry management has become increasingly common in the last two decades. Bergen et al (1998) assessed the use of data-driven simulation, dimensional accuracy and realism in a landscape visualization tool as a part of their research. Even then, computer-based simulations of landscapes were recognized as an effective tool for assessing the potential impact of land-use decisions and s were commonly used by decision makers to assess the visual impact of forest operations, such as road building and harvesting, and as an aid in designing mitigation strategies. Early tools for decision makers relied on using computers to manipulate two-dimensional scanned photographic or videotape images for visual assessment and mitigation design after harvest. This computerized image manipulation carried the advantages of speed, efficiency and flexibility, but with two major drawbacks. First, image manipulation as a method of landscape simulation was primary an 'artistic technique', and therefore disconnected from project data. The second major drawback was that image manipulation methods lacked dimensional accuracy, and translating design information from a manipulated 2D image to a 3D landscape was difficult, if not impossible.

Bergen et al. (1998) also offered a review of the early 3D landscape visualization tools, and noted that the development of these methods closely paralleled developments in computer technology. Early computer tools included the Perspective Plot software and PREVIEW, both of which were based on digital terrain model (DTM) representations of a landscape and displayed crude line drawings of terrain and vegetation. More complex, realistic and accurate

simulations followed with the development of the SmartForest and Vantage Point software, which at the time of this article represented the state-of-the-art. Both draw individual trees to form forest stands over a DTM. Vantage Point generated and displayed color images of forest landscapes up to 8000 ha, and was used in the evaluation of visual quality and the visual impact of forest operations. Both systems used measured data, which added validity and credibility to the resulting image. The tools solved the two drawbacks mentioned previously, by relying on actual data and solving the dimensional accuracy issue by allowing the user to interact more directly with 3D landscape data. Users could display and manipulate design information on a perspective image of the landscape.

Bergen et al. (1999) concluded by stating that several obstacles remained before landscape simulation tools could find wider acceptance and use. The 3D visualization tools of the time, while offering flexibility in representing and altering data sets, lacked realism. Images that appeared more realistic were less flexible and often not based on measured data. The authors posed two remaining questions: 1) From a theoretical perspective, how much realism and accuracy is required to make value judgments? 2) Is it practical and economical to gather enough data to create more realistic simulations? The authors claimed that more complex computer systems could create more detailed images faster, approaching real-time manipulation of photo-realistic images representing 3D data sets, but it was unknown whether theory and data gathering abilities would keep pace with the technology.

McGaughey (1998) also reviewed techniques for visualizing the effects of forestry operations. His research compared how geometric modeling, where mathematical models of individual components are built and then assembled to create a model of a forest stand or landscape, compares with video imaging. The research also explores a hybrid of these two methods as well as the method of video draping, or overlaying an image over a DTM. These four methods were compared with respect to their data requirements, level of realism in final scene, operational complexity and data integrity. The ultimate consideration in choosing a method was found to be reliant on the size of the project area, overall goal of the visualizations, amount of detail that must be shown, and amount of available data describing the area. Finally, the author reviewed the available software at the time, noting that commercial systems can be expensive, often need a specialized operator to produce results, and require that typical forestry data be converted into a suitable format. However, public domain visualization and image-editing capabilities suitable to forestry visualization were available at the time for little or no cost.

Since the time when SmartForest and Vantage Point were considered state-of-the-art, visualization tools have come a long way, and one reason for this is the rise in use of remote sensing capabilities such as LiDAR. Kao et al. (2005) point out in their research that the development of remote sensing capabilities has ushered in an era where large quantities of multidimensional and multivariate data are routinely analyzed. Most work to date, they noted, relied on statistical summaries (a.k.a. data aggregations) to characterize the distribution of data with a

small set of descriptors. These methods reduce the dimensionality of the data set, often making it impossible to access the primary data from the visualization, but making visualization straightforward. However, this approach fails when the distributions are nonparametric, and when they are multimodal. Kao et al. (2005) proposed instead allowing for exploration, query and comparison of LiDAR data distributions, in order to increase opportunities to query multi-valued data in new ways that better help scientists and other stakeholders understand the spatial distributions of geophysical and ecological phenomena. This, in theory, could be done both at single locations and across the spatial domain. The authors utilized so-called spatially distributed probability density functions (pdfs), created from multiple return LiDAR data, and noted that the major contribution of their work was a paradigm shift that allowed ecologists to think of and analyze data in terms of full distributions, not just summary statistics. The major contributions of this paper, as listed by the authors, were: 1) provide automated and interactive ways to analyze forest canopy distributions from LiDAR data, 2) make it easier for scientists to analyze distributions derived from LiDAR data, and 3) allow scientists to query distribution data for special features and then identify areas of the spatial field with similar distributions and discover potentially interesting distributions and their locations. Figure 32 shows a diagram of the visual analysis of distribution data made possible by this work.

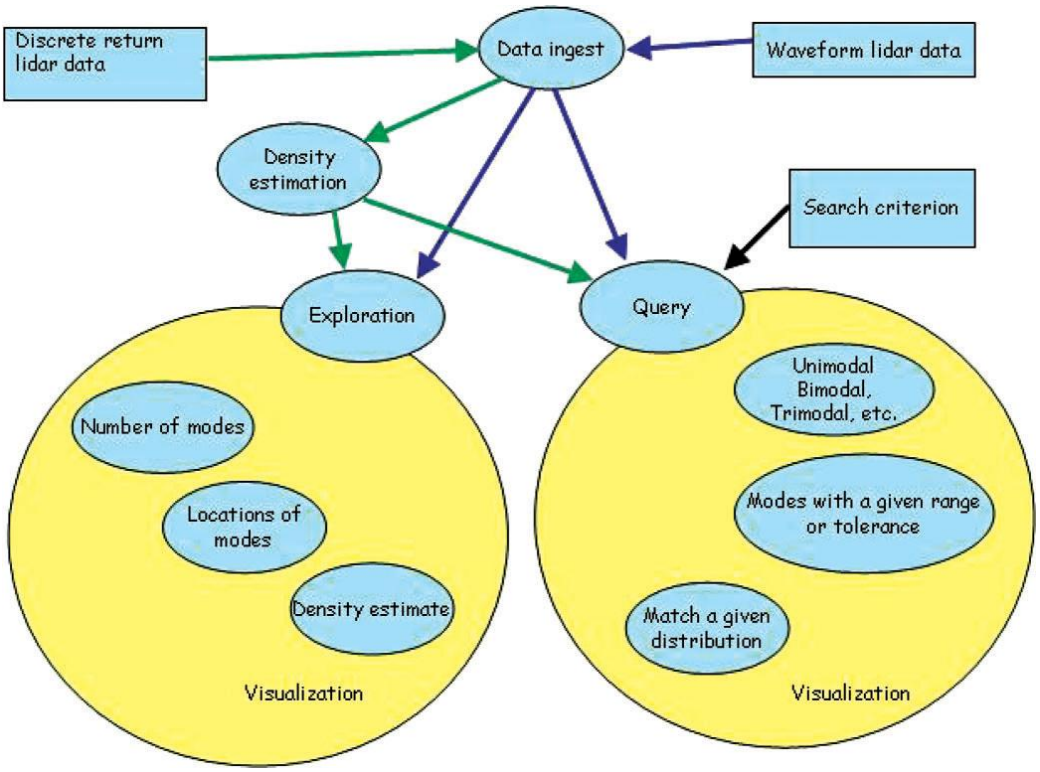

Figure 32. A diagram representing new types of visual analysis of LiDAR data could occur because of research by Kao et al. (2005).

Fujisaki et al. (2007) offered an update to forest visualization systems in their research paper describing stand assessment through LiDAR based forest visualization using immersive virtual environment technology. The systems mentioned include INFORMS, FMIS, Landscape Management System, and the Stand Visualization System (SVS), all of which aimed for higher perceptional effectiveness in forest visualization. These systems use advanced graphics techniques and display technologies to develop fully interactive 3D visualizations, referred to as immersive virtual environments (IVE). IVEs are used in many fields including vehicle simulations, entertainment, architectural design, medicine and surgery, and education, and the potential use of the technology for forest visualization was first noted by McGaughey and Carson (2003).

In their research, Fujisaki et al. (2007) set up an experiment to compare IVE methods to field recorded videos of immature and mature loblolly pine (*Pinus taeda*) stands in Mississippi. LiDAR data was used to create a virtual forest, which was then projected with an interactive room-sized stereoscopic display, so that participants could 'walk' through the forest. Other participants viewed only the field video recordings of the stands. Study participants' estimates of stand characteristics were then compared, and significant differences were found in the two groups' estimates of height class and rotation stage, even though estimates of stocking, tree size class, stand structure, and hardwood competition were similar. These results led the researchers to conclude that IVE technologies and visualizations in general could be potentially useful in natural resources management, and that further study of the economic aspects and interface development were required to further develop such technologies into an operational system.

Stoltman et al. (2004) saw visualization of forests as a pathway for public participation in the forest planning process. Working within the state of Wisconsin, USA, these researchers noticed that visualization technology at the time was used solely by researchers and consultants, and not by natural resource managers. The authors reviewed a 3D forest visualization system, developed for use by the Wisconsin Department of Natural Resources, which incorporated a library of photographs of trees, snags, and logging debris to realistically depict forest management activities. The system was linked to a GIS so that available forest survey data could be incorporated, and was built to be as user friendly as

possible, for use by managers without extensive computer knowledge. The authors found the system to be a success, noting that computer visualization of forest management facilitated continued public involvement in forest management. The key, the authors claimed, is getting the system into the hands of managers. Finally, the authors state that the development of forest visualization parallels the development of GIS, moving from being in the hands of only a few computer-literate individuals to being widely used by the broad scientific and natural resource management community.

Similarly, Kopytko et al. (2008) attempted to connect resource managers to visualizations and in doing so connect the managers with ecologists attempting to answer fundamental scientific questions regarding the natural world. This research points out the fundamental differences between how ecologists conduct their research and how managers make decisions. The translation of ecological values into management procedures is difficult, but there exists a push from the public to incorporate ecological values into decision making, in addition to traditional revenue maximization. The results of this research allowed for better characterization of canopy crowns, with an informatics tool to provide structure summaries that better enable people to look at the data and classify or cluster trees according to structural similarity. This said, the authors noted that new information technology was still needed to accomplish the ecology research goals, including 1) interpolation and extrapolation of missing data on geographically complex topographies, 2) better models and tools to develop complex situations,

and 3) better pattern recognition and visualization so data can be compared and contrasted.

METHODS

This section describes the methods used in this thesis research to achieve data visualization. Before visualization with FUSION could begin, the software requires that a FUSION project be built from various sources of data. First the raw LiDAR data was loaded. The original LiDAR data acquisition completed by Watershed Science, Inc., segmented the LiDAR data into 500 mB bins, which separated ground returns into 'ground bins', and canopy or non-ground returns into high_bins (Spies et al., 2011). This segmentation was done because otherwise the size of the data file would have been exceptionally large; it also separated ground returns from canopy returns which simplified analysis. Thus, the full HJA data set did not have to be loaded, but instead only the six bins that covered the spatial extent of WS1. The ground and high bins are related to one another by number, and the following ground and high bins were used: bin_017, bin_020, bin_21, bin_025, bin_026 and bin_031. Using the ground bins, a bare earth model was created in FUSION using the *ASCII raster terrain model* tool, which converts ASCII points from the bins into a .dtm file that FUSION can read and analyze. The ground bins were combined into one .dtm file, labeled All_WS1.dtm.

After the raw data and bare earth model were loaded, an image of WS1 was acquired. This image was downloaded from the USGS seamless image viewer/Oregon Imagery Explorer (http://nationalmap.gov/viewer.html) This site has orthophotographs for the entire state of Oregon, and the online interface

allows a user to zoom into an area, select the extent of image desired, and download the image as a 4 band National Agriculture Imagery Program (NAIP) image. An orthophotograph is an aerial image that is geometrically corrected, or orthorectified, so that the scale is uniform and distances can be accurately measured on the image itself. After the orthoimage was loaded into FUSION, the vegetation plot point shapefile (created during hemispherical photograph analysis (Chapter 2) was loaded into FUSION as a *point of interest* (POI) file.

Visualization of LiDAR Data for Plots and Transects

Once all the required data files were loaded into FUSION, creating visualizations using LDV was straightforward. In the FUSION interface a user can *stoke* or select any size rectangle or circle and LiDAR Data Viewer (LDV) automatically loads with the selected data visualized. The *sample options* button in the FUSION user interface was utilized to create original visualizations of the LiDAR point cloud for each plot and wider views of entire transects in which DHPs were taken. Since the plot centers were loaded into FUSION as a POI file, *snap sample points to nearest POI point* was selected from the options menu. Also, since a ground model had been loaded, the *subtract ground elevation from each return* was selected to normalize the point cloud, and give elevation of points above the ground rather than above sea level. The sample shape selected was a *fixed circle* with a diameter of 18 meters (to align with the 9 meter radius plots). The set shape, along with the snapping to the nearest POI ensured that not only a user click near a plot aligned with the center of the plot, but also that the outer edge of

the selection was matched to the plot itself. The visualizations of each plot were colored by height, normalized by ground model (Figures 37-55, left).

Visualization of TreeVaW Output Trees

Special help for this section of the thesis came from Lee Zeman, a collaborator on the VISTAS project who created images of TreeVaW's output using the visual programming language *Processing* (http://processing.org). The position and heights of the trees were read from TreeVaW's output files. DBH was approximated from height using the allometric equations given in Garman (1995); crown radius was approximated from DBH using the two-term allometric equation given in Gill (2000). All trees were assumed to be *Psuedotsuga menziesii*.

RESULTS

Watershed 1 Visualizations

Figures 33-36 are visualizations of LiDAR data created using FUSION software.

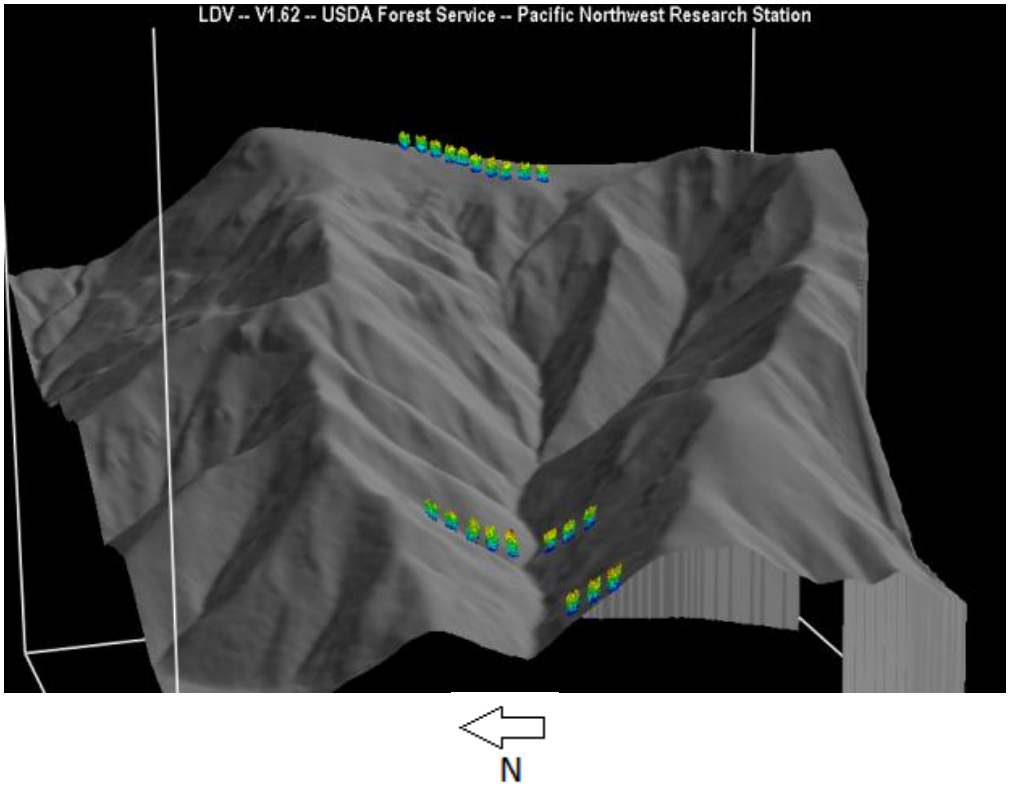

Figure 33. FUSION visualization of WS1 Digital Elevation Model (DEM) and LiDAR data of 19 vegetation plots where digital hemispherical photographs were taken.

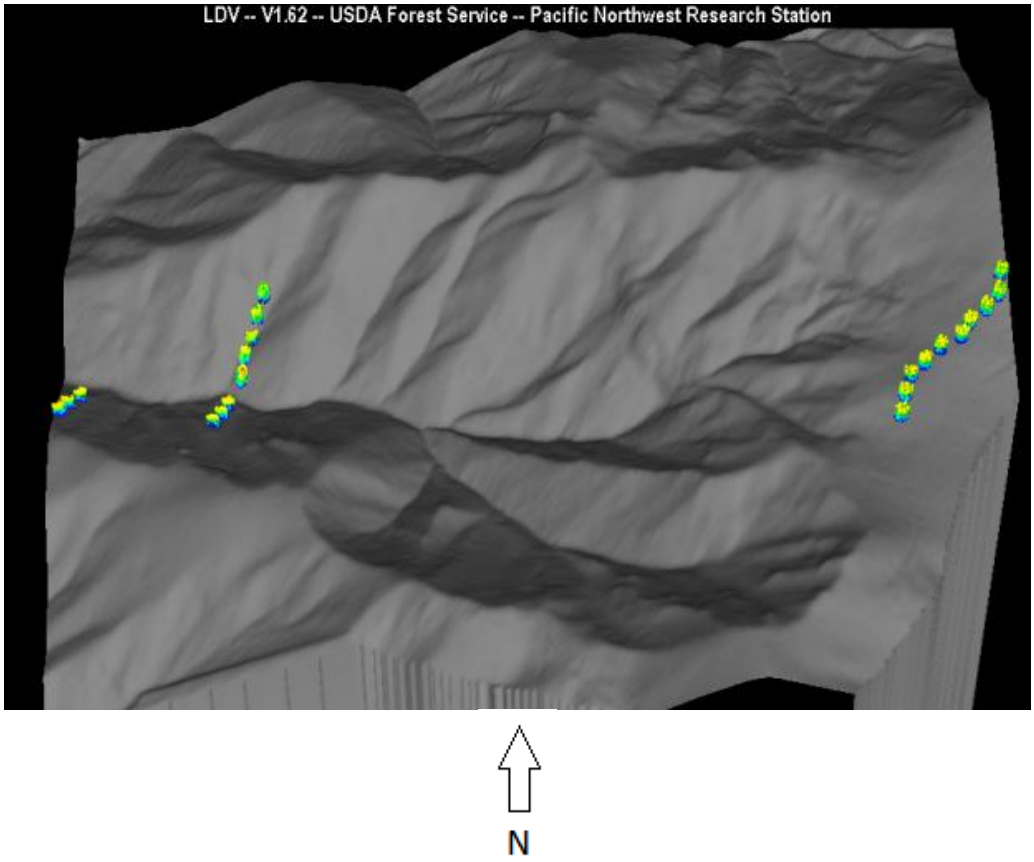

Figure 34. Overhead view visualization of WS1 DEM and LiDAR data of vegetation plots.

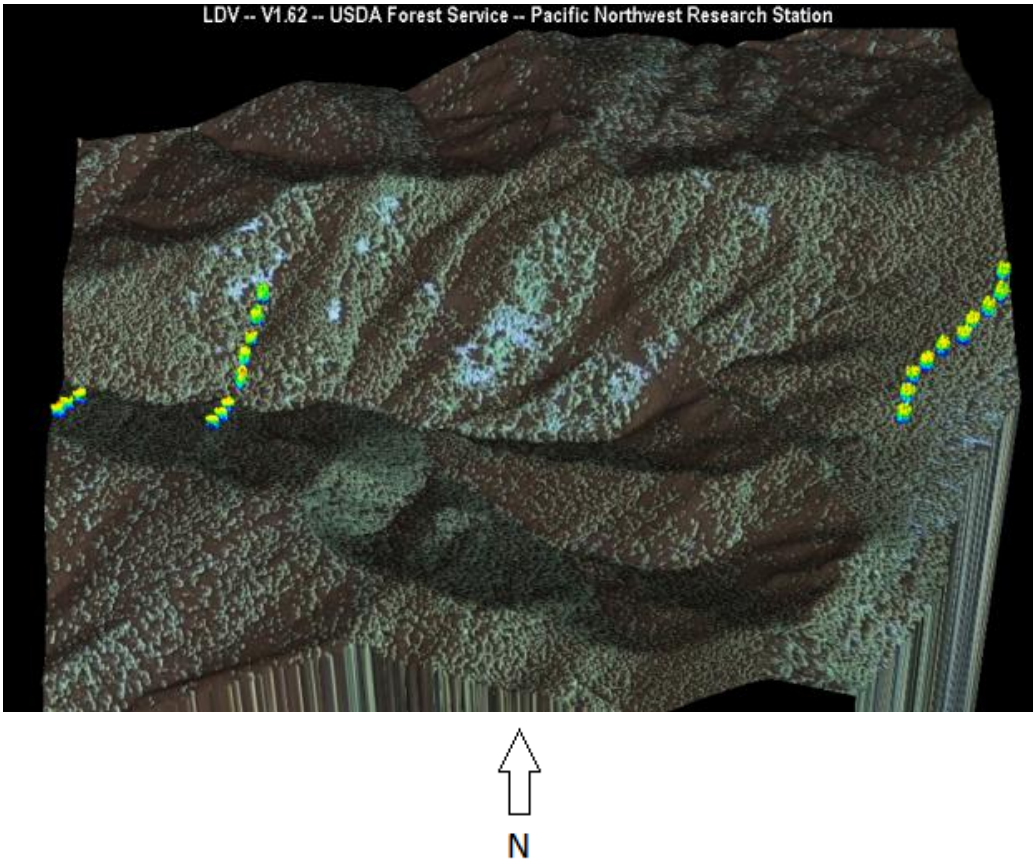

Figure 35. Overhead view visualization of WS1 DEM and LiDAR data of vegetation plots with digital orthophotograph of vegetation in the Watershed overlaid.

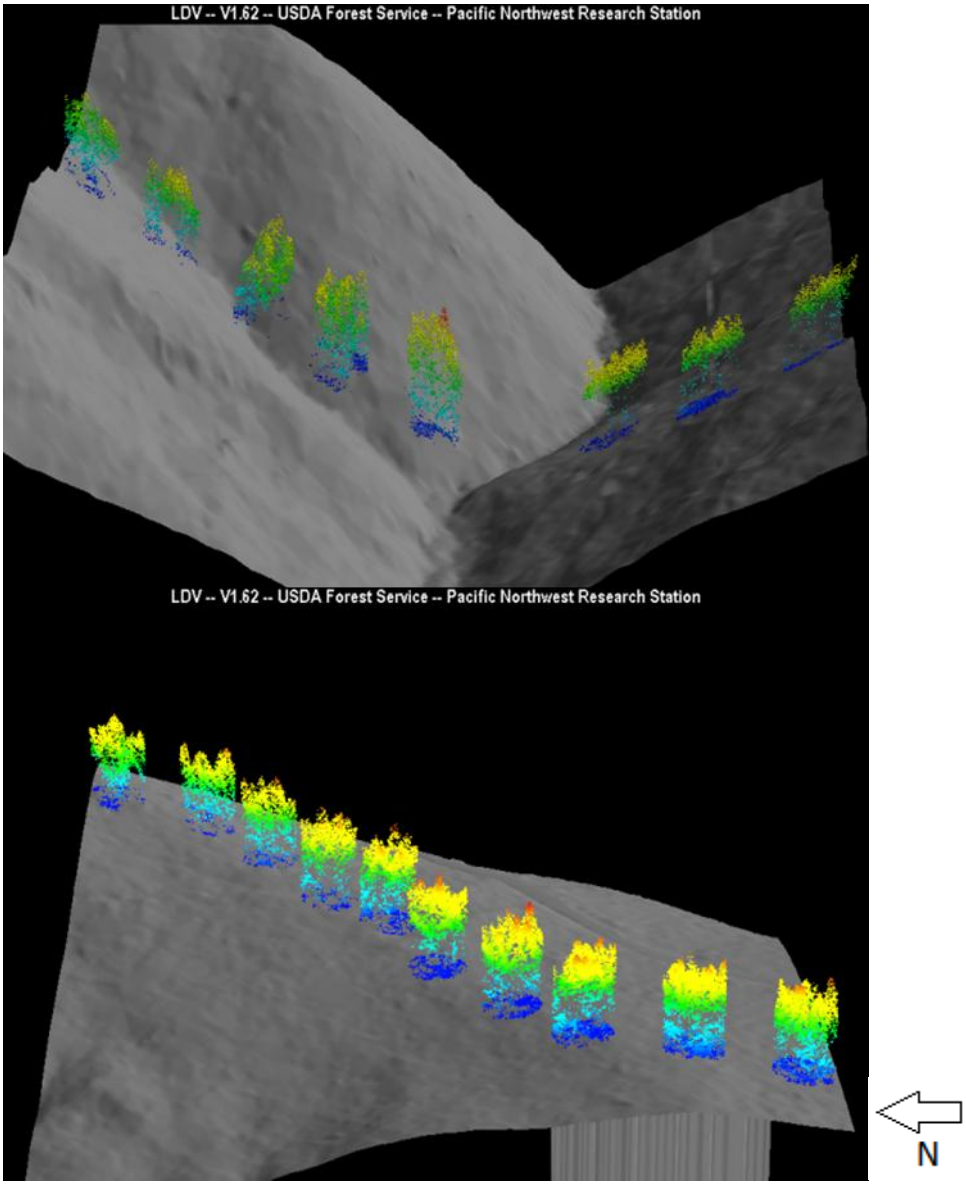

Figure 36. Visualization of LiDAR data and DEM of vegetation plots in transect 2 (above) and transect 6 (below).

Visualizations of LiDAR Point Cloud and TreeVaW Identified Trees

Figures 37-55 are visualizations created for each plot where digital hemispherical photographs were taken for LAI measurements (see Chapter 2). The image on the left of each figure is the visualization produced with FUSION, and the image on

the right is the visualization of trees identified using TreeVaW, created using *Processing* from data output by TreeVaW.

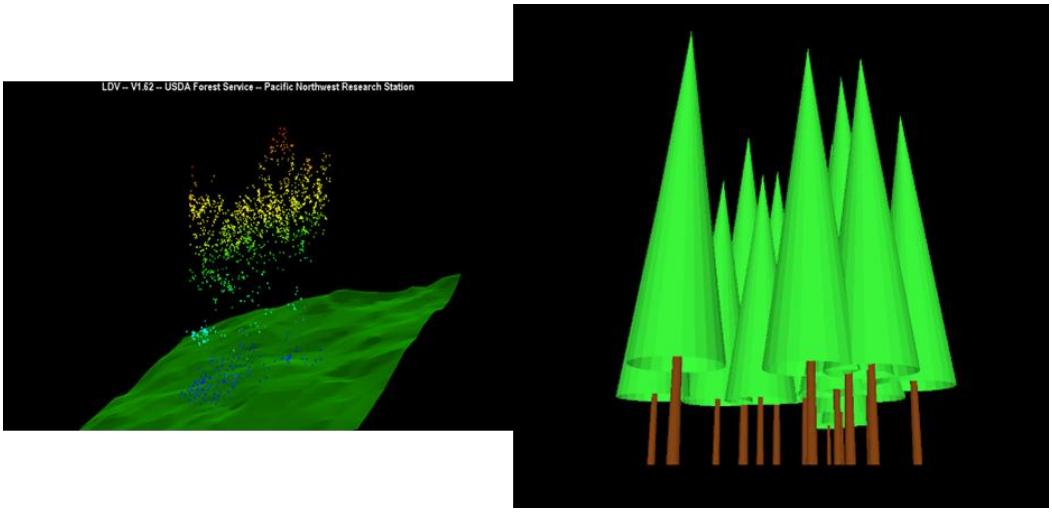

Figure 37. Transect 1, plot 9.

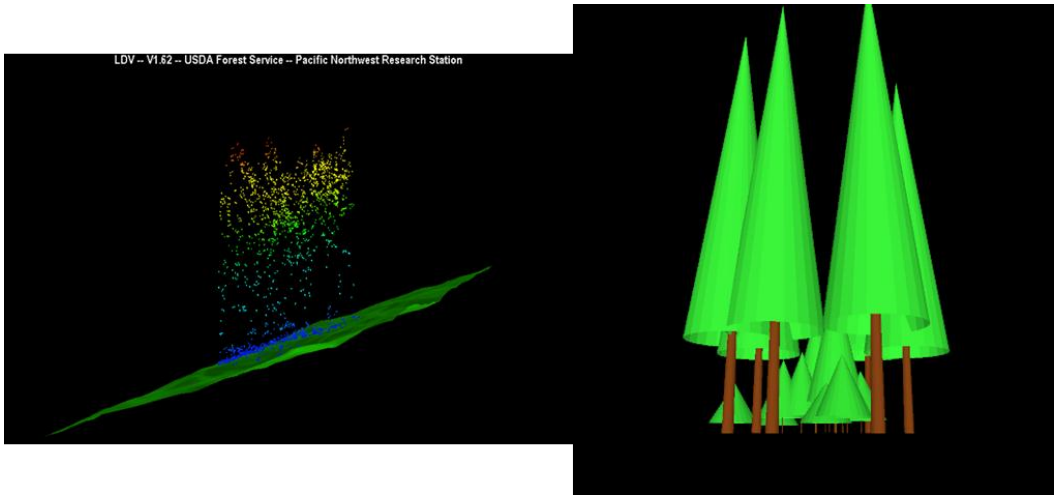

Figure 38. Transect 1, plot 10.

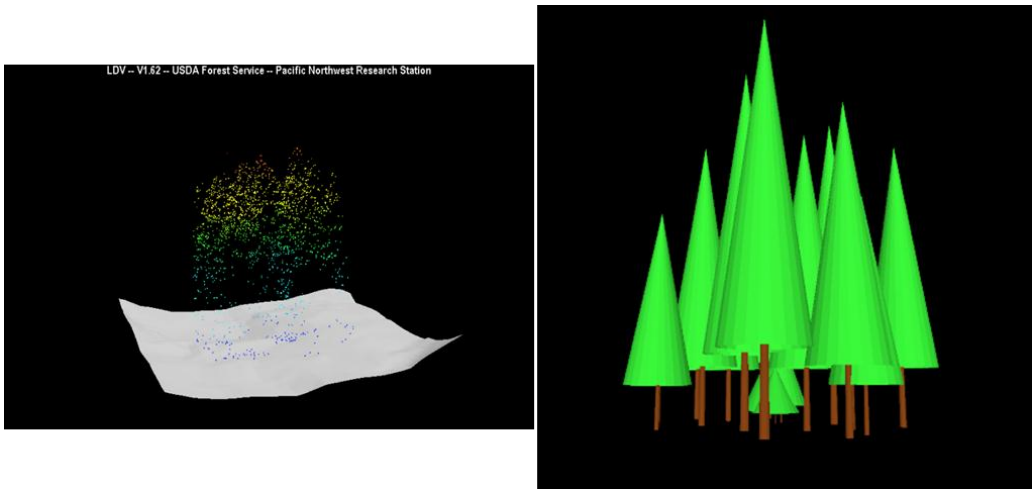

Figure 39. Transect 2, plot 5.

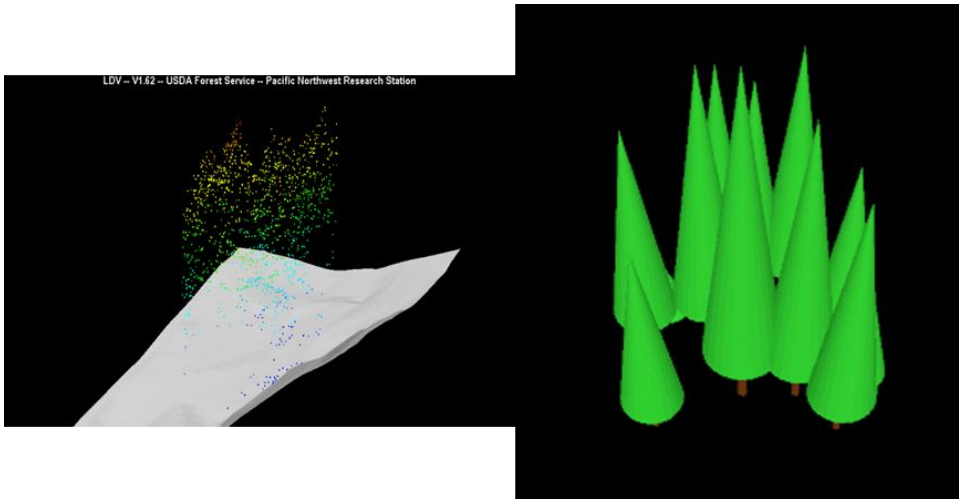

Figure 40. Transect 2, plot 6.

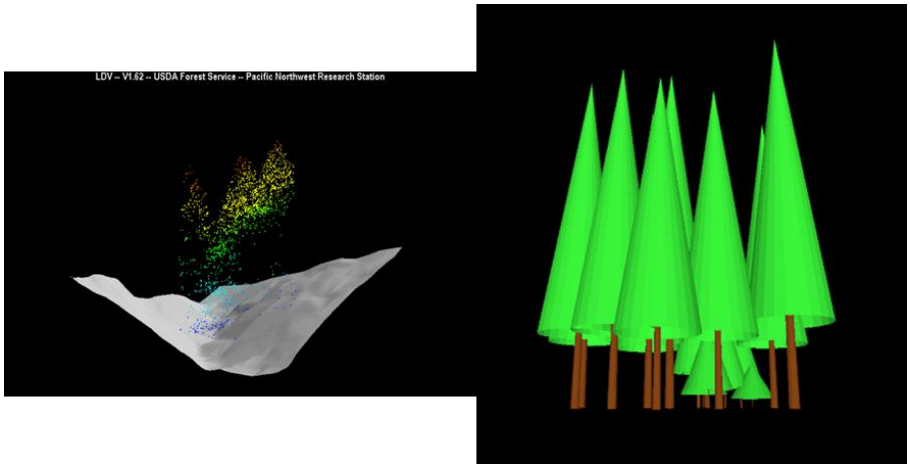

Figure 41. Transect 2, plot 7.

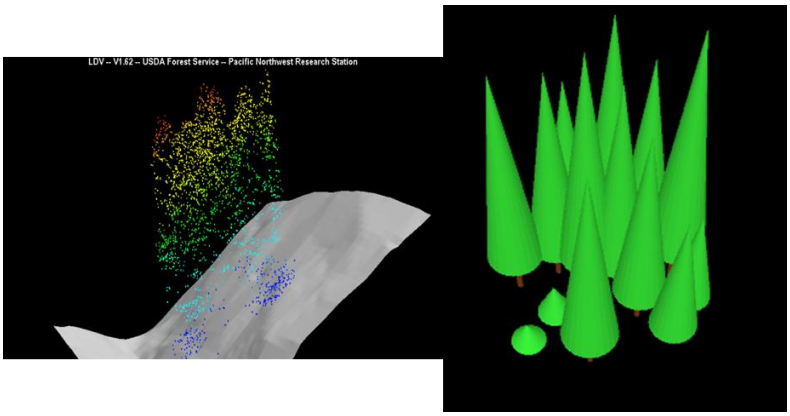

Figure 42. Transect 2, plot 8.

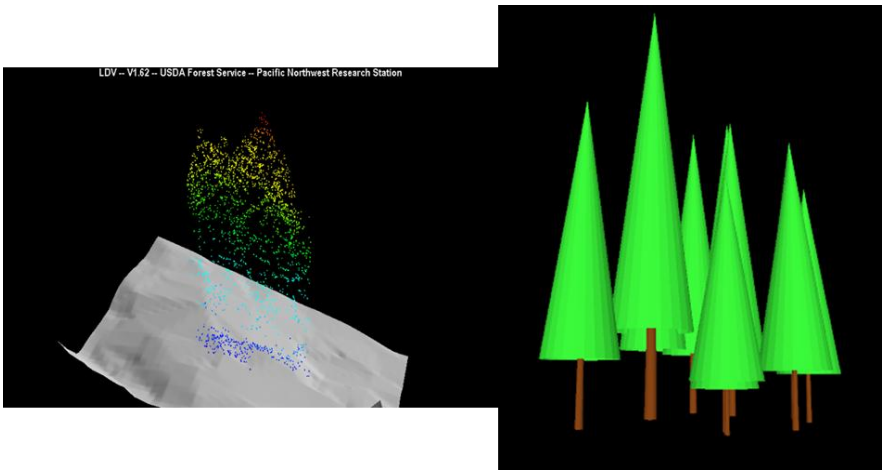

Figure 43. Transect 2, plot 9.

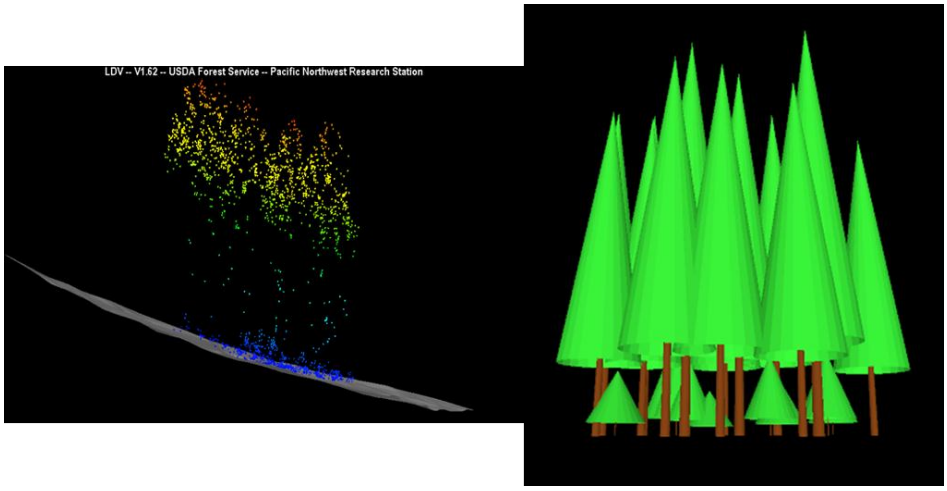

Figure 44. Transect 2, plot 12.

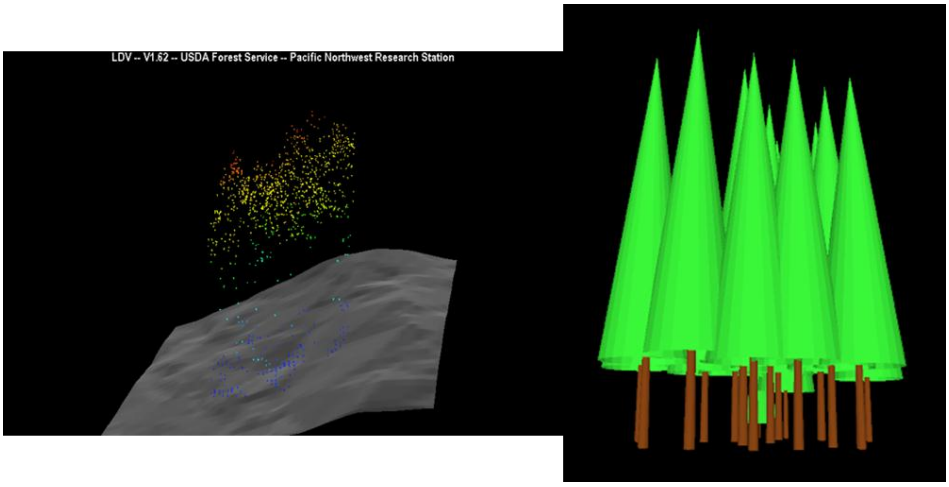

Figure 45. Transect 2, plot 13.

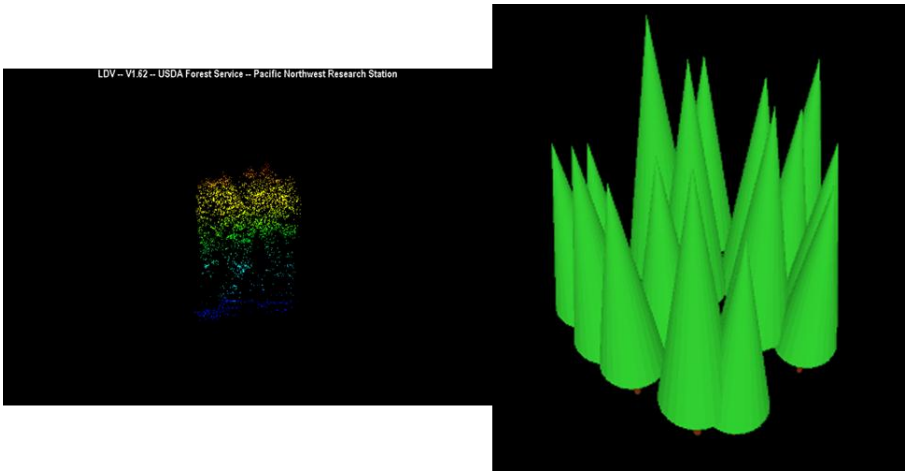

Figure 46. Transect 6, plot 8.

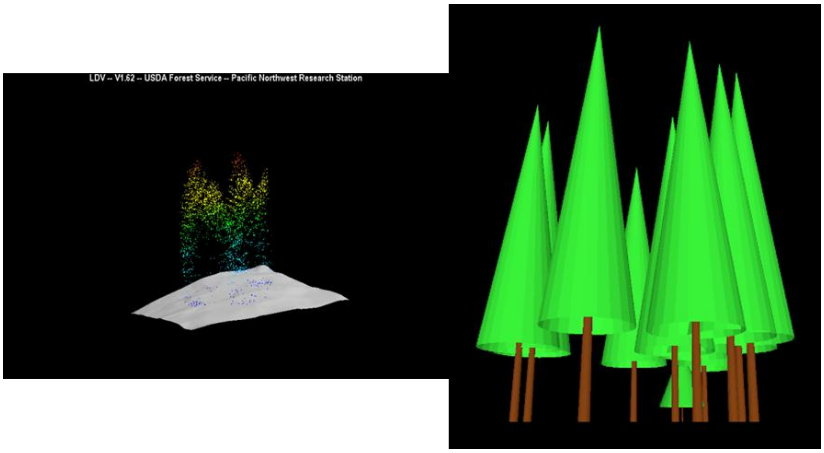

Figure 47. Transect 6, plot 9.

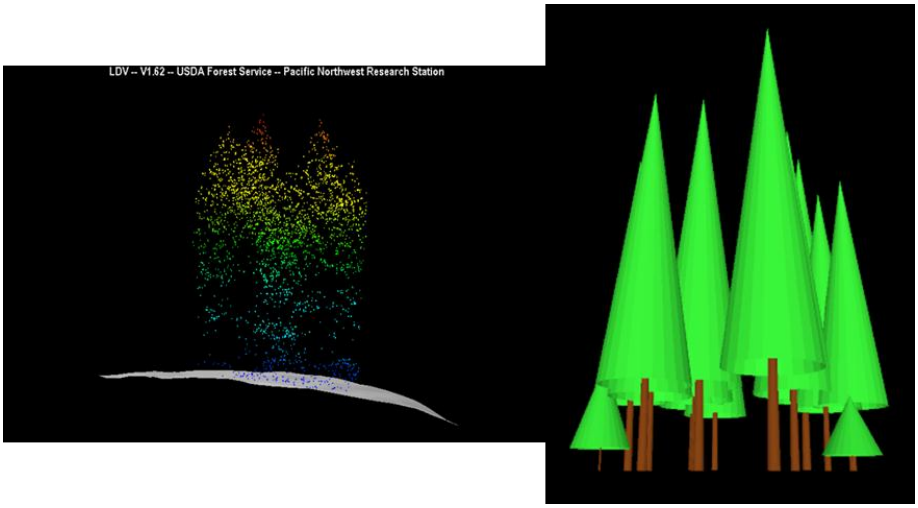

Figure 48. Transect 6, plot 10.

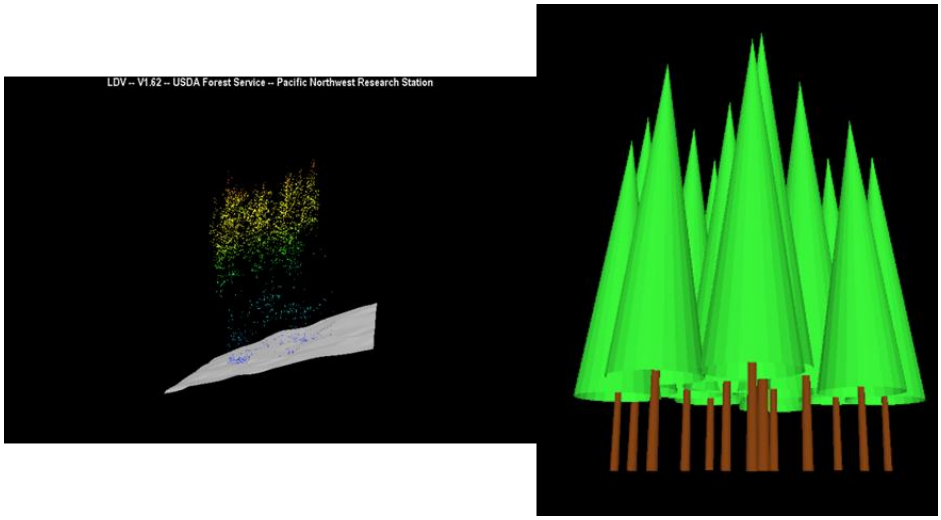

Figure 49. Transect 6, plot 11.

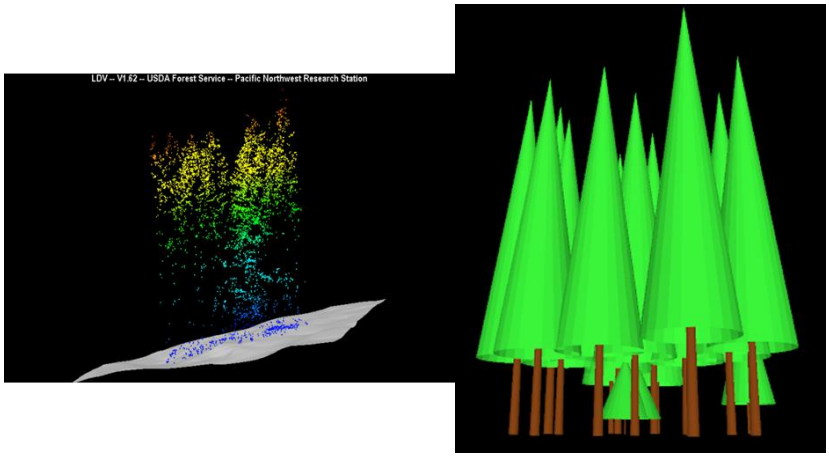

Figure 50. Transect 6, plot 12.

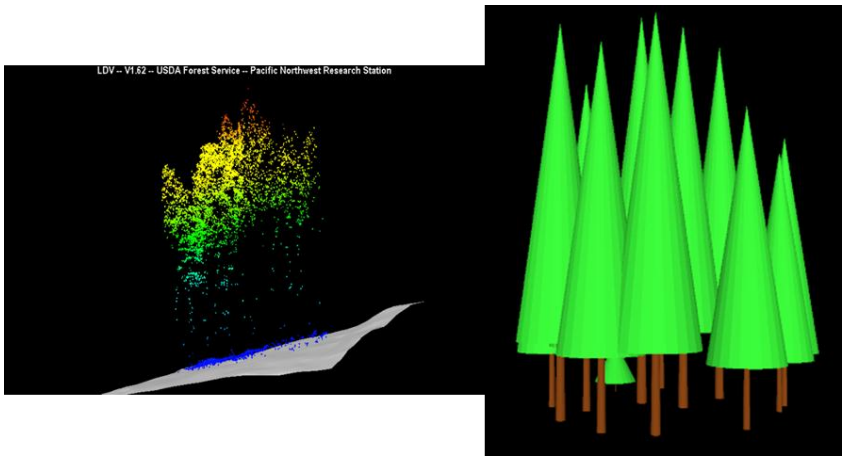

Figure 51. Transect 6, plot 13.

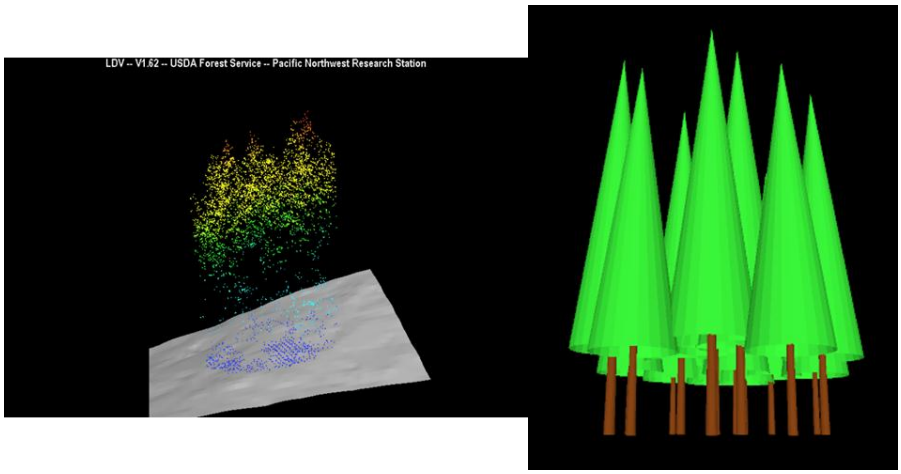

Figure 52. Transect 6, plot 14.

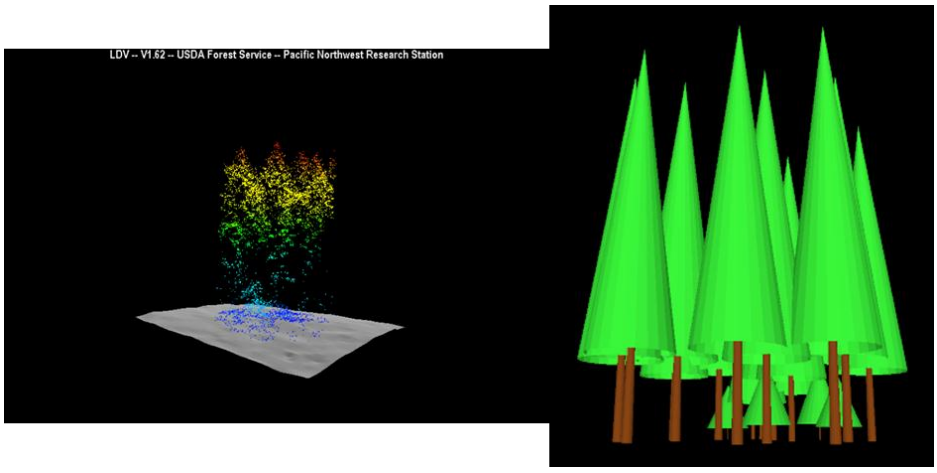

Figure 53. Transect 6, plot 15.

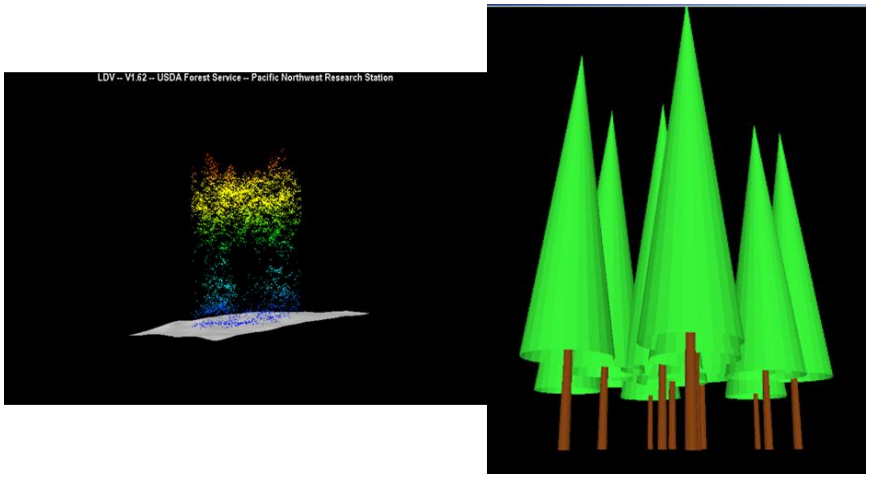

Figure 54. Transect 6, plot 16.

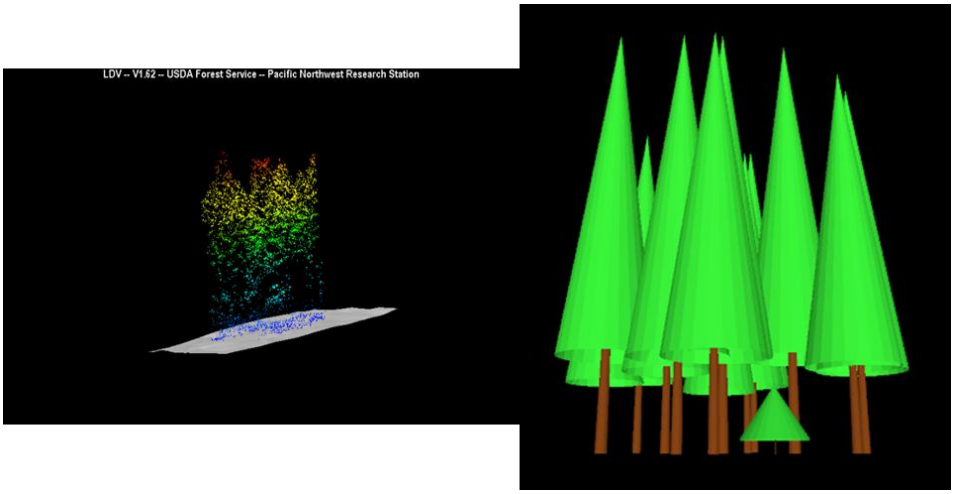

Figure 55. Transect 6, plot 17.

DISCUSSION

The FUSION visualizations of LiDAR data using are presented above. These visualizations show the lay of the land in WS1, highlighting the steepness of the terrain and the denseness of the forest canopy within the vegetation stands. These images show why estimation of LAI has been a difficulty in the past (see Chapter 2), and why on complex terrain with variable stand composition, visualization of forest structure has continued to be an issue even within this thesis.

The visualizations of 3D stem maps from the TreeVaW output are also presented. These images show the trees identified by TreeVaW in 19 vegetative plots in the WS1. However, since no x-y location information was available for the vegetation surveys, similar visualizations of the surveyed trees could not be completed. Although stem maps exist for some of the plots in WS1, they are not readily available and have not been verified recently enough to compare to LiDAR derived metrics and TreeVaW visualizations (Peterson, personal communication; Wooley, personal communication). If recent stem maps from the watershed's vegetation plots could be verified a visual comparison could be made. One purpose visualizing the TreeVaW output is to visually examine the trees that TreeVaW identified. With those visualizations, it became clear that where a thick over story of taller trees is present, as in P11109 (Figure 37) and P11616 (Figure 54). TreeVaw is able to identify more trees and predict their heights more accurately than where stand composition is complex, and understory trees are present in P11211 and P11212 (Figure 44). In the field, these two plots (P11109 and P11616) fall on areas where harvest regeneration attempts were highly successful. The north-facing aspect of WS1 was replanted with 1-1 seedlings (1 year total age, 1 year development at the nursery) only once, but soil conditions (deep, moist) fostered early coniferous development. Transect 1, at a low elevation, also has sufficient belowground moisture to foster a dense stand for much of the year. Transect 6, located along the ridgeline, is very near the second original landing from the harvest event. Areas around the landing were replanted specially, and they have very flat slopes and deep soils. Tree growth on this plot is

particularly well organized, with 1-1 and 2-1 (2 years total age, 1 year development at the nursery) seedlings planted in row arrangement that is still visible today. Strong canopy coverage from these successful plantings, combined with purposeful row spacing, leads to the development of a healthy overstory and precludes the establishment of understory species, with the exception of hardy shrubs. Thus, we note that on these plots, TreeVaw did not identify many, if any, smaller trees in the understory. However, where there were gaps present in the taller trees, such as P11110 (Figure 38) and P11208 (Figure 42) TreeVaW was better able to identify the smaller trees found underneath these gaps. On P11110, a windthrow event, likely corresponding with the floods of 1994-1995 and the odd weather patterns that season, caused great instantaneous mortality leading to the establishment of gaps. These gaps were readily seeded by *Tsuga heterophylla* blown in from neighboring stands. On P11208, which is located on the south facing slope, the presence of local topography, specifically a basaltic caprock feature, does not allow for the contiguous establishment of deep rooted conifers, thus smaller trees such as *Prunus emarginata, Cornus spp.,* and *Castanopsis chrysophylla* have established, needing less belowground resources for growth and structure and benefiting from the increased radiation on the south-facing slope (Peterson, 2012).

Visualization in Ecosystem Monitoring and Processes

The research presented in the introduction of this chapter explains how visualization of forests and trees have been used in forestry management; separate from this is visualization of forest stands for the purposes of understanding

ecosystem processes and function. Few articles in the literature have focused on visualization of ecological phenomena for purposes of understanding these basic ecological phenomena and functions. Below, I selected a short list of these studies.

Krisp (2004) examined the use of 3D visualization to measure ecological barriers to movement for species in Finland. To build a model for visualizing the effects of barriers, the authors assumed that different land covers and land uses have a dissimilar impact on wildlife movement, and they assigned a qualitative value to each landscape component considered, on a species-species basis. In general, the values assigned were low for natural elements and high for artificial ones. Then, by linking the qualitative value to the landscape components in a map the movement limitations for species could be assessed, first using a 2D map, and then a 3D map that had the ability to change the perspective or view. This work of modeling barrier effects in 3D can help visually identify ecological corridors, networks or bottlenecks. This research represents early work in environmental phenomena visualization.

Omasa et al. (2007) explored the use of LiDAR to produce 3D imaging not only for understanding canopy structure, similar to Chapter 3 of this thesis, but also for detecting and understanding plant responses to varying phenomena. The authors reviewed the development of LiDAR systems and their application from the leaf to canopy level remote sensing. Plant properties explored with 3D LiDAR imaging included canopy height, canopy structure, carbon stock, and species distribution, and plant responses (change in growth and shape) were also

assessed. Canopy height, an important variable needed to estimate the 3D properties of trees, was historically underestimated in LiDAR metrics because of low likelihood of pulses with a density of <1 pulse m-2 hitting the highest point on any given tree. More recently, high pulse densities have been used more often to solve this underestimation problem. Ground-based LiDAR provides a more precise 3D image of individual trees, with resolutions ranging from .05 -10 cm. Tree heights can be measured from these ground based systems, but if tree tops are blocked by other trees, estimating tree height can be difficult. A way around this problem is to take ground based LiDAR measurements in multiple locations around a tree of interest, and images from the different locations can be co-registered and merged.

Landscape Visualization

While visualization of forest processes has been scarce, visualizations of landscape phenomena have been more common. Paar (2005) examined the role of landscape visualization software for landscape and environmental planning in Germany. The author questioned hundreds of private consultancies and public authorities about the current and future use of 3D landscape visualizations in environmental decision making. Overall, the respondents had great expectations about where 3D visualizations would take landscape planning, with 91% of respondents believing that 3D visualizations would bring additional benefits to landscape planning. Many of the issues confronted by the respondents were based on software problems. Respondents who use visualization software mentioned technical problems, including insufficient representation of plants and habitats,

and slow rendering. The group representing ‘non-users’ of software mentioned the high cost of existing software as a barrier to use. Respondents from both groups mentioned training and usability of available software as a difficulty. The results of Paar’s surveys show that the application of visualizations facilitates improved communication between experts and laypersons, and the author concludes that new technological developments within computer graphics will continue to aid landscape planners and environmental managers with use of 3D landscape visualization tools, but that innovative, new 3D landscape visualization tools are needed to continue this trend.

Wang et al. (2006) described 3D visualizations of forest landscapes as “quantitative ecological information-based techniques that can be used to visualize forest structure, dynamics, landscape transformations and regional plans.” The authors posited that the use of existing public data sets to create visualizations can replace time consuming and expensive stand-level surveys. The authors utilized the Forest Inventory and Analysis d (http://www.fia.fs.fed.us) and several other existing vegetation databases to visualize a section of the Chequamegon National Forest in Wisconsin. The authors created visualizations from the individual stand to the landscape level, using two software packages: Tree Professional 5 and Visual Nature Studio 2.01, and concluded that public data sets are suitable and useful for visualizing the dynamics of forests and landscapes. This research shows that large pools of data are available, but they may be un- or under-utilized by researchers and decision makers.

Sherren et al (2011) examined lessons learned from visualizations of the landscape and in habitat assessment in the current trend of tree decline in Australia. The authors presented photo-realistic visualizations of landscapes to stakeholders representing the results of modeling of different future scenarios of tree decline. The visualizations represent likely outcomes of the 'status quo' compared to alternative tree planting remediation efforts in an attempt to show the consequences of each on landscape aesthetics and biodiversity. Through the visualizations the authors found that the current trend of tree decline is contrary to stakeholders' values concerning the region's social and ecological well-being. The authors showed that the visualizations could be used to create interdisciplinary collaboration and engage stakeholder involvement in forest management.

CONCLUSIONS

This chapter outlined the importance of visualizing forest and landscapes in the natural resource management and ecosystem research. Visualization of forest landscapes and structure for resource management has become common in recent years, but visualization of forest processes and function is just beginning. The data intensive nature of the work requires novel visualization tools to understand many and massive current data sets. Visualization also stands as a key communication tool in keeping decision makers, stakeholders and the general public connected and informed in decision making. The visualizations presented in this chapter suggest how LiDAR data might be used to visualize forest structure and represent actual trees. The use of remote sensing technologies such

as LiDAR greatly reduces the time, resources, and personnel needed to create visualizations for use in both natural resource management and ecosystem research.

Chapter 5- Conclusions and Future Research

This chapter summarizes conclusions already mentioned in Chapters 2-4, and looks forward to research directions for this field. The objectives of the thesis frame the following conclusions:

Thesis Objective 1: Determine accurate LAI estimates for a subset of permanent vegetation plots in WS1 using digital hemispherical photography (DHP)

Hemispherical photographs taken in 19 vegetation plots in WS1 were analyzed three different ways using SLIM software: 1) limiting the 'scope', or angle of view, to estimate for the plot only, 2) using a wider scope to estimate the immediate area around the plot, and 3) using the average LAI values for DHPs in four cardinal directions around the center of the plot. The three resulting estimates were not statistically correlated, which may be caused by either 1) the hillslope affecting the two wider measures of LAI, or 2) how light was measured in the DHPs for the software analysis.

Issues encountered in these LAI estimates are similar to previous work in WS1. The steepness of the terrain and the high vegetation density make accurate estimation of LAI very difficult.

Thesis Objective 2: Use estimates of LAI obtained from DHP to build a LiDAR based model of LAI for all 133 permanent vegetation plots

Using the estimates of LAI for the plots obtained from DHP, we developed a LiDAR based model to estimate LAI using the LiDAR metric surface volume, and used this to estimate LAI for all 133 vegetation plots in the watershed. The resulting LAI values also revealed a strong relationship when compared to

Cover*Height for each plot ($R^2 = 0.5467$, $p < 2.2e\text{-}16$). The use of LiDAR to estimate LAI for the watershed thus seems promising. The development of a LiDAR only model to estimate LAI is a possible solution to estimating LAI in steep, densely vegetated watershed, since LiDAR seems to adequately measure complex terrain.

Thesis Objective 3: Calibrate the LiDAR based model for LAI to create LAI maps for the entire watershed.

The LiDAR model for LAI could not be calibrated to create LAI maps for the watershed as a whole. A reason for this is the LiDAR derived volume metric used is not directly related to LAI, but rather to leaf area, which is mechanistically different because LAI incorporates ground area and is a dimensionless value (Richardson, personal communication). Because of this, TreeVaW software was used to estimate the total number of trees in the watershed, which could then be used with allometric relationships as an alternative for estimating LAI for the entire watershed. Future research will need to validate the number of trees in the watershed either through field measurements or another remotely sensed metric.

Thesis Objective 4: Test the ability of software programs to extract and identify individual trees from LiDAR data in all 133 permanent vegetation plots in WS1

The TreeVaW software program was used to extract and identify individual trees within all 133 vegetation plots in the watershed. Overall, TreeVaW identified over 82% of trees when compared to vegetation surveys completed in the plots. TreeVaW performed better in plots with lower tree density and those with taller

trees. TreeVaW was also used to identify all trees in the watershed, and identified nearly 77,300 trees. Since no comprehensive tree counts have been taken in the watershed the estimate of total trees could not be validated. However, the vegetation plots represent the entire range of slope, aspect, and elevation present in the watershed, it is reasonable to assume that the estimate of total trees would be comparable to the 82% of trees identified in the vegetation plots.

Thesis Objective 5: Create novel visualizations of LiDAR data and individual trees in the vegetation plots.

Visualizations were created from the LiDAR point cloud data using the FUSION and LiDAR Data Viewer (LDV) software. The output of individual trees from TreeVaW was also used to create 3D stem maps (stand visualizations) using the programming language *Processing* (http://processing.org). The latter visualizations clearly displayed gaps in the canopy of the plots where TreeVaW was better able to identify shorter trees, and also showed where the canopy was dense and limited TreeVaW's ability to identify understory trees.

Future Research Directions

This thesis research has answered some questions about LAI, LiDAR data and tree extraction, but has also made apparent potential directions for future research. First, a comprehensive look at why ground based measurements of LAI based on hemispherical photographs differ from LiDAR based methods is in order. The importance of LAI in ecosystems studies has been demonstrated by other prior research, but difficulties remain in obtaining accurate estimates LAI in densely vegetated, steep terrain. The use of LiDAR is promising for estimating LAI.

Incorporating slope correction into digital hemispherical photograph analysis and developing a site-specific model for correcting LiDAR estimates could make LAI estimates more accurate.

Secondly, a comprehensive examination of why TreeVaW performed very well in some vegetation plots but poorly in others is needed. The initial analysis showed that TreeVaW performed better in plots with lower tree density and taller trees. However, comparing the aspect, slope, or elevation of the plots may provide insight into what factors affected TreeVaW's identification of individual trees. Since the forest type in Texas, where TreeVaW was developed, differs considerably from the Pacific Northwest Cascades, changes to algorithms and the software itself may provide more accurate identification of trees. This could especially improve the estimates of crown width which were unusable for this research.

Thirdly, the visualizations of individual trees presented in this thesis could assist researchers in canopy gap research. These visualizations give the researcher the ability to "see" the size and shape of the gaps in the canopy, which could then be compared to remotely sensed metrics and topographic and climatic measurement. This gives the researcher the chance to assess variability on a subplot scale, without having to break the data down to the subplot scale.

Finally, further empirical data needs to be gathered to validate the estimations of LAI, number of trees, and tree heights at the individual tree scale. Current field measurements of LAI are inconsistent, and repeated sampling of the same geographic locations under a variety of seasons and meteorological

conditions could help determine which measures are most accurate under which conditions. The number of trees in the entire watershed also needs to be calculated to assess TreeVaW's accuracy on the watershed scale, perhaps from derived metrics other than the LiDAR data (local "peaks" in height at a sub-crown diameter scale). Finally, validation of tree heights from the ground needs to be conducted specifically on WS1; although some validations exist for the LiDAR data on the H.J. Andrews at large, these measurements were taken from the tallest trees (old growth) and may not be applicable to those on WS1.

The ability to accurately map individual trees and measure LAI on a watershed scale is increasingly important in both forest ecosystem research and management. This thesis combines ground and remotely sensed methods to measure LAI and utilizes current state-of-the-art software to identify individual and visualize individual trees. This research represents an interdisciplinary approach to solving complex environmental questions, and contributes novel analysis to the field. Moving forward, the combination of visualization, remote sensing analysis and software programming can move us closer to understanding environmental phenomena and processes from an ecological and management perspective.

LITERATURE CITED

Adams, T., P. Beets, and C. Parrish. 2012. Extracting more data from lidar in forested areas by analyzing waveform shape. Remote Sensing **4**: 682-702

Andersen, H.E., S. Reutebuch and G.F. Schreuder. Automated individual tree measurement through morphological analysis of LiDAR-based canopy surface model. Proceedings of the First International Forestry Cooperative Symposium. Seattle, WA. 2001.

Barilotti, A., S. Turco, and G. Alberti. 2006. LAI determination in forestry ecosystems by lidar data analysis. 3D Remote Sensing in Forestry international workshop. Online (www.wau.boku.ac.at/fileadmin/_/.../3drsforestry/.../8b.3-barilotti.pdf). Accessed 24 November 2012.

Barilotti, A., and S. Turco. 2006. A 3-D GIS for the sustainable management of forest resources. IUFRO Landscape Ecology Conference, Locorotondo, Bari, Italy. Online (http://geomatica.uniud.it/pubblicazioni/pdf/2006/IUFRO%2006%20Barilotti.pdf) Accessed 24 November 2012.

Barilotti, A., F. Sepic, E. Abramo, and F. Crosilla. 2007. Improving the morphological analysis for tree extraction: a dynamic approach to lidar data. ISPRS Workshop on Laser Scanning 2007 and SilviLaser 2007, Finland. Online (www.isprs.org/proceedings/XXXVI/3-W52/.../Barilotti_2007.pdf). Accessed 24 November 2012.

Barilotti, A., and F. Sepic. 2010. Assessment of forestry parameters at single-tree level by using methods of lidar data analysis and processing. Ambiência Guarapuava **6**: 81-92.

Bartelink, H.H. 1996. Allometric relationships on biomass and needle area of douglas-fir. Forest Ecology and Management **86**: 193-203.

Bergen, S.D., R.J. McGaughey and J.L. Fridley. 1998. Data-driven simulation, dimensional accuracy and realism in a landscape visualization tool. Landscape and Urban Planning **40**: 283-293.

Bond, B.J., J.A. Jones, G. Moore, N. Phillips, D. Post and J.J. McDonnell. 2002. The zone of vegetation influence on baseflow revealed by diel patterns of streamflow and vegetation water use in a headwater basin. Hydrological Processes **16**: 1671-1677.

Breda, N.J.J. 2003. Ground-based measurements of leaf area index: a review of methods, instruments, and current controversies. Journal of Experimental Botany **54**(392): 2403-2417.

Carlson, T.N., and D.A. Ripley. 1997. On the relation between NDVI, fractional vegetation cover, and leaf area index. Remote Sensing of Environment **62**: 241-252.

Chen, J.M. and T.A. Black. 1992. Defining Leaf-Area Index for non-flat leaves. Plant Cell Environment **15**: 421-429.

Chen, J.M., and J. Cihlar. 1995. Plant canopy gap-size analysis theory for improving optical measurement of leaf area index. Applied Optics **34**(27): 6211-6222.

Chen, X., L. Vierling, E. Rowell, and T. DeFelice. 2004. Using lidar and effective LAI data to evaluate IKONOS and landsat 7 ETM+ vegetation cover estimates in a ponderosa pine forest. Remote Sensing of Environment **91**: 14-26.

Chen. Q., D. Baldocchi, P. Gong and M. Kelly. 2006. Isolating individual trees in a savanna woodland using small footprint lidar data. Photogrammetric engineering and Remote Sensing. **72**(8): 923-932.

Chertov, O., A. Komarov, G. Andrienko, N. Andrienko, and P. Gatalsky. 2002. Integrating forest simulation models and spatial-temporal interactive visualization for decision making at landscape level. Ecological Modelling **148**: 47-65.

Clark, J. and G. Murphy. 2011. Estimating forest biomass components with hemispherical photography for Douglas-fir stands in northwest Oregon. Canadian Journal of Forest Research. **41**: 1060-1074.

Cohen, W.B., T.A. Spies, R.J. Alig, D.R. Oetter, T.K. Maiersperger, and M. Fiorella. 2002. Characterizing 23 years (1972-95) of stand replacement disturbance in western Oregon forests with landsat imagery. Ecosystems **5**(2): 122-137.

Comeau, Phil. LITE and SLIM Programs for Estimating Light Levels Beneath Tree Canopies.
http://www.ualberta.ca/~pcomeau/Light_Modeling/Lite_and_slim_intro.html
Accessed April 2012.

Coops, N.C., T. Hilker, M.A. Wulder, B. St-Onge, G. Newnham, A. Siggins, and J.A. Trofymow. 2007. Estimating canopy structure of douglas-fir forest stands from discrete return lidar. Trees **21**: 295-310.

Curtis, R.O. 1967. Height-diameter and height-diameter-age equations for second-growth douglas-fir. Forest Science **13**(4): 365-375.

Cushing, J. VISTAS Project Summary. National Science Foundation (NSF) proposal number 1062572. http://blogs.evergreen.edu/vistas

Cutini, A., G. Matteucci, and G. Mugozza. 1998. Estimation of leaf area index with the Licor LAI 2000 in deciduous forests. Forest Ecology and Management. **105** (1-3) 55-65.

Deblonde, G., M. Penner, and A. Royer. 1994. Measuring leaf area index with the li-cor LAI-2000 in pine stands. Ecology **75**(5): 1507-1511.

Dubayah, R., R. Knox, M. Hofton, J.B. Blair, J. Drake. Land surface characterization using lidar remote sensing. Pages 25-55 in Hill, M.J., and R.J. Aspinall. 2000. Spatial Information for Land Use Management. Gordan and Breach Science Publishers, The Netherlands.

Dufrene, E. and N. Breda. 1995. Estimation of deciduous forest leaf area index using direct and indirect methods. Oecologia **104**: 156-162.

Edson, C., and M.G. Wing. 2011. Airborne light detection and ranging (lidar) for individual tree stem location, height, and biomass measurements. Remote Sensing **3**: 2494-2528.

Erdody, T.L., and L.M. Moskal. 2008. Lidar derived canopy fuel metrics for wildlife modeling. Factsheet #4 Remote Sensing and Geospatial Application Laboratory, University of Washington, Seattle, WA. Online (http://dept.washington.edu/rsgal/). Accessed 24 November 2012.

Espana, M.L., F. Baret, and M. Weiss. 2008. Slope correction for LAI estimation from gap fraction measurements. Agricultural and Forest Meteorology **148**: 1553-1562.

ESRI (Environmental Systems Resource Institute). 2012. ArcMap 10. ESRI, Redlands, California.

Evans, J.R. and H. Poorter. 2001. Photosynthetic Acclimation of plants to growth irradiance. Specific Leaf Area and N-fixation. Plant, Cell and Environment **24**: 755-767.

Evans, J.S., and A.T. Hudak. 2007. A multiscale curvature algorithm for classifying discrete return lidar in forested environments. IEEE Transactions on Geoscience and Remote Sensing **45**(4): 1029-1038.

Falkowksi, M.J., A.M.S. Smith, P.E. Gessler, A.T. Hudak, L.A. Vierling, and J.S. Evans. 2008. The influence of conifer forest canopy cover on the accuracy of two individual tree measurement algorithms using lidar data. Canadian Journal of Remote Sensing **34**(2): S1-S13.

Feng, L., P. de Reffye, P. Dreyfus, and D. Auclair. 2012. Connecting an architectural plant model to a forest stand dynamics model—application to Austrian black pine stand visualization. Annals of Forest Science **69**: 245-255.

Frazer, G.W., J.A. Trofymow, and K.P. Lertzman. 2000. Canopy openness and leaf area in chronosequence of coastal temperate rainforests. Canadian Journal of Forest Research **30**(2): 239-256.

Fry, B. and Reas, C., Processing Library for Visual Arts and Design, http://www.processing.org. Accessed November 2012.

Fujisaki, I., D.L. Evans, R.J. Moorhead, D.W. Irby, M.J. Mohammadi-Aragh, S.D. Roberts, and P.D. Gerard. (2008) Stand assessment through LiDAR-based forest visualization using immersive virtual environment technology. Forest Science **54**(1): 1-7.

Garcia, M., D. Riano, E. Chuvieco, and F.M. Danson. 2010. Estimating biomass carbon stocks for a Mediterranean forest in central Spain using lidar height and intensity data. Remote Sensing of Environment **114**: 816-830.

Garman, S.L., S.A. Acker, J.L. Ohmann, and T.A. Spies. 1995. Asymptotic height-diameter equations for twenty-four tree species in western Oregon. Research contribution 10. College of Forestry Forest Research Laboratory, Oregon State University, Corvallis, OR. Online (ir.library.oregonstate.edu/xmlui/handle/1957/7655). Accessed 24 November 2012.

Gholz, H.L., C.C. Grier, A.G. Campbell, and A.T. Brown. 1979. Equations for estimating biomass and leaf area of plants in the pacific northwest. Research paper 41, Forest Research Lab, School of Forestry, Oregon State University, Corvallis, OR.

Gonsamo, A., and P. Pellikka. 2008. Methodology comparison for slope correction in canopy leaf area index estimation using hemispherical photography. Forest Ecology and Management **256**: 749-759.

Gonsamo, A., J.N. Walter, and P. Pellikka. 2010. Sampling gap fraction and size for estimating leaf area and clumping indices from hemispherical photographs. Canadian Journal of Forest Research **40**: 1588-1603.

Goodwin, N.R., N.C. Coops, and D.S. Culvenor. 2007. Development of a simulation model to predict lidar interception in forested environments. Remote Sensing of Environment **111**: 481-492.

Grier, C.C. and R.H. Waring. 1974. Conifer foliage mass related to sapwood area. Forest Science. **20**: 205-206.

Halpern, C. and J. Means. 2011. Pacific Northwest Plant Biomass Component Equation Library. Long-Term Ecological Research. Forest Science Data Bank, Corvallis, OR. [Database]

Hawk, G.M. 1970. Vegetation and stem mapping of watershed 10 H.J. Andrews experimental forest. Internal Report 97 US Internal Biological Program, Coniferous forest biome. Online (andrewsforest.oregonstate.edu/pubs/pdf/pub1862.pdf). Accessed 24 November 2012.

He, Q., C. Cao, E. Chen, G. Sun, F. Ling, Y. Pang, H. Zhang, W. Ni, M. Xu, Z. Li, and X. Li. 2012. Forest stand biomass estimation using ALOS PALSAR data based on lidar-derived prior knowledge in the Qilian mountain, western China. International Journal of Remote Sensing **33**(3): 710-729.

Heritage, G. and A. Large, eds. Laser Scanning for the Environmental Sciences. Wiley-Blackwell, 2009.

Hirata, Y., N. Furuya, M. Suzuki and H. Yamamoto. 2009. Airborne laser scanning in forest management: Individual tree identification and laser pulse penetration in a stand with different levels of thinning. Forest Ecology and Management **258**: 752-760.

H.J. Andrews Experimental Forest LTER. http://andrewsforest.oregonstate.edu/ 2011. Accessed June 2012.

Hopkinson, C., and L.E. Chasmer. 2007. Modelling canopy gap fraction from lidar intensity. ISPRS Workshop on Laser Scanning 2007 and Silvilaser 2007, Finland. Online (http://www.isprs.org/proceedings/XXXVI/3-W52/final_papers/Hopkinson_2007.pdf). Accessed 24 November 2012.

Hopkinson, C., and L. Chasmer. 2009. Testinf lidar models of fractional cover across multiple forest ecozones. Remote Sensing of Environment **113**: 275-288.

Hosoi, F., and K. Omasa. 2009. Estimating vertical leaf area density profiles of tree canopies using three-dimensional portable lidar imaging. Online (http://park.itc.u-tokyo.ac.jp/joho/Omasa/462.pdf). Accessed 24 November 2012.

Houldcroft, C.J., C.L. Campbell, I.J. Davenport, R.J. Gurney, and N. Holden. 2005. Measurement of canopy geometry characterisitics using lidar laser altimetry: a feasibility study. IEEE Transactions on Geoscience and Remote Sensing **43**(10): 2270-2282.

Hyde, P., R. Dubayah, B. Peterson, J.B. Blair, M. Hofton, C. Hunsaker, R. Knox, and W. Walker. 2005. Mapping forest structure for wildlife habitat analysis using waveform lidar: validation of montane ecosystems. Remote Sensing of Environment **96**: 427-437.

Hyde, P., R. Dubayah, W. Walker, J.B. Blair, M. Hofton, and C. Hunsacker. 2006. Mapping forest structure for wildlife habitat analysis using multi-sensor (lidar, sar/insar, etm+, quickbird) synergy. Remote Sensing of Environment **102**: 63-73.

Jensen, J.L.R., K.S. Humes, L.A. Vierling, and A.T. Hudak. 2008. Discrete return lidar-based prediction of leaf area index in two conifer forests. Remote Sensing of Environment **112**: 3947-3957.

Jensen, J.L.R, K.S. Humes, A.T. Hudak, L.A. Vierling, and E. Delmelle. 2011. Evaluation of the MODIS LAI product using independent lidar-derived LAI: a case study in mixed conifer forest. Remote Sensing of Environment **115**: 3625-3639.

Jonckheere, I., S. Fleck, K. Nackaerts, B. Muys, P. Coppin, M. Weiss, and F. Baret. 2004. Review of methods for in situ leaf area index determination part I. theories, sensors, and hemispherical photography. Agricultural and Forest Meteorology **121**: 19-35.

Junttila, V., T. Kauranne, and V. Leppänen. 2010. Estimation of forest stand parameters from airborne laser scanning using calibrated plot databases. Forest Science **56**(3): 257-270.

Kao, D.L., M.G. Kramer, A.L. Love, J.L. Dungan and A.T. Pain. (2005) Visualizing distributions from multi-return LiDAR data to understand forest structure. The Cartographic Journal **42**(1): 35-47.

Kopytko, N., J.B. Cushing, L. Zeman, N. Stevenson-Molnar, F. Martin, and E.S. Keeley. "Making ecology research results useful for resource management: a case study in visual analytics." In *Proceedings of the 10th Annual International Conference on Digital Government Research: Social Networks: Making Connections between Citizens, Data and Government*, pp. 206-215. Digital Government Society of North America, 2009.

Korhonen, L., I. Korpela, J. Heiskanen, and M. Maltamo. 2011. Airborne discrete-return lidar data in the estimation of vertical canopy cover, angular canopy closure and leaf area index. Remote Sensing of Environment **115**: 1065-1080.

Korpela, I. B. Dahlin, H. Schäfer, E. Bruun, F. Haapaniemi, J. Honkasalo, S. Ilvesniemi, V. Kuutti, M. Linkosalmi, J. Mustonen, M. Salo, O. Suomi, and H. Virtanen. 2007. Single tree forest inventory using lidar and aerial images for 3D treetop positioning, species recognition, height and crown width estimation. IAPRES Volume XXXVI, Part 3/W 52.

Korpela, I.S. 2008. Mapping of understory lichens with airborne discrete-return lidar data. Remote Sensing of Environment **112**: 3891-3897.

Krisp, J.M. 2004. Three-dimensional visualization of ecological barriers. Applied Geography. **24**: 23-34.

Lang, A.R.G. and Y. Xiang. 1986. Estimation of leaf area index from transmission of direct sunlight in discontinuous canopies. Agricultural and Forest Meteorology **37**: 229-243.

Lauenroth, W.K., D.L. Urban, D.P. Coffin, W.J. Parton, H.H. Shugart, T.B. Kirchner and T.M. Smith. 1993. Modeling vegetation structure- ecosystem process interactions across sites and ecosystems. Ecological Modeling **67**: 49-80.

Leblanc, S.G., J.M. Chen, R. Fernandes, D.W. Deering, and A. Conley. 2005. Methodology comparison for canopy structure parameters extraction from digital hemispherical photography in boreal forests. Agricultural and Forest Meteorology **129**: 187-207.

Lee, A.C., and R.M. Lucas. 2007. A lidar-derived canopy density model for tree stem and crown mapping in Australian forests. Remote Sensing of Environment **111**: 493-518.

Lefsky, M.A., W.B. Cohen, S.A. Acker, G.G. Parker, T.A. Spies, and D. Harding. 1999. Lidar remote sensing of the canopy structure and biophysical properties of douglas-fir western hemlock forests. Remote Sensing of Environment **70**: 339-361.

Lefsky, M.A., W.B. Cohen, D.J. Harding, G.G. Parker, S.A. Acker, and S.T. Gower. 2001. Lidar remote sensing of aboveground biomass in three biomes. International Archives of Photogrammetry and Remote Sensing XXXIV-3/W4: 22-24.

Lefsky, M.A., W.B. Cohen, G.G. Parker, and D.J. Harding. 2002. Lidar remote sensing for ecosystem studies. BioScience **52**(1): 19-30.

Lefsky, M.A. 2005. Geographic variability in lidar predictions of forest stand structure in the Pacific Northwest. Remote Sensing of Environment **95**(4): 532-548.

Li, W., Q. Guo, M.K. Jakubowski, and M. Kelly. 2012. A new method for segmenting individual trees from lidar point cloud. Photogrammetric Engineering & Remote Sensing **78**(1): 75-84.

Lim, K., P. Treitz, K. Baldwin, I. Morrison and J. Green. 2003. Lidar remote sensing of biophysical properties of tolerant northern hardwood forests. Canadian Journal of Remote Sensing **29**(5): 658-678.

Lovell, J.L., D.L.B Jupp, D.S. Culvenor, and N.C. Coops. 2003. Using airborne and ground-based ranging lidar to measure canopy structure in Australian forests. Canadian Journal of Remote Sensing **29**(5): 607-622.

Lutz, J.A. 2005. The contribution of mortality to early coniferous forest development. Seattle, WA: University of Washington. 95 p. M.S. thesis.

Macfarlane, C., M. Hoffman, D. Eamus, N. Kerp, S. Higginson, R. McMurtrie, and M. Adams. 2007. Estimation of leaf area index in eucalypt forest using digital photography. Agricultural and Forest Meteorology **143**: 176-188.

Makela, A. 1986. Implications of the pipe model theory on dry matter partitioning and height growth in trees. Journal of Theoretical Biology **123**: 103-120.

Magnussen, S., and P. Boudewyn. 1998. Derivations of stand heights from airborne laser scanner data with canopy-based quantile estimators. Canadian Journal of Forest Research **28**: 1016-1031.

Marcell, W., M. Eriksson, and S. Popescu. 2009. Systematic sampling of scanning lidar swaths. Online (ftp://www.iscc.org/people/vanaardt/Silvilaser/.../S5.../Marcell_64.pdf). Accessed 24 November 2012.

McGaughey, R. 1998. Techniques for visualizing the appearance of forestry operations. Journal of Forestry **96**(6): 9-14.

McGaughey, R.J., AND W.W. Carson. 2003. Fusing LIDAR data, photographs, and other data using 2D and 3D visualization techniques. P. 16–24 in *Proc. of Terrain Data: Applications and Visualization-Making the Connection,*

Charleston, SC. American Society for Photogrammetry and Remote Sensing, Bethesda, MD.

McGaughey, R.J. *Fusion/LDV: Software for LiDAR Data Analysis and Visualization*; USDA Forest Service, Pacific Northwest Research Station: Portland, OR, USA, 2012. Available online: http://forsys.cfr.washington.edu/JFSP06/lidar_&_ifsar_tools.htm Accessed: January 2012.

Martens, S.N., S.L. Ustin, and R.A. Rouseau. 1993. Estimation of tree canopy leaf area index by gap fraction analysis. Forest Ecology and Management **61**: 91-108.

Means, J.E., S.A. Acker, D.J. Harding, J.B. Blair, M.A. Lefsky, W.B. Cohen, M.E. Harmon, and W.A. McKee. 1999. Use of large-footprint scanning airborne lidar to estimate forest stand characteristics in the Western Cascades of Oregon. Remote Sensing of Environment **67**: 298-308.

Montes, F., P. Pita, A. Rubio, I. Canellas. 2007. Leaf area index estimation in mountain even-aged Pinus silvestris L. stands from hemispherical photographs. Agricultural and Forest Meteorology **145**: 215-228.

Morrison, H., C. Hopkinson, L. Chasmer, and N. Kljun. 2011. Generating an automated approach to optimize effective leaf area index by Canadian boreal forest species using airborne lidar. Silvilaser 11th international conference on lidar applications for assessing forest ecosystems Hobart, Australia. Online (http://www.iufro.org/download/file/8239/5065/40205-silvilaser2011_pdf). Accessed 24 November 2012.

Morrison, H., C. Hopkinson, and M.A. Wulder. 2011. Optimal lidar gridding parameterization for effective leaf area estimation in the boreal forest Yukon Territory, Canada. SilviLaser 2011, Hobart, Australia. Online (www.cabdirect.org/abstracts/20123180564.html). Accessed 24 November 2012.

Morsdorf, F., B. Kötz, E. Meier, K.I. Itten, and B. Allgöwer. 2006. Estimation of LAI and fractional cover from small footprint airborne laser scanning data based on gap fraction. Remote Sensing of Environment **104**: 50-61.

Moskal, L.M., T. Erdody, A. Kato, J. Richardson, G. Zheng, and D. Briggs. 2009. Lidar applications in precision forestry. Silvilaser College Station, TX.

Negron Juarez, R.I., H. Ribeiro da Rocha, A.M. Silva e Figueira, M.L. Goulden, and S.D. Miller. 2009. An improved estimate of leaf area index based on the histogram analysis of hemispherical photographs. Agricultural and Forest Meteorology **149**: 920-928.

Norman, D. 2012. The detection of forest structures in the Monongahela National Forest using lidar. Thesis. Marshall University. 53 pages.

Omasa, K., F. Hosoi, and A. Konishi. 2007. 3D lidar imaging for detecting and understanding plant response and canopy structure. Journal of Experimental Botany **58**(4): 881-898.

Paar, P. 2006. Landscape visualizations: Applications and requirements of 3D visualization software for environmental planning. Computers, Environment and Urban Systems **30**: 815-839.

Peduzzi, A., R.H. Wynne, T.R. Fox, R.F. Nelson, and V.A. Thomas. 2012. Estimating leaf area index in intensively managed pine plantations using airborne laser scanner data. Forest Ecology and Management **270**: 54-65.

Pekin, B., and C. Macfarlane. 2009. Measurement of crown cover and leaf area index using digital cover photography and its application to remote sensing. Remote Sensing **1**: 1298-1320.

Peterson, F. 2012. Post-harvest establishment influences ANPP, Soil C, and DOC export in complex terrain. Doctoral Dissertation, Oregon State University, Corvallis, OR.

Peterson, F. and K. Lajtha. 2012. Soil C and DOC dynamics in complex terrain. Submitted to *JGR-Biogeosciences*, December 2012.

Peterson, K.S. 2010. Calculating leaf area index on watershed one and relationships with other indices. Unpublished internal document. Oregon State University, Corvallis, OR.

Popescu. S.C. and R. Wynne. 2004. Seeing the trees in the forest: Using LiDAR and multispectral data fusion with local filtering and variable window size for estimating tree height. Photogrammetric Engineering and Remote Sensing **70**(5): 589-604.

Popescu, S.C., and K. Zhao. 2008. A voxel-based lidar method for estimating crown base height for deciduous and pine trees. Remote Sensing of Environment **112**: 767-781.

Popescu, S.C., K. Zhao, A. Neuenschwander, and C. Lin. 2011. Satellite lidar vs. small footprint airborne lidar: comparing the accuracy of aboveground biomass estimates and forest structure metrics at footprint level. Remote Sensing of Environment **115**: 2786-2797.

Popescu, S.C. *TreeVaW: Tree Variable Window;* Spatial Sciences Laboratory, Texas A&M University: College Station, TX, USA. Available online: http://ssl.tamu.edu/personnel/s_popescu/TreeVaW/download.htm Accessed 7th July 7 2012

Poulos, H.M., A.E. Camp, R.G. Gatewood, and L. Loomis. 2007. A hierarchical approach for scaling forest inventory and fuels data from local to landscape scales in the Davis mountains, Texas, USA. Forest Ecology and Management **244**: 1-15.

Pypker, T.G., M.H. Unsworth, A.C. Mix, W. Rugh, T. Ocheltree, K. Alstad and B.J. Bond. 2007. Using nocturnal cold air drainage flow to monitor ecosystem processes in complex terrain. Ecological Applications **17**: 702-714.

R Development Core Team (2012). R: A language and environment for statistical computing, reference index version 2.15.12. R Foundation for Statistical Computing, Vienna, Austria. ISBN 3-900051-07-0, URL http://www.R-project.org. Accessed July 2012.

Riano, D., J. Sanchez-Pena, M. Patricio, F. Valladares, J. Greenberg and S.L. Ustin. 2006. A simple model to calculate leaf area index from lidar data. American Geophysical Union, Fall Meeting. http://adsabs.harvard.edu/abs/2006AGUFM.B41A0160R Accesed: 24th November 2012.

Riano, D., F. Valladares, S. Condes, and E. Chuvieco. 2004. Estimation of leaf area index and covered ground from airborne laser scanner (lidar) in two contrasting forests. Agricultural and Forest Meteorology short communication.

Richardson, J.J. 2008. Estimating leaf area index from multiple return, small footprint aerial lidar at the Washington park arboretum. Thesis. College of Forest Resources, University of Washington, Seattle, WA. M.S. Thesis.

Richardson, J.J., L.M. Moskal, and S. Kim. 2008. Estimating urban forest leaf area index (LAI) from aerial lidar. Factsheet #5. Remote Sensing and Geospatial Application Laboratory, University of Washington, Seattle, WA. Online (http://dept.washington.edu/rsgal/). Accessed 24 November 2012.

Richardson, J.J., L.M. Moskal, and S. Kim. 2009. Modeling approaches to estimate effective leaf area index from aerial discrete-return lidar. Agricultural and Forest Meteorology **149**: 1152-1160.

Richardson, A.D., D.B. Dail, and D.Y. Hollinger. 2011. Leaf area index uncertainty estimates for model-data fusion applications. Agricultural and Forest Meteorology **151**: 1287-1292.

Richardson, J.J., and L.M. Moskal. 2011. Strengths and limitations of assessing forest density and spatial configuration with aerial lidar. Remote Sensing of Environment **115**: 2640-2651.

Roth, B.E., K. Clint Slatton, and M.J. Cohen. 2007. On the potential for high-resolution lidar to improve rainfall interception estimates in forest ecosystems. Frontiers of Ecology and the Environment **5**(8): 421-428.

Rothacher, J., C.T. Dyrness, and R.L. Fredriksen. 1967. Hydrologic and related characteristics of three small watersheds in the Oregon Cascades. Portland, OR: U.S. Department of Agriculture, Forest Service, Pacific Northwest Forest and Range Experiment Station. 54 p.

Ryu, Y., T. Nilson, H. Kobayashi, O. Sonnentage, B.E. Law, and D.D. Baldocchi. 2010. On the correct estimation of effective leaf area index: does it reveal information on clumping effects? Agricultural and Forest Meteorology **150**: 463-472.

Schleppi, P., M. Conedera, I. Sedivy, and A. Thimonier. 2007. Correcting non-linearity and slope effects in the estimation of the leaf area index of forests from hemispherical photographs. Agricultural and Forest Meteorology **144**: 236-242.

Sea, W.B., P. Choler, J. Beringer, R.A. Weinmann, L.B. Hutley, and R. Leuning. 2011. Documenting improvement in leaf area index estimates from MODIS using hemispherical photos from Australian savannas. Agricultural and Forest Meteorology **151**: 1453-1461.

Seidel, D., S. Fleck, and C. Leuschner. 2012. Analyzing forest canopies with ground-based laser scanning: A comparison with hemispherical photography. Agricultural and Forest Meteorology **154-155**: 1-8.

Seidl, R., T.A. Spies, W. Rammer, E.A. Steel, R.J. Pabst, and K. Olsen. 2012. Multi-scale drivers of spatial variation in old-growth forest carbon density disentangled with lidar and an individual-based landscape model. Ecosystems. 15 pages.

Sherren, K., J. Fischer, H. Clayton, A. Hauldren, and S. Dovers. Lessons from visualizing the landscape and habitat implications of tree decline—and its remediation through tree planting—in Australia's grazing landscapes. Landscape and Urban Planning **103**: 248-258.

Smith, A.M.S., M.J. Falkowski, A.T. Hudak, J.S. Evans, A.P. Robinson, and C.M. Steele. 2009. A cross-comparison of field, spectral, and lidar estimates of forest canopy cover. Canadian Journal of Remote Sensing **35**(5): 447-459.

Solberg, S., E. Naesset, K. Holt Hanssen, and E. Christiansen. 2006. Mapping defoliation during a severe insect attack on Scots pine using airborne laser scanning. Remote Sensing of Environment **102**: 364-376.

Specht, R.L and Specht, A. Australian plant communities: dynamics of structure, growth and biodiversity. 1999.

Spies, T. 2011. LiDAR data (August 2008) for the Andrews Experimental Forest and Willamette National Forest study areas. H.J. Andrews Experimental Forest. Forest Science Data Bank, Corvallis, OR. [Database]

Stojanova, D., P. Panov, V. Gjorgjioski, A. Kobler, and S. Džeroski. 2010. Estimating vegetation height and canopy cover from remotely sensed data with machine learning. Ecological Informatics **5**(4): 256-266.

Stoltman, A. M., V.C. Radeloff and D.J. Mladenoff. (2004) Forest Visualization for management and planning in Wisconsin. Journal of Forestry **102**(4) 7-13.

Strunk, J.L., S.E. Reutebuch, and J.R. Foster. 2008. Lidar inventory and monitoring of a complex forest. ASPR Annual Conference, Portland, OR. Online (www.asprs.org/a/publications/proceedings/portland08/0076.pdf). Accessed 24 November 2012.

Suarez, J.C., C. Ontiveros, S. Smith and S. Snape. 2005. Use of airborne LiDAR and aerial photography in the estimation of individual tree heights in forestry. Computers and Geosciences **31**: 253-262.

Tiede, D., G. Hocheimer and T. Blaschke. 2005. A full GIS-based workflow for tree identification and tree crown delineation using laser scanning. In CMRT05, Vol. XXXVI, Part 3/W24. Vienna, Austria.

Turner, D.P., W.B. Cohen, R.E. Kennedy, K.S. Fassnacht, and J.M. Briggs. 1999. Relationships between leaf area index and landsat tm spectral vegetation indices across three temperate zone sites. Remote Sensing of Environment **70**: 52-68.

United States Department of Agriculture (USDA), Forest Service. Forest Inventory and Analysis National Program. http://www.fia.fs.fed.us/ December 2012.

United States Geological Survey (USGS). The National Map Viewer. http://nationalmap.gov/viewer.html. December 2012 Accessed August 2012.

Van Gardingen, P.R., G.E. Jackson, S. Hernandez-Daumas, G. Russell, and L. Sharp. 1999. Leaf area index estimates obtained for clumped canopies using hemispherical photography. Agricultural and Forest Meteorology **94**: 243-257.

Vose, J.M., P.M. Dougherty, J.N. Long, F.W. Smith, H.L. Gholz and P.J. Curran. 1994. Factors influencing the amount and distribution of leaf area of pine stands. Ecological Bulletin (Copenhagen) **43**: 102-114.

Walter, J.N., and E.F. Torquebiau. 2000. The computation of forest leaf area index on slope using fish eye sensors. Life Sciences **323**: 801-813.

Wang, W., B. Song, J. Chen, D. Zheng and T.R. Crow. 2006. Visualizing forest landscapes using public data sources. Landscape and Urban Planning **75**: 111-124.

Waring, R.H., H.L. Gholz, C.C. Grier and M.L. Plummer. 1977. Evaluating stem conducting tissue as an estimator of leaf area in four woody angiosperms. Canadian Journal of Botany **55**:1474-1477.

Waring, R.H. 1998. Lessons learned while extending physiological principles from growth chambers to satellite studies. Tree Physiology. **18**: 491-497.

Watershed Sciences. *Lidar Remote Sensing Data Collection: HJ Andrews & Willamette National Forest*; Watershed Sciences Inc.: Corvallis, OR, USA November 2008; 25 p.

Weiss, M., F. Baret, G.J. Smith, I. Jonckheere, and P. Coppin. 2004. Review of methods for in situ leaf area index (LAI) determination part II. Estimation of LAI, errors and sampling. Agricultural and Forest Meteorology **121**: 37-53.

Wilson, J.W. 1960. Inclined point quadrats. New Phytol. **59**: 1-8.

Wilson, J.W. 1963. Estimation of foliage denseness and foliage angle by inclined point quadrats. Australian Journal of Botany **11**: 95-105.

Zhao, K., S. Popescu, and R. Nelson. 2009. Lidar remote sensing of forest biomass: a scale-invariant estimation approach using airborne lasers. Remote Sensing of Environment **113**: 182-196.

Zhao, K., and S. Popescu. 2009. Lidar-based mapping of leaf area index and its use for validating GLOBCARBON satellite LAI product in a temperate forest of the southern USA. Remote Sensing of Environment **113**: 1628-1645.

Zheng, G., and L.M. Moskal. 2009. Retrieving leaf area index (LAI) using remote sensing: theories, methods, and sensors. Sensors **9**: 2719-2745.

APPENDIX A: LiDAR Calculated LAI, Surface Volume and Cover*Height Value for All Permanent Vegetation Plots.

Plot	LiDAR LAI	Volume	Cover*Height
P11101	4.56	2851.99	1304.86
P11102	7.21	3881.91	1810.46
P11103	9.36	4716.75	2108.04
P11104	6.47	3592.73	1688.23
P11105	9.66	4832.69	2129.69
P11107	5.87	3361.66	1499.25
P11109	8.32	4313.06	1970.07
P11110	6.12	3457.18	1552.28
P11111	9.59	4804.17	2191.74
P11112	15.97	7283.14	3269.34
P11201	0.64	1327.74	537.41
P11203	1.77	1765.31	1634.25
P11205	6.18	3481.56	1851.11
P11206	7.48	3984.75	1709.26
P11207	7.50	3992.86	1723.01
P11208	6.99	3793.14	1841.66
P11209	7.79	4104.92	1857.40
P11210	7.85	4130.72	2321.76
P11211	10.17	5029.63	1482.66
P11212	6.70	3682.82	1928.78
P11213	8.58	4412.35	1883.05
P11214	7.61	4036.64	1684.53
P11215	6.84	3737.21	1876.32
P11216	7.85	4130.42	1558.30
P11217	6.43	3579.44	1976.15
P11218	8.51	4384.02	1930.42
P11301	8.34	4317.79	2036.53
P11302	8.56	4406.24	1626.86
P11303	6.27	3513.99	1466.32
P11304	5.39	3173.55	1449.60
P11305	5.11	3066.43	538.83
P11306	0.77	1377.15	1142.32
P11307	4.06	2656.61	581.40
P11308	0.78	1384.11	733.49
P11309	2.48	2042.33	698.31
P11310	1.58	1695.09	1465.79
P11311	5.54	3231.37	1546.48

P11312	5.42	3186.17	2147.66
P11313	9.49	4766.61	2150.88
P11314	9.68	4840.79	2302.55
P11315	10.32	5089.58	2250.21
P11316	10.07	4990.19	2096.08
P11317	9.33	4703.48	1867.13
P11318	7.63	4044.01	1925.33
P11319	8.13	4237.20	1758.08
P11320	7.51	3996.70	1773.62
P11321	7.22	3883.21	1712.32
P11322	6.91	3764.93	1683.36
P11323	6.71	3687.65	2254.25
P11324	9.59	4804.72	1925.11
P11401	7.79	4107.68	1777.88
P11402	6.90	3759.48	1529.96
P11403	5.75	3312.53	1835.90
P11404	7.26	3901.58	2125.42
P11405	9.25	4674.50	2039.21
P11406	8.71	4464.90	1576.06
P11407	6.39	3561.29	1550.84
P11408	5.60	3255.33	1406.38
P11409	4.74	2921.07	1916.22
P11410	8.04	4203.01	932.02
P11411	2.60	2090.99	1478.81
P11412	5.31	3140.85	1913.67
P11413	8.26	4286.63	1944.52
P11414	8.18	4257.79	1471.17
P11415	6.03	3422.51	1840.87
P11416	8.32	4312.89	328.52
P11419	3.26	2347.27	1210.87
P11420	4.10	2672.14	836.08
P11421	1.96	1840.46	1686.62
P11422	6.56	3628.07	1923.78
P11423	7.80	4108.20	879.63
P11424	2.02	1864.88	1185.66
P11425	3.55	2458.25	977.30
P11426	3.10	2283.98	1814.15
P11501	7.73	4081.92	1913.26
P11502	5.20	3100.67	1496.04
P11503	5.74	3308.71	1510.65
P11504	8.47	4368.29	1993.34

P11505	3.64	2492.18	1026.51
P11506	5.98	3403.64	1602.89
P11507	9.12	4623.31	1846.26
P11508	8.47	4369.43	1971.16
P11509	7.30	3913.96	1814.08
P11510	6.11	3451.69	1615.55
P11511	6.43	3576.48	1558.77
P11512	8.44	4359.61	1985.29
P11513	7.83	4122.42	1843.08
P11514	8.39	4337.04	1967.35
P11515	7.82	4118.74	1889.00
P11516	2.00	1858.20	835.13
P11517	1.95	1836.35	875.49
P11518	4.59	2861.19	1377.29
P11520	5.45	3196.52	1430.11
P11521	0.28	1189.14	402.75
P11522	2.56	2073.50	898.35
P11523	1.97	1844.66	768.83
P11524	7.14	3853.28	1799.12
P11525	5.29	3133.00	1467.19
P11526	5.44	3192.00	1376.24
P11527	6.16	3471.17	1542.90
P11601	6.21	3493.93	1572.30
P11602	5.48	3209.01	1543.77
P11603	5.75	3313.64	1522.65
P11604	5.74	3309.35	1576.71
P11605	6.92	3767.20	1740.94
P11606	5.81	3337.78	1526.60
P11607	8.04	4203.94	1907.45
P11608	8.05	4208.02	1907.70
P11609	7.64	4046.03	1864.89
P11610	7.91	4153.80	1915.59
P11611	9.33	4704.49	2150.82
P11612	8.60	4419.24	1994.95
P11613	9.13	4625.23	2067.91
P11614	9.31	4697.41	2135.11
P11615	8.29	4299.38	1872.71
P11616	9.25	4674.68	2048.82
P11617	7.80	4109.04	1936.86
P11618	8.90	4538.78	2073.92
P11619	6.77	3709.65	1752.57

P11620	10.10	5002.62	2233.84
P11621	8.77	4486.22	2025.14
P11622	10.47	5145.32	2291.59
P11623	7.85	4127.45	1865.50
P11624	6.43	3576.04	1655.44
P11625	5.76	3317.49	1557.57
P11626	4.70	2907.34	1341.70

APPENDIX B: TreeVaW Tree Identification Results for all 133 Permanent Vegetation Plots

PLOT	Observed Trees	Predicted Trees	% Trees Id'ed
			Plots in which DHPs were taken
P11108	28	12	42.86%
P11109	23	17	73.91%
P11110	23	18	78.26%
P11205	17	17	100.00%
P11206	17	15	88.24%
P11207	15	18	120.00%
P11208	12	14	116.67%
P11209	25	11	44.00%
P11211	38	15	39.47%
P11212	46	22	47.83%
P11213	28	17	60.71%
P11608	24	17	70.83%
P11609	15	12	80.00%
P11610	18	14	77.78%
P11611	19	14	73.68%
P11612	21	17	80.95%
P11613	30	15	50.00%
P11614	19	15	78.95%
P11615	25	20	80.00%
P11616	21	14	66.67%
P11617	13	14	107.69%
			All other WS1 plots
P11102	35	15	42.86%
P11103	43	13	30.23%
P11104	16	19	118.75%
P11105	14	14	100.00%
P11107	23	13	56.52%
P11111	46	11	23.91%
P11112	80	8	10.00%
P11201	18	48	266.67%
P11202	5	30	600.00%
P11203	11	29	263.64%
P11210	18	21	116.67%
P11214	54	15	27.78%
P11215	45	15	33.33%

P11216	27	14	51.85%
P11217	62	14	22.58%
P11218	52	12	23.08%
P11301	36	16	44.44%
P11302	18	16	88.89%
P11303	44	21	47.73%
P11304	29	20	68.97%
P11305	34	21	61.76%
P11306	4	31	775.00%
P11307	17	24	141.18%
P11308	6	54	900.00%
P11309	18	35	194.44%
P11310	11	39	354.55%
P11311	7	33	471.43%
P11312	5	28	560.00%
P11313	30	14	46.67%
P11314	44	14	31.82%
P11315	22	14	63.64%
P11316	40	16	40.00%
P11317	46	18	39.13%
P11318	36	17	47.22%
P11319	20	15	75.00%
P11320	24	17	70.83%
P11321	35	23	65.71%
P11322	36	19	52.78%
P11323	64	12	18.75%
P11324	44	10	22.73%
P11401	27	15	55.56%
P11402	16	19	118.75%
P11403	8	15	187.50%
P11404	14	15	107.14%
P11405	21	12	57.14%
P11406	13	10	76.92%
P11407	23	14	60.87%
P11408	9	42	466.67%
P11409	20	37	185.00%
P11410	16	15	93.75%
P11411	15	46	306.67%
P11412	49	21	42.86%
P11413	47	12	25.53%
P11414	23	11	47.83%

P11415	16	14	87.50%
P11416	15	11	73.33%
P11417	11	68	618.18%
P11418	14	29	207.14%
P11419	20	29	145.00%
P11420	28	30	107.14%
P11421	22	46	209.09%
P11422	16	16	100.00%
P11423	34	14	41.18%
P11424	28	55	196.43%
P11425	24	31	129.17%
P11426	13	30	230.77%
P11427	43	26	60.47%
P11501	30	14	46.67%
P11502	22	20	90.91%
P11503	37	19	51.35%
P11504	36	14	38.89%
P11505	12	26	216.67%
P11506	11	18	163.64%
P11507	18	9	50.00%
P11508	23	12	52.17%
P11509	18	13	72.22%
P11510	32	19	59.38%
P11511	8	34	425.00%
P11512	15	16	106.67%
P11513	24	13	54.17%
P11514	17	16	94.12%
P11515	23	14	60.87%
P11516	11	34	309.09%
P11517	3	53	1766.67%
P11518	28	25	89.29%
P11519	4	71	1775.00%
P11520	9	29	322.22%
P11521	8	64	800.00%
P11522	22	39	177.27%
P11523	21	40	190.48%
P11524	32	14	43.75%
P11525	16	18	112.50%
P11526	22	23	104.55%
P11527	70	16	22.86%
P11601	24	21	87.50%

P11602	13	26	200.00%
P11603	28	24	85.71%
P11604	29	14	48.28%
P11605	34	15	44.12%
P11606	19	22	115.79%
P11607	22	22	100.00%
P11618	16	14	87.50%
P11619	17	24	141.18%
P11620	26	10	38.46%
P11621	35	16	45.71%
P11622	30	14	46.67%
P11623	27	17	62.96%
P11624	51	19	37.25%
P11625	84	15	17.86%
P11626	99	25	25.25%
TOTAL	3407	2810	82.48%